QUAECUMQUE VERA

Structural Engineering Report 178

THE FLEXURAL BEHAVIOUR OF CONCRETE-FILLED HOLLOW STRUCTURAL SECTIONS

by

YUE QING LU

and

D. J. LAURIE KENNEDY

APRIL, 1992

RECENT STRUCTURAL ENGINEERING REPORTS

Department of Civil Engineering
University of Alberta

151. *Behaviour and Ultimate Strength of Partial Joint Penetration Groove Welds* by D.P. Gagnon and D.J.L. Kennedy, July 1987.

152. *KBES for Design of Reinforced Concrete Columns* by A. Bezzina and S.H. Simmonds, July 1987.

153. *Compressive Behavior of Gusset Plate Connections* by S.Z. Hu and J.J. Cheng, July 1987.

154. *Development of Structural Steel Design Standards* by P.J. Marek and D.J.L. Kennedy, October 1987.

155. *Behaviour of Bolted Joints of Corrugated Steel Plates* by R.W.S. Lee and D.J.L. Kennedy, January 1988.

156. *Masonry Veneer Wall Systems* by W.M. McGinley, J. Warwaruk, J. Longworth and M. Hatzinikolas, January 1988.

157. *Stability of Concrete Plates* by A.O. Aghayere and J.G. MacGregor, February 1988.

158. *The Flexural Creep Behaviour of OSB Stressed Skin Panels* by P.C.K. Wong, L. Bach and J.J. Cheng, April 1988.

159. *Ultimate Strength of Eccentrically Loaded Fillet Welded Connections* by D.F. Lesik and D.J.L. Kennedy, May 1988.

160. *Fatigue Strength of Coped Steel Beams* by M.C.H. Yam and J.J. Cheng, June 1988.

161. *Analysis of Concrete Panels* by B. Massicotte, A.E. Elwi and J.G. MacGregor, July 1988.

162. *Behavior and Design of Reinforced Concrete Ice-Resisting Walls* by R.M. Ellis and J.G. MacGregor, November 1988.

163. *An Analysis of the Performance of Welded Wide Flange Columns* by D.E. Chernenko and D.J.L. Kennedy, December 1988.

164. *Nonlinear Dynamic Analysis of Caisson-Type Offshore Structures* by I.R. Soudy and T.M. Hrudey, March 1989.

165. *NORCO - A Program for Nonlinear Finite Element Analysis of Reinforced Concrete Structures - Users' Manual* by S. Balakrishnan, A.E. Elwi and D.W. Murray, April 1989.

166. *An Eigenvector-Based Strategy for Analysis of Inelastic Structures* by J. Napoleao, Fo., A.E. Elwi and D.W. Murray, May 1990.

167. *Elastic-Plastic and Creep Analysis of Casings for Thermal Wells* by S.P. Wen and D.W. Murray, May, 1990.

168. *Erection Analysis of Cable-Stayed Bridges* by Z. Behin and D.W. Murray, September 1990.

169. *Behavior of Shear Connected Cavity Walls* by P.K. Papanikolas, M. Hatzinikolas and J. Warwaruk, September 1990

170. *Inelastic Transverse Shear Capacity of Large Fabricated Steel Tubes*, by K.H. Obaia, A.E. Elwi and G.L. Kulak, April 1991.

171. *Fatigue of Drill Pipe* by G.Y. Grondin and G.L. Kulak, April 1991.

172. *The Effective Modulus of Elasticity of Concrete in Tension* by Atif F. Shaker and D.J. Laurie Kennedy, April 1991.

173. *Slenderness Effects in Eccentrically Loaded Masonry Walls* by Muqtadir, Mohammad A., Warwaruk, J. and Hatzinikolas, M.A., June 1991.

174. *Bond Model For Strength of Slab-Column Joints* by Scott D.B. Alexander and Sidney H. Simmonds, June 1991.

175. *Modelling and Design of Unbraced Reinforced Concrete Frames* by Yehia K. Elezaby and Sidney H. Simmonds, February 1992.

176. *Strength and Stability of Reinforced Concrete Plates Under Combined Inplane and Lateral Loads* by Mashhour G. Ghoneim and James G. MacGregor, February 1992.

177. *A Field Study of Fastener Tension in High-Strength Bolts* by G.L. Kulak and K. H Obaia, April 1992.

178. *The Flexural Behaviour of Concrete-Filled Hollow Structural Sections* by Yue Qing Lu and D.J. Laurie Kennedy, April 1992.

THE FLEXURAL BEHAVIOUR OF CONCRETE-FILLED HOLLOW STRUCTURAL SECTIONS

BY

Yue Qing Lu

D. J. Laurie Kennedy

DEPARTMENT OF CIVIL ENGINEERING

UNIVERSITY OF ALBERTA

Edmonton, Alberta, Canada, T6G 2G7

April, 1992

Abstract

Prior to the current edition of CSA standard CAN/CSA S16.1-M89, the moment resistance used in the interaction equation for concrete-filled hollow structural steel section beam-columns was taken as that of the steel section alone with no contribution of the concrete. In S16.1-M89, the concrete contribution was acknowledged as an alternative approach, but no method of assessing it was given. Preliminary studies had indicated that the concrete increased the ultimate moment capacity, the initial flexural stiffness and the ductility, and delayed local buckling of the steel thus enhancing the behaviour considerably.

A series of four flexural tests on hollow structural steel sections and twelve on concrete-filled sections were undertaken to assess the general behaviour of these composite sections. The properties of the test specimens were chosen to examine the effects of different ratios of depth/width and therefore of the proportions of steel and concrete in compression, and of different values of shear-span/depth as related to the transfer of forces from one to the other when no direct means is provided for this transfer. The tests showed that the ultimate flexural strength of the concrete-filled sections is increased by about 10 to 30% over that of the bare steel sections depending on the relative proportions of steel and concrete. In all cases, slip between the steel and concrete was not detrimental even though shear-span/depth ratios as low as one were

tested.

Two models, a relatively simple model suitable for design and a somewhat more complex model suitable for research purposes, are proposed to predict the flexural resistance of concrete-filled hollow structural steel sections.

Acknowledgements

I am indebted to Professor D. J. L. Kennedy for his supervision and valued counsel throughout the course of this work.

This thesis is based on tests conducted by Esther Barber in the I. F. Morrison Structural Laboratory, University of Alberta. The author would like to express his appreciation to Esther Barber for her sincere cooperation in providing the test results for analysis.

In addition the author would like to express his appreciation to Dr. J. R. Colbourne, Dr. J. G. MacGregor and Dr. J. J. Cheng for their guidance and suggestions.

I gratefully acknowledge the financial support of the NSERC as research assistant to Dr. Kennedy, the graduate students' personal interest and suggestions of the Department of Civil Engineering, University of Alberta, the assistant of the technical staff of the I. F. Morrison Structural Laboratory, University of Alberta, and the valuable assistance of librarians of the Cameron Library.

Table of Contents

List of Tables

List of Figures

List of Symbols

a	Shear span
A	Area
A_c	Area of concrete in compression
A_{sc}	Area of a steel beam in compression
A_s	Steel area
A_{st}	Area of a steel beam in tension
b	Width of the section
c	Distance from top of concrete to neutral axis
C_c	Compressive force in concrete
C_s	Compressive force in steel
d	Overall depth of a section
e	Lever arm between compressive resistance C_s, and the tensile resistance, T_s
E	Modulus of elasticity of steel
E_c	Modulus of elasticity of concrete
e'	Lever arm between C_c and T_s
f_r	Modulus of rupture
f_y	Measured yield strength of steel
F_y	Specified minimum yield stress
f'_c	Uniaxial compressive strength of concrete at 28 days
f''_c	Uniaxial compression strength of concrete at time of testing
G	Shear modulus of elasticity
I	Moment of inertia

I_x	Moment of inertia about x axis
I_y	Moment of inertia about y axis
J	St. Venant torsional constant
k_3	The ratio of the maximum stress, f''_c, in the compression zone of a beam to the cylinder strength, f'_c
L	Length of beam
m	Length of constant moment region
M_c	Composite moment
M_m	Maximum moment
M_n	Penultimate moment
M_p	Plastic moment
M_r	Unfactored moment resistance of the composite beam
M_t	Test moment
M_u	Critical elastic moment of a laterally unbraced beam
M_x	Moment about x axis
M_y	Moment about y axis, Yield moment
N.A.	Neutral axis
P_s	Load in steel stub column
r	Outside corner radius of steel shell
S	Elastic section modulus of steel section
t	Wall thickness, time
T_s	Tensile force in steel
V	Coefficient of variation
y_{sc}	Distance from centre of compressive area to neutral axis
y_{st}	Distance from centre of tensile area to neutral axis
Z	Plastic section modulus of steel section
α	Non-dimensional ratio of force in steel beam to that in

	composite beam
ε	Strain
ε_p	Strain at proportional limit
ε_y	Yield strain
ε_0	Strain at maximum compressive strength
ϕ	Curvature
μ	Mean value
σ	Stress
σ_p	Proportional limit
σ_u	Ultimate stress
σ_y	Yield stress of steel
ω_2	Coefficient used to account for increased moment resistance of a laterally unsupported beam segment when subject to a moment gradient

Chapter 1. Introduction

1.1 General

Only in 1989, in Canadian structural steel design standards, the contribution of the concrete to the flexural resistance of concrete-filled hollow structural steel sections (HSS's) was recognized in the interaction equations for the design of beam-columns. Even then, this recognition appeared only as an alternative to the formulation where the concrete contribution was assumed to be zero and, moreover, no method of calculating the flexural resistance of the composite section was given. This approach was apparently taken, because of the lack of a general method for the design to take into account the different factors affecting the behaviour that may exist in practice.

Such factors include different proportions of the concrete and steel in compression that can exist when rectangular hollow structural sections with different width/depth ratios are used rather than square sections. As well, because bond must be relied upon to transfer the shear forces between the steel shell and the concrete, when no mechanical devices are provided, high moment gradients may preclude the development of the full flexural capacity. In general the presence of the concrete modifies the behaviour of the composite member in flexure, not only because it contributes to the compression resistance but also because local buckling of the steel in compression, supported laterally by the concrete, is delayed. With the concrete carrying part of the compressive force, more of the steel section is available to provide the tensile portion of the internal resisting couple.

Work reported in the literature on the flexural behaviour of concrete-filled HSS's has been limited chiefly to that of square sections without examination of the effects of different proportions of steel and concrete in compression. The rate of development of compressive force in the concrete has not been examined closely.

1.2 Objectives

The objectives of this study were:

1. to examine experimentally the flexural behaviour of concrete-filled hollow structural sections as related to different proportions of steel and concrete in compression and to different shear-span/depth ratios,

2. to develop analytical models to predict the flexural resistance of these sections, consistent with the observed behaviour,

3. to determine whether limitations need be imposed on the shear-span/depth ratios (moment gradient) so that the predicted flexural resistance is reached, and

4. to outline areas of future work.

1.3 Scope

A total of four different cold formed square and rectangular hollow structural steel sections were tested, with two-point loading providing a constant moment region, to determine the flexural characteristics of the steel sections alone and to provide the basis for comparison for a total of twelve similar flexural tests on concrete-filled sections. The concrete-filled rectangular sections were tested both with the major axis oriented horizontally and vertically to achieve different proportions of steel and concrete in compression. Shear-span/depth ratios ranging from 1 to 5 were tested to investigate moment gradient effects. All loads were increased monotonically under the short term loading.

Extensive ancillary tests were conducted. For the steel sections, tension coupon tests, residual stress measurements and stub column tests were undertaken. For the concrete, compressive cylinder tests and split cylinder tests were made. Stub column tests on composite sections were also performed.

All tests were conducted by E. Barber.

Based on the analysis of the test results, two models to predict the flexural resistance of concrete-filled HSS's have been developed. The research model closely reflects the observed behaviour, particularly the strains achieved, and is useful as a research tool. The design model is somewhat simplified but gives good test/predicted ratios and is useful for design purposes.

No limitations on the use of the models due to excessive moment gradients need be applied.

1.4 Outline

This chapter closes with a brief literature review including a description of the steel beam tests, composite beam tests, and ancillary tests and the analysis of the latter. The test programme is discussed in Chapter 2.

The detailed analysis of the flexural tests is presented in Chapter 3. The methods to predict the flexural resistance of the composite sections are developed there.

In Chapter 4, engineering applications including design considerations and procedures to use the design model are presented.

A summary, conclusions and recommendations for future work are presented in Chapter 5.

1.5 Literature Review

The more salient aspects of the review of the literature carried out by Barber are reported here.

Furlong (1969) conducted one test on a composite square hollow structural section. He reported a test/predicted ratio of 1.5 times that of comparable concrete sections without the steel shell. For the encased sections he took the ultimate concrete flexural stress as $1.00f'_c$ rather than $0.85f'_c$ as used for ordinary reinforced concrete.

Knowles and Park (1969) found test/predicted ratios of the flexural capacity of concrete-filled steel tubes of 0.93 to 1.15. The predicted strength was again based on ultimate strength reinforced concrete theory, with the steel stress at the yield level and, the concrete in compression at $0.85f'_c$. Concrete in tension was considered to have no strength.

Tomii and Sakino (1979) tested a number of square sections under fixed axial loads and increasing uniform bending moments. As part of this program, four specimens were tested with zero axial load. They proposed for this case that the maximum moment be taken as:

[1.1] $$M_c = \left[1 + \frac{(1 - \alpha)(1 - 4t/d)}{3(1 - 4t/d + (2t/d)\alpha)}\right] M_p$$

where $\alpha = \dfrac{A_s f_y}{A_s f_y + A_c f'_c}$

This expression is based on rectangular stress blocks for the steel and concrete in compression with the steel stress taken as the yield stress and the concrete as f'_c as suggested by Furlong. On this basis, their test/predicted values ranged from 0.93 to 1.03 and a value of 1.35 was determined for Furlong's single test.

Redwood (1983) suggested that the flexural strength be based on the steel stressed to the yield level in tension and compression and the concrete to $0.85f'_c$.

Barber et al (1987) proposed two models based on four tests on square sections. For the research model, rectangular stress blocks are assumed for both the steel and the concrete. The stress in the steel in tension is that corresponding to 10 000 $\mu\varepsilon$ while in compression is that corresponding to 6 000 $\mu\varepsilon$. The rectangular stress block for the concrete, assumed to be stressed to $0.85f'_c$, extends 85% of the depth to the neutral axis which is positioned such that the sum of the internal forces is zero. For the design model, the moment capacity was determined based on the 0.2% offset yield strength of the steel and a compressive stress of $0.85f'_c$ for the concrete.

For the four tests, the research model gives test/predicted ratios of 0.991 to 1.071 with a mean value of 1.025 and a coefficient of variation of 0.034, while the design model gives ratios of 1.090 to 1.178 with a mean value of 1.128 and a coefficient of variation of 0.034.,

All these methods were based on a relatively small number of tests on square sections, with no assessment of different proportions of concrete and steel in compression and with little assessment of the shear transfer problem.

Chapter 2 Experimental Programme

2.1 General

The objectives of the experimental programme were to examine the flexural behaviour of concrete-filled hollow structural steel sections so that a model could be developed to predict the moment resistance of such members with sufficient accuracy to be used in design. For the model to be generally applicable, practical ranges of the several parameters that could affect the moment resistance had to be tested.

As both the steel and concrete contribute to the compressive resistance of the internal resisting couple, different ratios of the steel and concrete area in compression were used. This was accomplished by using steel sections of the same size but with different wall thicknesses, resulting in a considerable change in steel area relative to the concrete, and also by testing rectangular sections oriented for bending about both the strong and weak axes. As inelastic action occurs the upward shift of the neutral axis results in changed proportions of the compressive steel and concrete areas in the two cases.

For steel sections alone, the flexural resistance depends on the maximum strains that can be developed before local buckling occurs. All the 126 HSS's listed in the CISC handbook (CISC, 1991), when made of grade 350W steel, except four, are class 2 or better and therefore capable of reaching M_p. The exceptions occur only when relatively thin sections are bent about their weak axes. Therefore it was considered appropriate to use sections that were nominally Class 1 and Class 2 as being representative of Canadian production. By testing such sections, the effect, if any, of the concrete infill on delaying buckling could be determined as could the answer to the question whether the buckling mode would be changed to allow significantly higher strains to be reached in not compression.

No direct means was provided for the shear transfer of load from the steel to the concrete between the points of zero and maximum moment as this uncluttered form of construction would likely be prefered in the field. As the rate of transfer depends on the moment gradient or ratio of shear-span/depth, different ratios were used to determine whether a critical value existed above which the maximum composite flexural resistance was compromised.

An extensive series of ancillary tests to establish material and cross-sectional behaviour was also made. This included stub column tests, both on steel sections and composite sections, tension tests on coupons cut from the sections and residual stress measurements. Concrete cylinder tests were carried out to determine the compressive strength of the concrete and split cylinder tests to determine its tensile strength.

2.2 Flexural Tests

2.2.1 Flexural Specimens

In the main programme, the flexural specimens were tested with a monotonically increasing load using stroke control under short term loading. Two-point loading was used to provide a constant moment region in which to determine moment-curvature relationships and to observe the mode of failure. A length of 1 000 to 1 500 mm proved adequate for the strain gauges and the demc gauges applied for these purposes.

Beam sections were selected within a set of geometric and loading constraints. A least interior width of 130 mm was chosen so that concrete fill, with 12 mm aggregate, could be placed and adequately compacted using both a pencil vibrator and an external vibrator, when the specimens were standing vertically.

Wall thicknesses were selected to provide both width-thickness of Classes 1 and 2 based on nominal thicknesses and yield strengths. The more readily available sections, manufacturing Class C, of CSA G40.21 grade M350W steel with a nominal yield strength of 350 MPa were selected. These manufacturing Class C sections are cold formed to their final shape from tubular shapes produced by welding a flat-rolled sheet longitudinally. Ratios of shear-span/depth of 1, 1.5, 3 and 5, based on limited previous experience as being likely to divulge any problems of shear transfer, were selected.

The HSS's selected were 152 x 152 x 4.8 for SB1 and CB12, CB13 and CB15; 152 x 152 x 9.5 for SB2 and CB22; 254 x 152 x 6.4 for SB3 and CB31, CB33 and CB35 (bent about the strong axis); 254 x 152 x 9.5 for SB4 and CB41 and CB45 (bent about the strong axis) and 254 x 152 x 6.4 for SB5 and CB51, CB53 and CB55 (bent about the weak axis).

Data of the five HSS steel beam tests carried out to establish the basis for comparison and the twelve composite beam tests are given in Table 2.1. The steel beam tests are designated SB and the composite beam tests, CB. The subsequent digit denotes the specimen number as given in the table and for the composite beams, the last digit denotes the shear-span/depth ratio to the nearest whole number. The first entry in the table for SB1 gives the results for a test done by Kennedy and MacGregor (1984), as this same section was used for tests CB12, 13 and 15.

The concrete selected was type 10 normal weight concrete with a specified 28 day strength of 30 MPa, a maximum aggregate size of 12 mm and 70 mm slump. With temporary bottom end plates tack-welded in place to retain the concrete and the HSS's standing vertically, the concrete was cast in short lifts and compaction was carried out using internal pencil vibrators and external vibrators. All specimens and test cylinders were cast from the same batch of concrete and cured under polyethylene until the time of testing. In each case the compressive strength of the concrete was determined at the time of the flexural test. The end plates were removed from the flexural specimens and bearing plates, 200 x 12 mm extending across the width of the specimens were tack-welded in place at the load and reaction points.

The test results are presented and discussed in Chapter 3.

Table 2.2 gives the manufacturers and the chemical composition for the four different HSS used in these tests. Also given are the chemical composition limits as specified in CSA standard CAN3-G40.21-M84 for grade 350 W steel. All sections meet the chemical composition requirements of the standard.

Table 2.3 gives the measured dimensions of the cross sections. In all cases the sections meet the tolerances given by G40.21-M84. However the wall thickness tends to be less than the specified value, sometimes as much as 7%. The classification of the sections in bending based on the measured values of the wall thickness, flange width and yield strength (as determined subsequently) are given in the Table 2.4. Because the wall thicknesses are less than the nominal values, the b/t ratios are higher than the nominal values. Because the yield strengths are greater than the nominal value, the classification limits are reduced. Therefore, in one case the section classification has degraded by one class.

The cross-sectional properties based on the measured cross-sectional dimensions and assuming that the outside corner radius was 2 times the thickness of the tube wall are given in Table 2.5. Two lines of entries are given for the HSS 254 x 152 x 6.4 depending on whether it is bent about its strong or weak axis. In Table 2.6, the cross-sectional areas, determined by three different methods, are compared. The first method assumes, as used in Table 2.4, that the corner radius is 2 times the wall thickness while the second method is based on the measured radius and in the third method the cross-sectional area was determined by measuring the mass of a short length of the section and dividing by its measured density. The measured areas are less than the nominal values given in the Handbook of Steel Construction, (CISC, 1991) by 4 to 7 %. The tolerance on the mass in CAN/CSA G40.20-M, and therefore the area, of minus 3.5 or plus 10 percent are given in the table. Three of the four sections are under the minimum tolerance.

2.2.2 Test Set-up

A schematic diagram of the test set-up is given in Figure 2.1. Loads were applied by the MTS 6000 with a compressive capacity of 6600 kN. At each load and reaction point, load cells were provided to measure the loads, knife edges to allow free rotation, and a set of rollers to allow longitudinal movement. Thus the beam was tested under simple support and loading conditions. As the beam deflects and the upper surface shortens the rollers under the load points allow them to move toward each other and similarly the rollers at the reactions allow them to move outward. The resulting change in the shear-span was recorded and of course the bending moment at any load was based on the shear-span at that instant.

At the start of a test, the specimen was aligned in the testing machine and about 1/10 of the expected maximum load was applied. If the load cells at the load and reactions showed that the load was not being applied symmetrically, the load was removed and adjustments were made to ensure that a constant moment region was indeed obtained.

2.2.3 Instrumentation

The Instrumentation can be categorized based on the measurements taken: loads, displacements, strains and shear displacements or slip measurements. Figure 2.2 shows the locations of the instrumentation used to measure displacements and strains.

2.2.3.1 Load Measurement

In addition to the measurement of the total applied load by the internal load cell of the MTS machine each reaction and load was measured using a calibrated load cell. These provided a check on statics, included the weight of the distributing beam that was not recorded by MTS load cell, and allowed alignment to be carried out as discussed previously to ensure that the central region of the flexural specimens were subject to a uniform moment.

2.2.3.2 Displacements

Calibrated linear variable displacement transformers (LVDT's) were generally used to measure displacements. Care was taken that these instruments was used only in their linear ranges. Locations of the LVDT's are shown in Figure 2.2. LVDT's 1 and 2 at the west end and 3 and 4 at the east end were positioned to measure the relative movement of the steel and concrete at mid height of the beam and therefore to determine any slips that may occur between them. LVDT's 5, 6 and 7 measured the vertical deflections at the load points and the midspan deflection. LVDT's 8, 9, 10 and 11 measured the inward longitudinal movement of the loads and outward longitudinal movement of the reactions so that the shear-span could be deduced at every load step.

2.2.3.3 Strains

Steel strains were determined from a total of sixteen foil type electrical resistance strain gauges applied in the constant moment region as shown in Figure 2.2. Five were applied on the outer surface of the top and bottom flanges and three were applied on each side.

Concrete strains were measured between demec points fastened to the concrete on a 254 mm gauge length at 3 levels on each side of the specimens in the compression zone. The demec points were centred in 12 mm diameter holes drilled through the steel web of the HSS's. By placing a demec point on the steel, 50 mm from each point mounted on the concrete, two measurements of the relative movement between the concrete and steel at each of 3 levels was obtained on one side of the specimens.

All measurements were taken at each load step. The electronic measurements (strain gauges, LVDT's and load cells) were recorded automatically on the Data General Eclipse S/120 data acquisition system while the demec readings were recorded manually. Photographic and written records were also kept.

2.3 Ancillary Tests

2.3.1 Steel Tests

The ancillary tests carried out on the steel consisted of tension tests on coupons cut from the hollow structural steel cross sections, residual strain measurements and steel stub column tests.

2.3.1.1 Tension Coupons

Tension coupons were used to determine the stress-strain characteristics of the steel for the three distinct regions, the flats, the corners and the longitudinal weld, of the hollow structural sections. Sixteen specimens were sawn from the square sections and twenty from rectangular sections as shown in Fig. 2.3. The coupons were made and tested in accordance with ASTM Standard A 370-77, Part 1, except that the corner coupons did not have a central portion of reduced width. These coupons were packed at the ends for gripping in the jaws of the testing machine. Cross-sectional areas were determined prior to testing from measurements of the reduced cross section for the flat and weld coupons and volumetrically for the corner coupons.

Strains of up to two percent were determined from a pair of electrical resistance strain gauges mounted on opposite face and wired in conjunction with two dummy gauges to give a full bridge system with double sensitivity. Larger strains were determined from caliper measurements.

The test results for the three sections tested in this program, the 152 x 152 x 9.5, the 254 x 152 x 6.4 and the 254 x 152 x 9.5, designated section members 2, 3 and 4 respectively are summarized in Tables 2.7, 2.8 and 2.9. The modulus of elasticity was determined by a moving 5 point average using a least squares fit. When the stress-strain curve becomes non-linear both the computed values of the modulus and its correlation coefficient decrease. Using judgement, the proportional limit can be defined and a value of the modulus up to the proportional limit is found using least squares for all the relevant data. The yield strength and corresponding strain were obtained from the 0.2% offset method. Mean values and coefficients of variation for the modulus of elasticity and yield strength for the three regions, flats, corners and welds (when more than one observation was made) are also tabulated. Chauvenet's criterion was used to reject outliers. Overall weighted averages for the cross section based on the relative area of the flats, corners and welds are also given for the modulus of elasticity and the yield strength.

In Tables 2.10, 2.11 and 2.12 are given coefficients that describe a fifth degree polynomial:

[2.1] $$\sigma = A + B\varepsilon + C\varepsilon^2 + D\varepsilon^3 + E\varepsilon^4 + F\varepsilon^5$$

that approximates closely the mean stress-strain curves for different strain ranges for the flats, corners and welds of the 152 x 152 x 9.5, 254 x 152 x 6.4 and 254 x 152 x 9.5 hollow structural sections respectively. With these data and having the residual strain at any point in the cross section, as presented subsequently, for a given strain distribution across the cross section the stress on any element can be determined. From these, the summation on the stress resultants on the elements leads to the resultant force system.

2.3.1.2 Residual Strains

Longitudinal residual strains were determined for the three cross sections using the method of sections as discused by Tebedge et al (1973). As the slices bowed substantially on sectioning a correction had to be made to the measured strains on the inner and outer faces to account for the fact that the gauge measures the final length on a chord rather than on the arc. Such corrections were made and the average of the corrected strains on the inner and outer faces gives the average longitudinal residual strain.

The location and size of the residual strain coupons which were used with a gauge of 254 mm gauge length are given in Fig. 2.4. The longitudinal residual strain distributions are given in Figs. 2.5, 2.6 and 2.7 for section numbers 2, 3 and 4 respectively and the values of residual strains through the thickness in Figs. 2.8, 2.9 and 2.10 respectively.

In each of Figs. 2.5 to 2.10, tensile residual strains (+) are plotted away from the cross section and compressive residual strains (-) are plotted towards the cross section. The manufacturing process in which the flat rolled sheet is formed into a circular tube and closed by welding longitudinally and then subsequently cold formed into a square or rectangular cross section leaves the members with a most complex and apparently random residual strain distribution. The variation in longitudinal residual strains through the thickness are consistent with the residual strain resulting from forming the tube into a circular cross section, with longitudinal tensile residual strains on the outside surface and compressive residual strains on the inside. The average longitudinal residual strain in Figs. 2.5 to 2.7 is 650, 361 and 270 microstrain respectively.

Obviously, the strains have not been corrected to ensure that the sum of the corresponding stress resultants based on the average stress-strain curves for the flats, corners and welds of the respective sections, nor the sum of the moments of the stress resultants about the principal axes are zero. This is quite a labourious procedure and entails a trial and error solution because inelastic strain may occur. However, assuming elastic behaviour, strain corrections for axial load and moment about the two axes are given in Table 2.13 where the strain correction for moments indicates that a tensile strain is to be applied for positive x or y values. Of course, the values of residual axial force and moment about the two axes to which these approximate corrections apply were determined taking the shape of the stress-strain curve into account.

2.3.1.3 Stub Columns

Stub column tests were conducted on the 3 HSS's introduced in this study, following the procedures of the SSRC (1976), to obtain the overall stress-strain relationship in compression. Electrical resistance strain gauges were mounted at mid-height on the center of each of the sides and demec points on a 254 mm gauge length were also mounted here on 2 opposite sides to provide both auxiliary and larger strain measurements. The stress-strain curves for the three tests are given in Fig. 2.11 There is no sharply defined yield stress and proportional limits ranging from 103 to 139 MPa are only about one-fourth to one-third of the yield strength determined by the 0.2% offset method. The overall shapes of the stress-strain curves (not considering local buckling for the moment) are similar to those obtained from the tension coupons, and both become non-linear at relatively low stress levels. This shape of curve is characteristic of heavily cold-worked steels and, in addition, the residual stresses play a role in the gradual yielding process. For the tension coupons, the variation of stresses through the thickness is seen to be significant as the tension coupons would have to straightened to be tested while for the stub columns both these stresses and the net longitudinal residual stresses have an effect.

It is noted that the HSS 254 x 152 x 6.4 failed by local buckling before the yield strength was reached. This is not unexpected as when the long side is in uniform compression (when the section was designated section 5), the section is classified as a

Class 4 section in bending as given in Table 2.4.

In Table 2.14 are compared the stress-strain characteristics for the three HSS's obtained from the stub column tests and the weighted averages obtained for the tension coupons. The values for section No. 1 determined previously by Kennedy and MacGregor (1984) are also given. The values obtained from any section by the two methods are in reasonable agreement. Differences could be expected in the proportional limit and the yield strength because of residual stress effects while differences in the modulus of elasticity and ultimate strength (ranging up to 4%) are a measure of experimental error.

In Table 2.15 coefficients A through F are given for fifth degree polynomials that describe the stub column load-strain curves for section numbers 2, 3 and 4, Thus

$$P_s = A + B\varepsilon + C\varepsilon^2 + D\varepsilon^3 + E\varepsilon^4 + F\varepsilon^5 \qquad [2.2]$$

The limiting values of strain to which these equations apply are also given in the table.

2.3.2 Concrete Tests

The ancillary tests carried out on the concrete from the single batch used for all flexural tests consisted of compression tests on standard 152 mm x 305 mm cylinders and split cylinder tests to determine the tensile strength. The cylinders were tested at 7 to 85 days after casting so that strengths were available at the time the main flexural tests were done. The cylinders were cast in steel molds and cured under polyethylene along with the composite flexural specimens.

2.3.2.1 Compression Cylinders

Table 2.16 gives the results of the concrete cylinder tests. Thirty-one compression cylinders were tested with 2 to 3 cylinders being tested at a time. Fig. 2.12 shows the variation of the compressive strength with time and the least squares best fit third-degree polynomial

$$f''_c = 26.86 + 0.413t - 0.00193t^2 - 0.805\times10^{-6}t^3 \quad [2.3]$$

for the test data. Strengths corresponding to [2.3] are also given in Table 2.16

The modulus of elasticity of the concrete was determined for each test in accordance with the CSA standard CAN3 A 23.2-9C-M90 (1990) by dividing the difference between the stress at 40% of the ultimate load and the stress at 0.005% strain (50 $\mu\varepsilon$) by the corresponding difference in strain. These values are given in Table 2.16 and plotted against experimental values of $\sqrt{f''_c}$ in Fig. 2.13. A least squares fit of a linear equation is

$$E_c = 3550\sqrt{f''_c} \quad [2.4]$$

This modulus is only 71% of the value prescribed in CSA Standard CAN3-A23.3-M84 (1984). In Fig. 2.14, is plotted the variation of the modulus of elasticity of the concrete with time. In addition to the experimental values, values determined from [2.4] and the measured cylinder strengths are plotted as is the line using [2.3] and [2.4] together.

2.3.2.2 Split Cylinders

Five split cylinders were tested in accordance with CSA Standard A23.2-13C-M90 (1990) to determine the split cylinder tensile strength. The experimental values are given in Table 2.16. Empirical values given by

[2.5] $$f_r = 0.52\sqrt{f''_c}$$

rather then the same equation with the usual coefficient of 0.60 are seen to be in good agreement with the test values.

2.3.2.3 Stress-strain Curve for Concrete

Fig. 2.15 shows an idealized uniaxial stress-strain curve for the concrete in compression that could be used to predict the unconfined compressive resistance based on the empirical data of this investigation. It consists of 3 parts:

(i) An elastic-brittle stress-strain relationship is assumed for concrete in tension. The modulus of elasticity in tension is set equal to the modulus of elasticity in compression, given by [2.4]. The maximum tensile stress is given by [2.5]

(ii) An elastic stress-strain relationship is assumed for concrete in compression up to a value of stress equal to 0.4 times the compressive strength, given by [2.3] with the modulus of elasticity determined from [2.4].

(iii) The inelastic compressive stress portion is described by the Todeschini et al (1964) stress-strain curve. The value ε_o is the strain at maximum compressive strength, f''_c. By constraining the Todeschini curve to pass through the point corresponding to a stress equal to $0.4f''_c$ and a strain of $0.4f''_c/E_c$, the value of ε_0 is equal to 4.79 times the strain at $0.4f''_c$, ε_p, as shown.

2.3.3 Composite Stub Column Tests

Composite stub column tests were conducted on the four hollow structural sections, 1, 2, 3 and 4 following the SSRC procedures with strain gauging as used in the steel stub column tests. Both ends of the stub column were grouted to provide a smooth surface for uniform bearing.

Stub column load-strain curves for the four sections are plotted in Figs. 2.16, 2.17 2.18 and 2.19 respectively. In each figure are also plotted: (i) the load-strain curve for the steel section alone (ii) the deduced load in the concrete, taken as the difference between the composite stub column load and the steel column load, (iii) the uniaxial unconfined concrete load based on the idealized stress-strain curve for the concrete using the maximum strength corresponding to the date of test from [2.4] (iv) the difference in the load in the concrete as deduced in (ii) and that based on the uniaxial stress-strain curve used in (iii).

For the steel sections alone (see section 2.3.1.3), the failure modes consisted of local buckling of the four HSS walls under essential hinged edge support with two buckles forming inward and two outward as the corners rotate as a hinge and offer little rotational resistance. As would be expected, the ultimate strain developed varies inversely as the width-thickness ratio and section 3 (Class 4) did not even reach the yield strain.

The behaviour of the composite stub column is largely controlled by the behaviour of the steel and therefore by the width-thickness ratio of the steel shell. Composite Section 2, with a 152 x 152 x 9.5 HSS having a low b/t ratio of 17.0, exhibited great ductility. The load in the concrete core finally exceeds that uniaxial unconfined compressive resistance and the concrete continues to carry significant load to strains as high as 0.012. Composite Section 4, with a 254 x 152 x 9.5 HSS having the next lowest b/t ratio of 28.0, also exhibited great ductility reaching a strain of 0.02. This could only be achieved, as the steel section alone buckled at a lesser strain, by interaction between the steel and concrete, with the concrete confined properly in a crushed state by the steel but preventing it from buckling inward. Composite Section 1, with a 152 x 152 x 4.8 HSS having a b/t ratio of 34.4, and composite Section 3, with a 254 x 152 x 6.4 HSS having a b/t ratio of 41.1, both failed in a brittle mode with a rapid decrease in load from the maximum load when the steel shell buckled followed quickly by the crushing of the concrete.

Therefore the only composite section to maintain its maximum load while straining significantly was the square section with the low b/t ratio. Rectangular Section 4 (with a b/t ratio corresponding to a Class 2 section) had significant ductility but lost about 25% of its capacity before final failure. The "thin" sections, Section 1 and 3 failed in a brittle manner.

In Table 2.17, 2.18, 2.19 and 2.20 are given coefficients that describe fifth degree polynomials fitted to the load-strain curve for the four sections tested.

Table 2.1 Flexural Test Specimens

Specimen	HSS		Test Dimensions, mm				a/d	b/t	Concrete	
	Number	Designation	a	m	L	d			Age at Testing, Days	Strength, f''_c
SB1	1	152 x 152 x 4.8	500	1000	2000	152	3.3	31.7	-	-
SB2	2	152 x 152 x 9.5	500	1000	2000	152	3.3	16.0	-	-
SB3	3	254 x 152 x 6.4	500	1000	2000	254	2.0	23.8	-	-
SB4	4	254 x 152 x 9.5	500	1000	2000	254	2.0	16.0	-	-
SB5	5	152 x 254 x 6.4	500	1000	2000	152	3.3	39.7	-	-
CB12	1	152 x 152 x 4.8	235	1305	1975	152	1.54	31.7	79	47.0
CB13	1	152 x 152 x 4.8	463	1305	2430	152	3.03	31.7	51	42.8
CB15	1	152 x 152 x 4.8	768	1305	3040	152	5.04	31.7	44	41.2
CB22	2	152 x 152 x 9.5	236	1305	1976	152	1.54	16.0	78	46.9
CB31	3	254 x 152 x 6.4	261	1508	2231	254	1.03	23.8	76	46.7
CB33	3	254 x 152 x 6.4	766	1508	3243	254	3.03	23.8	64	45.2
CB35	3	254 x 152 x 6.4	1276	1508	4260	254	5.03	23.8	59	44.3
CB41	4	254 x 152 x 9.5	261	1508	2231	254	1.03	16.0	71	46.2
CB45	4	254 x 152 x 9.5	1276	1508	4260	254	5.03	16.0	56	43.8
CB52	5	152 x 254 x 6.4	235	1305	197	152	1.55	39.7	80	47.1
CB53	5	152 x 254 x 6.4	463	1305	2432	152	3.05	39.7	48	42.1
CB55	5	152 x 254 x 6.4	768	1305	3041	152	5.05	39.7	41	40.5

Table 2.2 Manufacturer and Chemical Composition of HSS

Section Designation	Manufacturer or Standard	Chemical Composition, %				
		C	Mn	P	S	Si
152 x 152 x 4.8	Standard Tube Canada Ltd.	0.18	0.82	0.009	0.016	-
152 x 152 x 9.5	Prudential Steel Ltd.	0.15	1.05	0.011	0.011	0.026
254 x 152 x 6.4	Prudential Steel Ltd.	0.14	0.98	0.013	0.015	0.015
254 x 152 x 9.5	Prudential Steel Ltd.	0.15	0.92	0.012	0.011	0.029
	CAN/CSA-G40.21 -M84 Grade 350W	≤ 0.23	0.50--1.50	≤ 0.04	≤ 0.05	≤ 0.40

Table 2.3 Measured Dimensions of HSS's

Section	Number	Dimension	Number of Measurements	Mean Value, mm	C.O.V.	Measured / Specified	Tolerance Limit, mm (CAN/CSA G40.20-M)
152 x 152 x 4.8	1	thickness	344	4.43	0.0099	0.927	4.30--5.26
		width (depth)	64	152.4	0.0016	1.000	150.9--153.9
152 x 152 x 9.5	2	thickness	48	8.95	0.0132	0.939	8.58--10.48
		width (depth)	64	152.4	0.0016	1.000	150.9--153.9
254 x 152 x 6.4	3,5	thickness	120	6.17	0.0119	0.972	5.72--6.99
		width	72	253.4	0.0011	0.998	251.5--256.5
		depth	72	152.0	0.0018	0.997	150.1--154.7
254 x 152 x 9.5	4	thickness	60	9.04	0.0109	0.949	8.58--10.48
		width	40	253.0	0.0008	0.996	251.5--256.5
		depth	32	152.2	0.0013	0.999	150.1--154.7

Table 2.4 Classification of Sections

Section	Fy	Class Limits			b/t		Section Class	
		1	2	3	Nominal	Actual	Nominal	Actual
		$420/\sqrt{F_y}$	$525/\sqrt{F_y}$	$670/\sqrt{F_y}$				
	350	22.4	28.1	35.8				
1	389	21.3	26.6	34.0	27.8	30.4	2	3
2	432	20.2	25.3	32.2	12.0	13.0	1	1
3	377	21.6	27.0	34.5	20.0	20.6	1	1
4	394	21.1	26.4	33.8	12.0	12.8	1	1
5	377	21.6	27.0	34.5	36.0	37.1	4	4

Table 2.5 Cross Sectional Properties of HSS's

Section		A (mm^2)	I (mm^4)	Z (mm^3)	S (mm^3)
Designation	Number				
152 x 152 x 4.8	1	2571	9.29×10^6	142.2×10^3	121.6×10^3
152 x 152 x 9.5	2	4930	16.54×10^6	261.3×10^3	217.1×10^3
254 x 152 x 6.4	3	4735	41.51×10^6	398.7×10^3	327.7×10^3
254 x 152 x 9.5	4	6788	57.20×10^6	558.7×10^3	452.2×10^3
152 x 254 x 6.4	5	4735	18.89×10^6	280.8×10^3	248.5×10^3

Table 2.6 Comparison of Cross Sectional Areas

Method	Area of Section, mm^2			
	1	2	3	4
Assuming $r = 2t$	2571	4930	4735	6788
Measured r	——	4948	4752	6791
Volumetric	2570	4967	4727	6851
Handbook	2760	5210	4900	7150
Tolerance	2663--3036	5027--5731	4728--5390	6900--7865

Table 2.7 Parameters of Stress-strain Curves for Tension Coupons, Section 2

Section		Coupon		$E \times 10^{-3}$	σ_p	ε_p	σ_y	ε_y	σ_u
Designation	No.	No.	Location	MPa	MPa	$\mu\varepsilon$	MPa	$\mu\varepsilon$	MPa
152 x 152 x 9.5	2	2	flat	192.9	64	326	445	4320	475
		4	flat	205.6	64	314	438	4140	466
		6	flat	209.6	117	557	521	4460	532
		8	flat	206.2	63	306	420	4060	455
		12	flat	210.4	168	582	---	----	523
		μ		204.9			456	4245	490
		V		0.031			0.10	0.042	0.07
		3	corner	210.3	146	697	529	4480	552
		7	corner	194.0	72	374	---	---	456
		11	corner	206.0	72	355	423	4060	455
		15	corner	208.9	117	565	518	4480	561
		μ		204.8			490	4340	506
		V		0.036			0.12	0.056	0.12
		1	weld	216.7	113	528	507	4340	561
		Overall mean		206.1			475.1	4295	
		V		0.036			0.100	0.042	

Table 2.8 Parameters of Stress-strain Curves for Tension Coupons, Section 3

Section		Coupon		$E \times 10^{-3}$	σ_p	ε_p	σ_y	ε_y	σ_u
Designation	No.	No.	Location	MPa	MPa	$\mu\varepsilon$	MPa	$\mu\varepsilon$	MPa
254 x 152 x 6.4	3	3	flat	208.5	93	451	493	4370	517
		5	flat	203.9	91	391	367	3820	405
		6	flat	209.1	106	515	534	4550	543
		7	flat	207.7	116	566	420	4020	427
		9	flat	207.8	103	502	422	4030	430
		11	flat	208.9	129	616	437	4090	444
		12	flat	210.8	143	687	497	4320	517
		15	flat	209.3	153	731	500	4380	552
		17	flat	206.1	105	510	419	4030	434
		μ		208.0			454	4179	474
		V		0.010			0.12	0.056	0.12
		4	corner	207.5	91	441	379	3840	440
		1	weld	215.4	119	553	469	4210	521
		Overall mean		208.6			448.8	4151	
		V		0.014			0.119	0.056	

Table 2.9 Parameters of Stress-strain Curves for Tension Coupons, Section 4

Section		Coupon		$E \times 10^{-3}$	σ_p	ε_p	σ_y	ε_y	σ_u
Designation	No.	No.	Location	MPa	MPa	$\mu\varepsilon$	MPa	$\mu\varepsilon$	MPa
254 x 152 x 9.5	4	2	flat	195.1	70	366	419	4110	431
		3	flat	207.5	154	748	445	4130	466
		6	flat	207.1	124	605	457	4200	464
		7	flat	199.5	62	305	419	4080	429
		9	flat	184.7	90	482	385	4040	410
		12	flat	207.5	133	649	469	4240	481
		13	flat	-----	---	---	---	----	419
		15	flat	208.5	139	685	438	4110	450
		μ		201.4			433	4130	444
		V		0.044			0.07	0.017	0.06
		4	corner	193.4	44	228	405	4320	416
		1	weld	-----	172	721	---	----	530
		Overall mean		200.4			429.6	4145	
		V		0.044			0.065	0.022	

Table 2.10 Stress-strain Curve Coefficients, Section 2

Portion	Coefficient	Strain Range, $\mu\varepsilon$				
		0--958	958--2015	2015--4435	4435--20601	20601--33603
Flat	A	-0.72207	4.136×10^{3}	726.15	682.35	-34.115×10^{3}
	B	0.20071×10^{6}	-15.237×10^{6}	-0.65526×10^{6}	-7.6923×10^{3}	7.1764×10^{6}
	C	80.448×10^{6}	22.565×10^{9}	0.41907×10^{9}	14.567×10^{6}	-0.58409×10^{9}
	D	-0.33438×10^{12}	-16.147×10^{12}	-0.12401×10^{12}	-1.3750×10^{9}	23.388×10^{9}
	E	0.45683×10^{15}	5.6441×10^{15}	19.209×10^{12}	64.113×10^{9}	-0.46125×10^{12}
	F	-0.21658×10^{18}	-0.77141×10^{18}	-1.2500×10^{15}	-1.1446×10^{12}	3.5881×10^{12}
		0--726	726--2013	2013--4695	4695--15984	15984--107907
Corner	A	10.635	342.60	-2.086×10^{3}	939.89	445.97
	B	96.830×10^{3}	-1.1567×10^{6}	3.3949×10^{6}	-0.28773×10^{6}	7.9586×10^{3}
	C	0.88735×10^{9}	2.1570×10^{9}	-1.9098×10^{9}	62.092×10^{6}	-0.31559×10^{6}
	D	-2.9269×10^{12}	-1.7012×10^{12}	0.54696×10^{12}	-6.0927×10^{9}	5.5389×10^{6}
	E	4.1251×10^{15}	0.65517×10^{15}	-78.375×10^{12}	0.27960×10^{12}	-45.003×10^{6}
	F	-2.1122×10^{18}	-99.859×10^{15}	4.4573×10^{15}	-4.8516×10^{12}	0.13696×10^{9}
		0--4325	4325--18422	18422--50726		
Weld	A	-5.7566	38.468	564.35		
	B	0.24942×10^{6}	0.22939×10^{6}	-7.0309×10^{3}		
	C	-44.954×10^{6}	-40.933×10^{6}	0.77309×10^{6}		
	D	8.3332×10^{9}	3.4668×10^{9}	-33.805×10^{9}		
	E	-1.7827×10^{12}	-0.13918×10^{12}	0.65201×10^{9}		
	F	0.15087×10^{15}	2.1365×10^{12}	-4.5855×10^{9}		

Table 2.11 Stress-strain Curve Coefficients, Section 3

Portion	Coefficient	Strain Range, $\mu\varepsilon$				
		0--1022	1022--2500	2500--3918	3918--19651	19651--32639
Flat	A	-0.71963	-1.1887×10^{3}	3.6905×10^{3}	678.92	63.045×10^{3}
	B	0.21015×10^{6}	3.9585×10^{6}	-5.0981×10^{6}	-0.12325×10^{6}	-12.044×10^{6}
	C	-19.453×10^{6}	-4.6215×10^{9}	3.0145×10^{9}	25.793×10^{6}	0.92341×10^{9}
	D	72.747×10^{9}	2.7822×10^{12}	-0.85788×10^{12}	-2.5341×10^{9}	-35.264×10^{9}
	E	-0.11608×10^{15}	-0.82652×10^{15}	0.11894×10^{15}	0.11882×10^{12}	0.67063×10^{12}
	F	0.56722×10^{15}	96.137×10^{15}	-6.4594×10^{15}	-2.1292×10^{12}	-5.0790×10^{12}
		0--4747	4747--36339			
Corner	A	-0.57897	376.75			
	B	0.21552×10^{6}	4.8282×10^{3}			
	C	-18.974×10^{6}	-0.20582×10^{6}			
	D	-6.1290×10^{9}	5.5056×10^{6}			
	E	0.57425×10^{12}	-76.811×10^{6}			
	F	65.217×10^{12}	0.4538×10^{9}			
		0--3315	3315--66696			
Weld	A	-84.835x10	428.7			
	B	0.20306×10^{-3}	5.4342×10^{3}			
	C	46.503×10^{6}	-0.15492×10^{6}			
	D	-40.505×10^{6}	3.756×10^{6}			
	E	7.5912×10^{9}	-57.399×10^{6}			
	F	-0.44563×10^{12} 15	0.34680×10^{9}			

Table 2.12 Stress-strain Curve Coefficients, Section 4

Portion	Coefficient	Strain Range, $\mu\varepsilon$				
		0--1082	1082--2201	2201--5290	5290--14561	14561--25858
Flat	A	-1.1092	-2.9507×10^{3}	1.2188×10^{3}	-3.3065×10^{3}	4.6046×10^{3}
	B	0.20841×10^{6}	10.151×10^{6}	-1.3202×10^{6}	2.0850×10^{6}	-0.79391×10^{6}
	C	-9.5102×10^{6}	-13.197×10^{9}	0.75453×10^{9}	-0.44825×10^{9}	49.292×10^{6}
	D	-62.552×10^{12}	8.5953×10^{12}	-0.20289×10^{12}	46.607×10^{9}	-0.69624×10^{9}
	E	0.11365×10^{15}	-2.7566×10^{15}	26.448×10^{12}	-2.3502×10^{12}	-32.010×10^{9}
	F	-0.58701×10^{15}	-0.34731×10^{18}	-1.3513×10^{15}	46.156×10^{12}	0.84691×10^{12}
		0--4192	4192--19269			
Corner	A	2.0946	371.04			
	B	0.18256×10^{6}	12.697×10^{3}			
	C	-19.313×10^{6}	-2.3330×10^{6}			
	D	-0.95333×10^{9}	0.22328×10^{9}			
	E	53.070×10^{9}	9.7535×10^{9}			
	F	17.091×10^{12}	0.15553×10^{12}			
		0--7995	7995--94579			
Weld	A	-5.9080	500.01			
	B	0.21552×10^{6}	2.6069×10^{3}			
	C	-18.974×10^{6}	-64.306×10^{6}			
	D	-6.1290×10^{9}	0.78612×10^{6}			
	E	0.57425×10^{9}	-4.3910×10^{6}			
	F	65.217×10^{12}	7.8733×10^{9}			

Table 2.13 Elastic Correction to Residual Strain

Section		Maximum Residual Strain, $\mu\varepsilon$				Strain Correction, $\mu\varepsilon$		
Designation	Number	Longitudinal		Through-thickness		Axial	Mx(max)	My(max)
				Outside	Inside			
152 x 152 x 9.5	2	1784	-849	3286	-3313	-650	139	167
254 x 152 x 6.4	3	1100	-1053	3634	-1977	-361	8	143
254 x 152 x 9.5	4	1433	-483	3174	-3427	-270	52	139

Table 2.14 Average Stress-strain Characteristics for HSS's

HSS		Tension Coupons (Weighted Average)				Stub Column			
Designation	Number	E MPa x 10^3	σ_p MPa	σ_y MPa	σ_u MPa	E MPa x 10^3	σ_p MPa	σ_y MPa	σ_u MPa
152 x 152 x 4.8	1	212.0	177	383	466	210.7	175	389	---
152 x 152 x 9.5	2	205.4	97.7	467	489	210.8	139	432	508
254 x 152 x 6.4	3	208.4	110.5	431	467	207.4	129	377	---
254 x 152 x 9.5	4	200.0	97.8	425	433	208.0	103	394	426

Table 2.15 Coefficients Describing Steel Stub Column Load-strain Curve

Section	Coefficients						Maximum Strain, $\mu\varepsilon$
	A	B	C	D	E	F	
152 x 152 x 9.5	1.8397	0.22462×10^{6}	-44.845×10^{6}	4.9828×10^{9}	-0.31847×10^{12}	9.4893×10^{12}	0-8790
	2004.6	-0.61869×10^{6}	99.236×10^{6}	-7.8140×10^{9}	0.30340×10^{12}	-4.6524×10^{12}	8790-19200
254 x 152 x 6.4	3.3968	0.98384×10^{6}	0.14663×10^{9}	-0.32251×10^{12}	0.12486×10^{15}	-16.073×10^{15}	3400
254 x 152 x 9.5	9.5432	1.5925×10^{6}	-45.844×10^{9}	10.182×10^{12}	-0.14528×10^{12}	85.238×10^{15}	6350

Table 2.16 Stress-strain Data for Concrete

Time t, day	Compressive Strength f''_c, MPa		Modulus of Elasticity E_c, MPa x 10^3		Tensile Strength f_r, MPa	
	Experimental	Empirical*	Experimental	$3550\sqrt{f''_c}$	Experimental	$0.52\sqrt{f''_c}$ **
7	29.8	29.7	18.9	19.4		
7	28.4		18.5	18.9		
14	33.2	32.3	21.3	20.4		
14	32.5		19.6	20.2		
21	34.0	34.7	20.8	20.7		
21	35.9		20.1	21.3		
28	39.2	36.9	21.9	22.2	3.10	3.16
28	35.8		21.6	21.2		
28	37.5		21.0	21.8		
35	39.0	38.9	22.1	22.2		
35	40.4		22.0	22.5		
35	39.1		21.6	22.2		
42	38.8	40.7	22.9	22.1	3.11	3.32
42	40.1		23.1	22.5		
42	40.8		22.1	22.7		
49	44.7	42.4	23.1	23.7		
49	42.8		23.5	23.2		
49	41.3		21.9	22.8		
56	44.2	43.8	22.3	23.6	3.26	3.44
56	44.3		22.6	23.6		
56	44.4		22.5	23.6		
63	44.4	45.0	23.0	23.7		
63	45.9		23.3	24.1		
63	43.8		23.9	23.5		
70	44.9	46.0	24.2	23.8	3.66	3.53
70	47.1		25.1	24.4		
77	47.5	46.9	26.6	24.5		
77	48.4		26.4	24.7		
77	46.6		23.7	24.2		
85	48.0	47.5	26.6	24.6	3.86	3.59
85	46.2		24.9	24.1		

Notes: *. $f''_c = 26.86 + 0.4134\,t - 0.00193\,t^2 - 0.805 \times 10^{-6}\,t^3$

**. $f_r = 0.52\sqrt{f''_c}$, where f''_c is based on the empirical Equation 2.3

Table 2.17 Coefficients Describing Load-strain Curve for Composite Stub Column, Section 1

Coefficients	Strain Range $\times 10^{-6}$
	0—3482
A	9.3854
B	1.0610×10^{6}
C	-0.2848×10^{9}
D	71.893×10^{9}
E	-3.978×10^{12}
F	-1.6391×10^{15}

Table 2.18 Coefficients Describing Load-strain Curve for Composite Stub Column, Section 2

Coefficients	Strain Range $\times 10^{-6}$
	0—12506
A	93.474
B	1.3178×10^{6}
C	-0.17600×10^{9}
D	5.5764×10^{9}
E	0.50673×10^{12}
F	-30.367×10^{12}

Table 2.19 Coefficients Describing Load-strain Curve for Composite Stub Column, Section 3

Coefficients	Strain Range $\times 10^{-6}$				
	0—955	955—1943	1943—3518	3518—5834	5834—22851
A	-13.953	-30.306×10	4.5644×10^{3}	23.490×10^{3}	0.18649×10^{6}
B	0.80054×10^{6}	2.7269×10^{6}	-7.2537×10^{6}	-23.563×10^{6}	-0.12778×10^{9}
C	1.9278×10^{9}	-4.7854×10^{9}	5.6287×10^{9}	9.8263×10^{9}	35.128×10^{9}
D	-4.7258×10^{12}	4.6758×10^{12}	-2.0144×10^{12}	-1.9719×10^{12}	-4.7839×10^{12}
E	4.2035×10^{15}	-2.1096×10^{15}	0.35375×10^{15}	0.19327×10^{15}	0.32349×10^{15}
F	-1.3628×10^{18}	0.35647×10^{18}	-24.548×10^{15}	-7.3148×10^{15}	-8.6956×10^{15}

Table 2.20 Coefficients Describing Load-strain Curve for Composite Stub Column, Section 4

Coefficients	Strain Range $\times 10^{-6}$				
	0—677	677—1394	1394—11152	11152—12410	12410—20581
A	-42.941	9.1496×10^{3}	-42.805	0.32595×10^{9}	-40.207×10^{3}
B	7.6391×10^{6}	-38.139×10^{6}	-3.3923×10^{6}	-0.13526×10^{12}	14.812×10^{6}
C	-14.935×10^{9}	75.833×10^{9}	-1.0318×10^{9}	22.444×10^{12}	-1.9716×10^{9}
D	15.932×10^{12}	-71.168×10^{12}	0.14938×10^{12}	-1.8616×10^{15}	0.12855×10^{12}
E	-2.1768×10^{15}	32.922×10^{15}	-10.458×10^{12}	77.175×10^{15}	-4.1266×10^{12}
F	-5.0906×10^{18}	-6.0436×10^{18}	0.28261×10^{15}	-1.2794×10^{18}	52.296×10^{12}

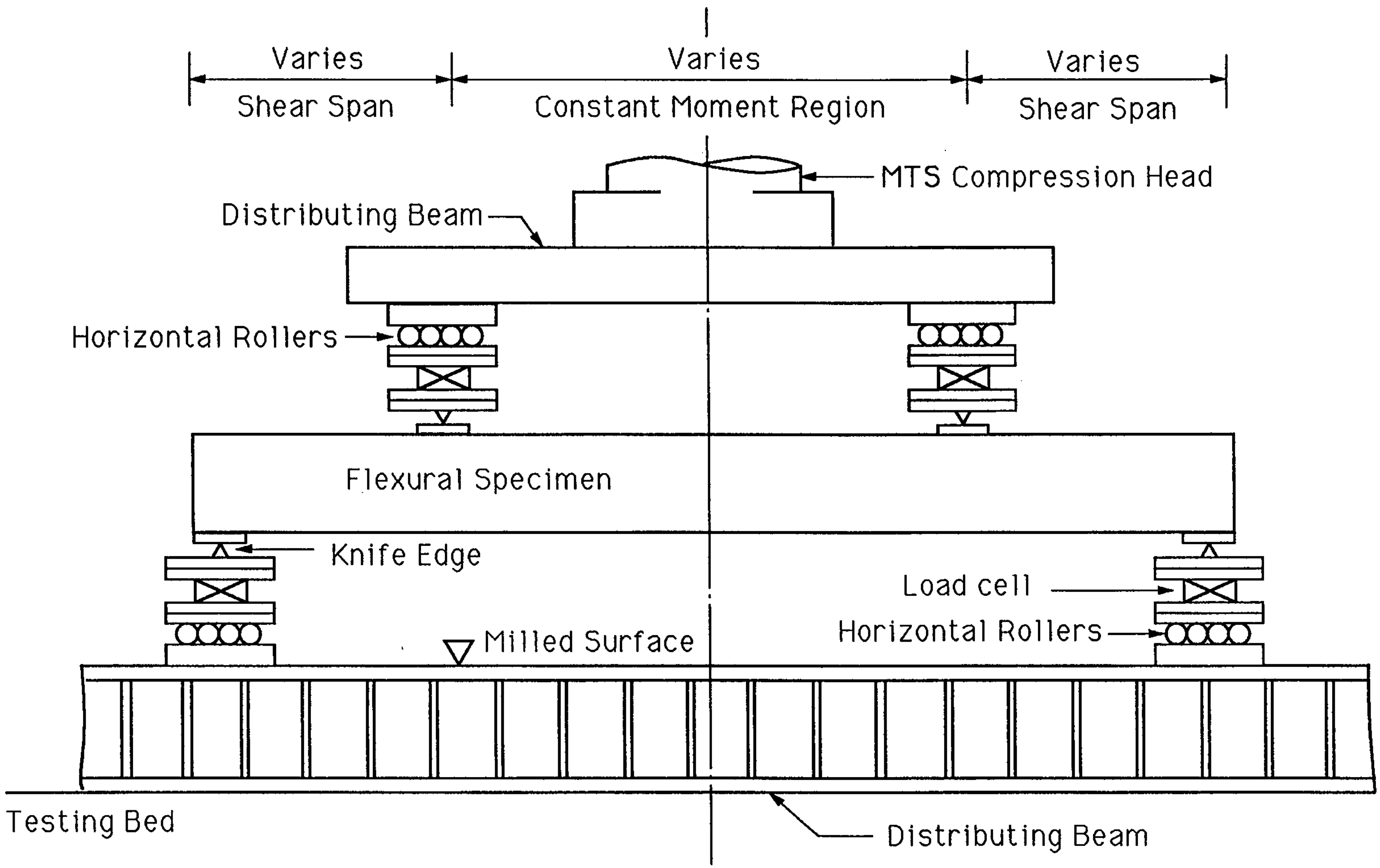

Figure 2.1 Schematic Diagram of Test Set-up

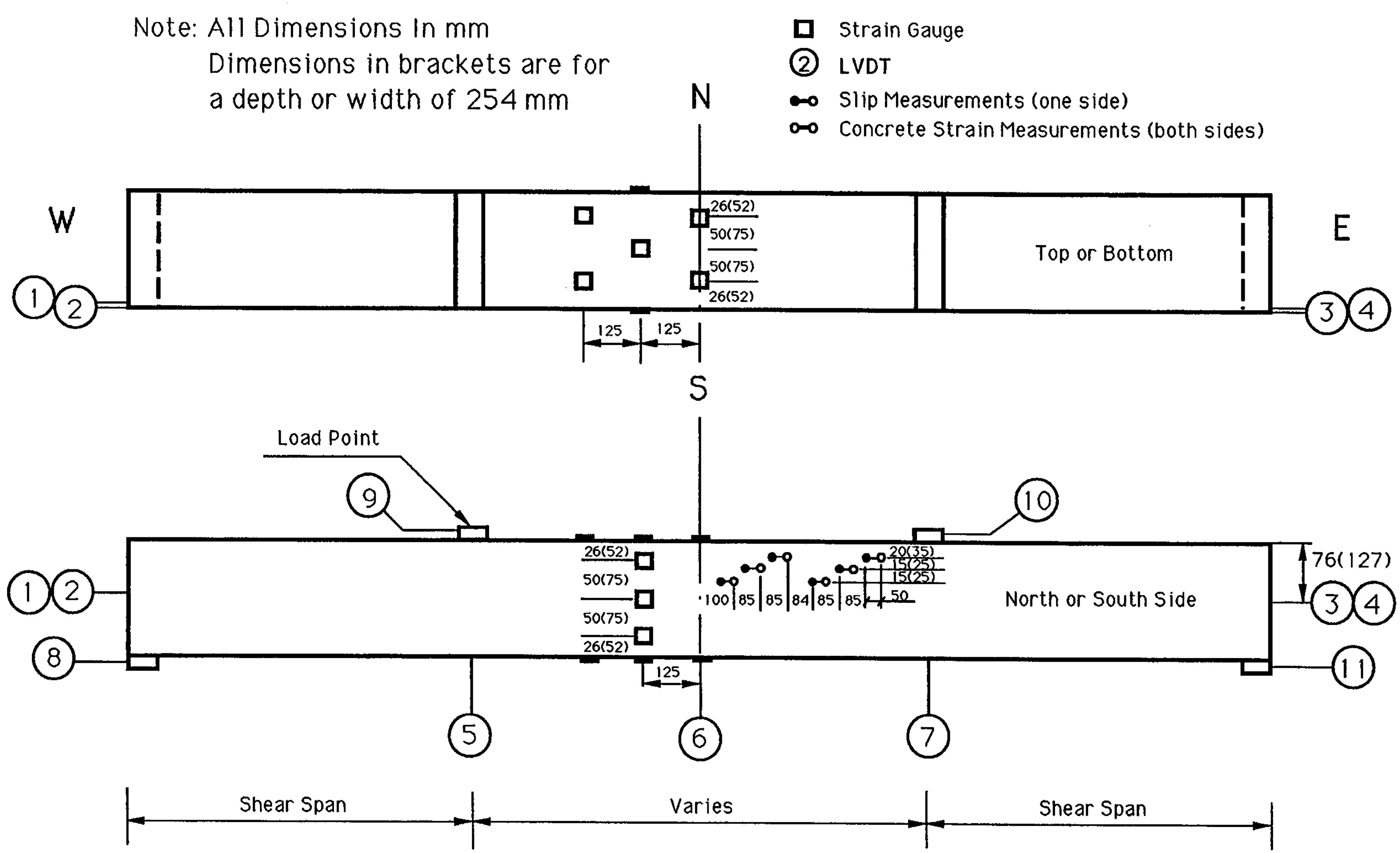

Fig. 2.2 Schematic Digram of Instrumentation

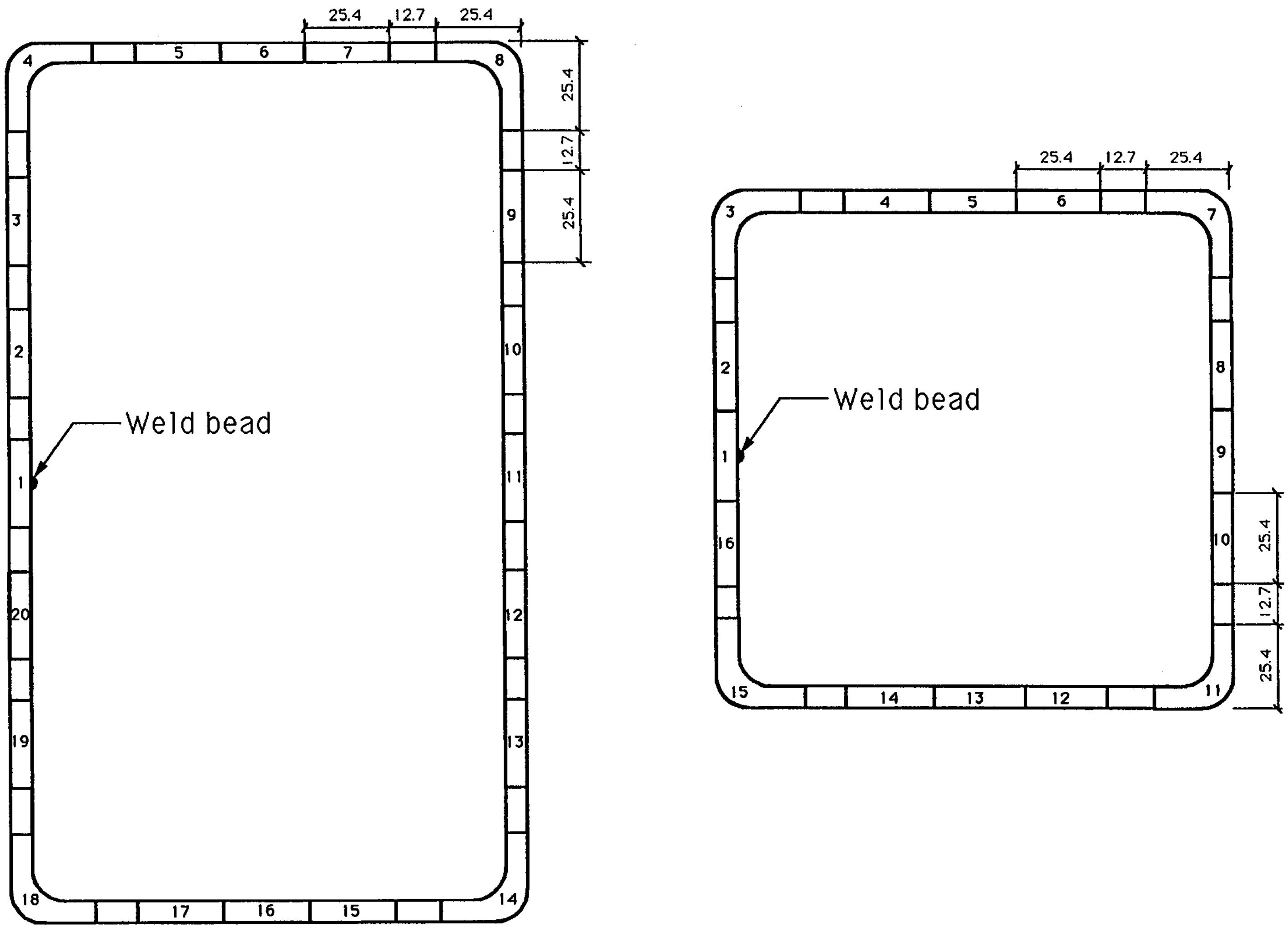

Fig. 2.3 Tension Coupons

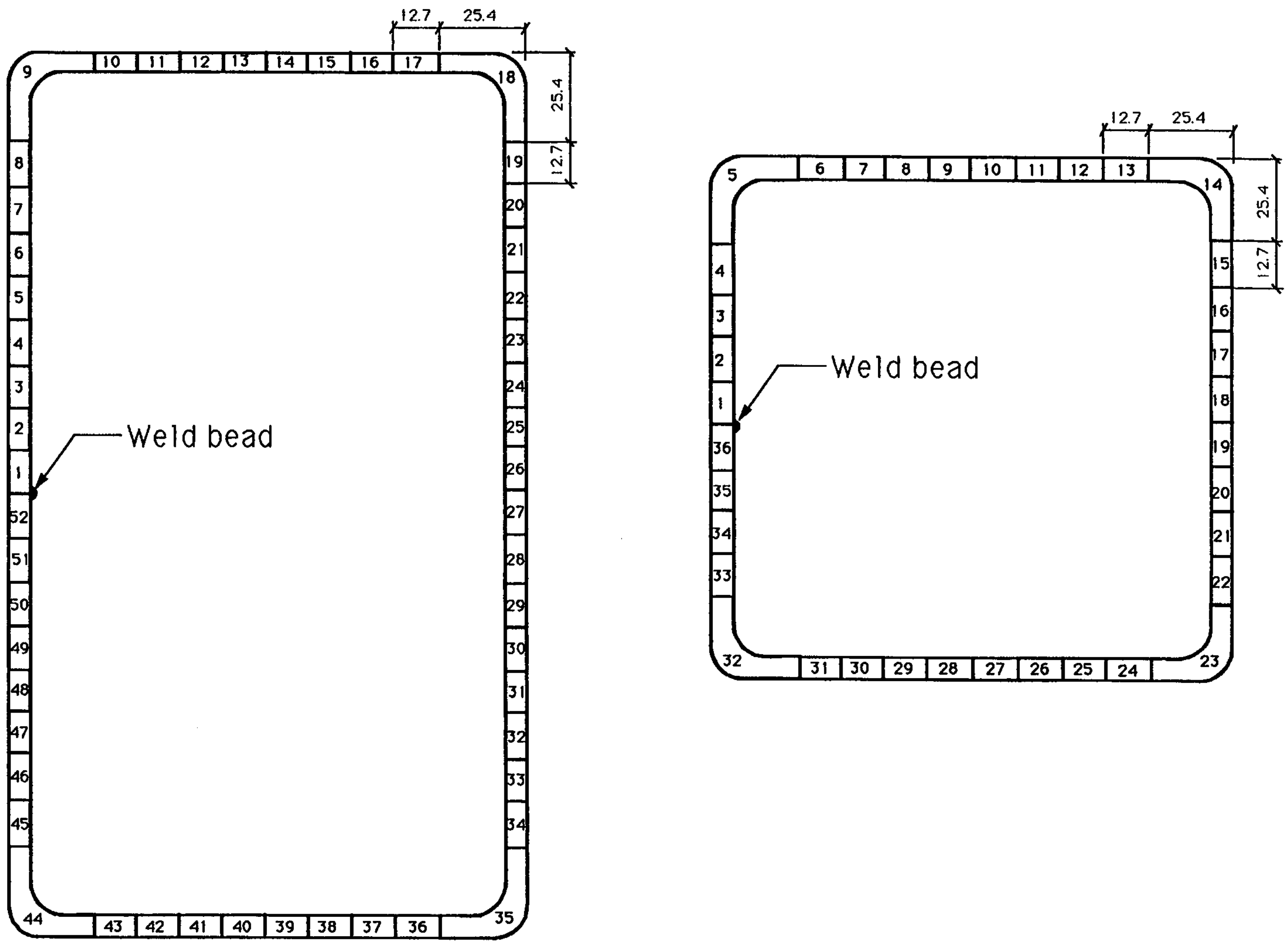

Fig. 2.4 Residual Strain Coupons

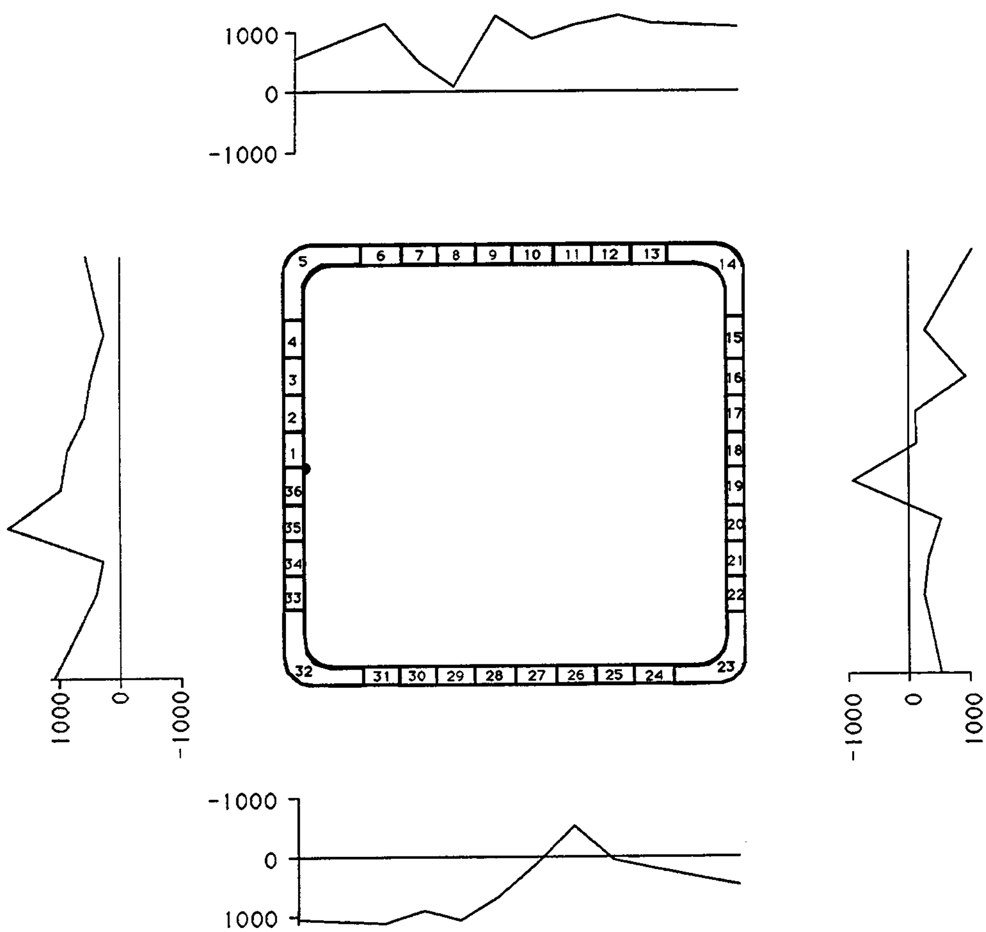

Figure 2.5 Longitudinal Residual Strain Distribution, Section 2

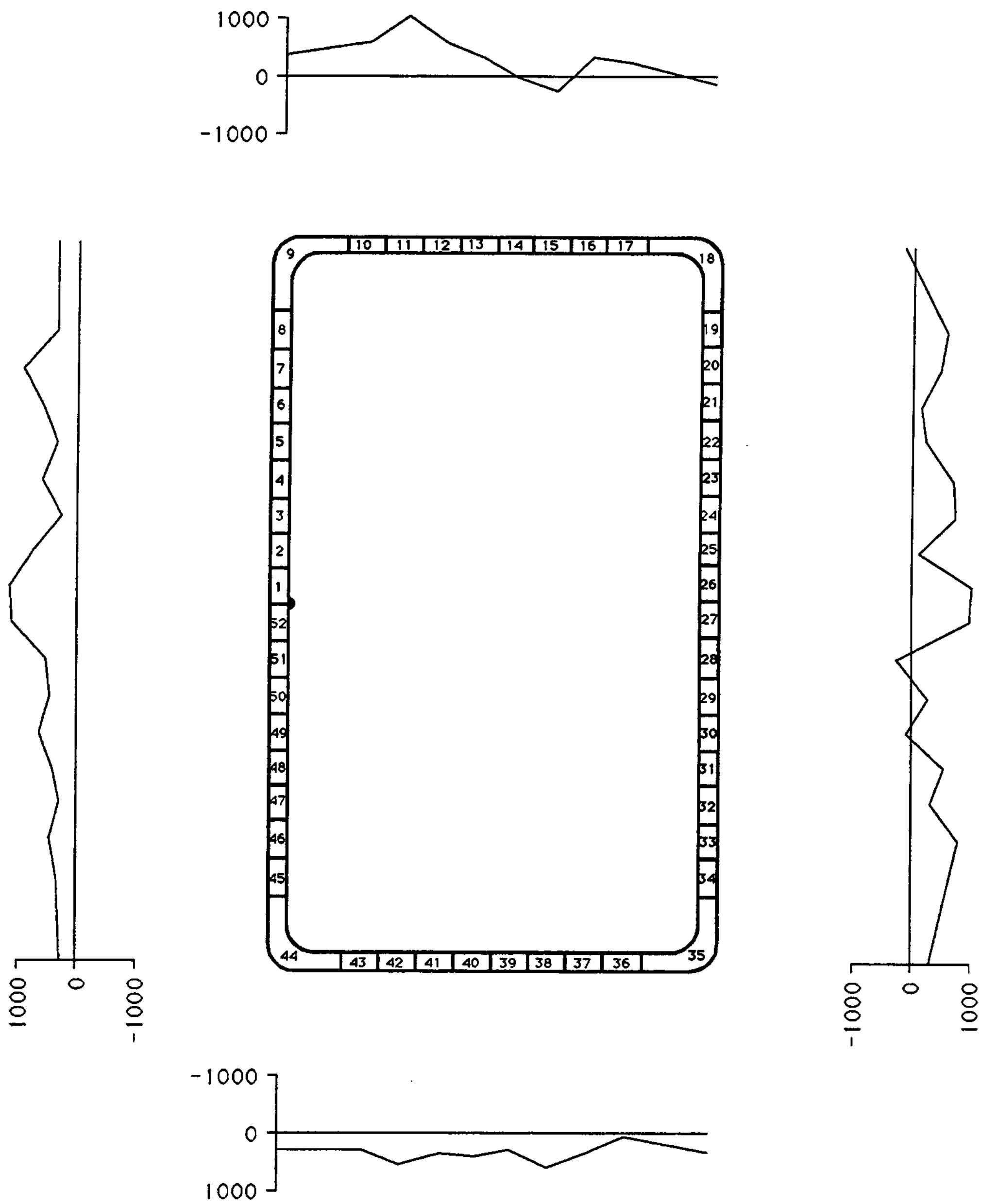

Figure 2.6 Longitudinal Residual Strain Distribution, Section 3

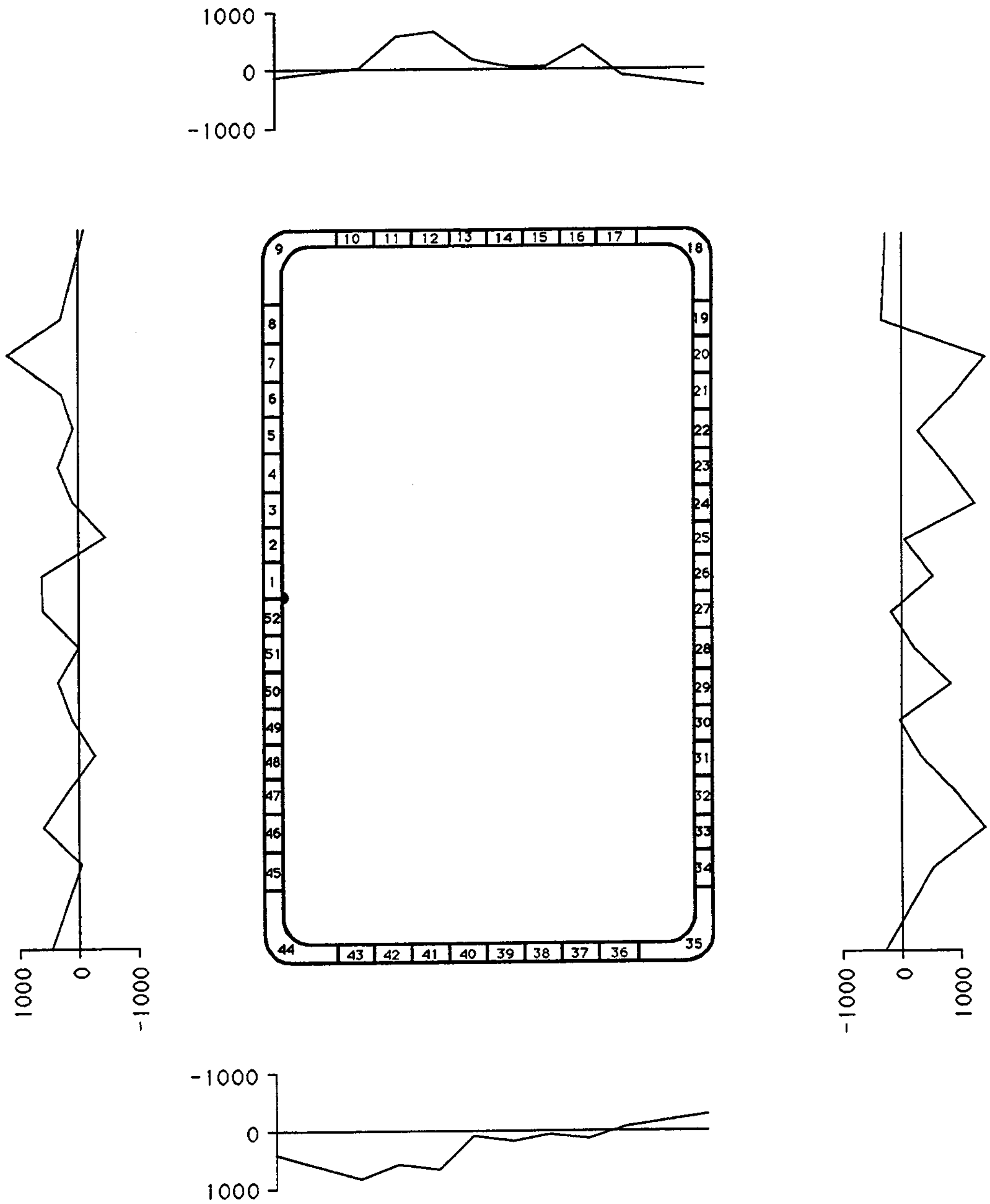

Figure 2.7 Longitudinal Residual Strain Distribution, Section 4

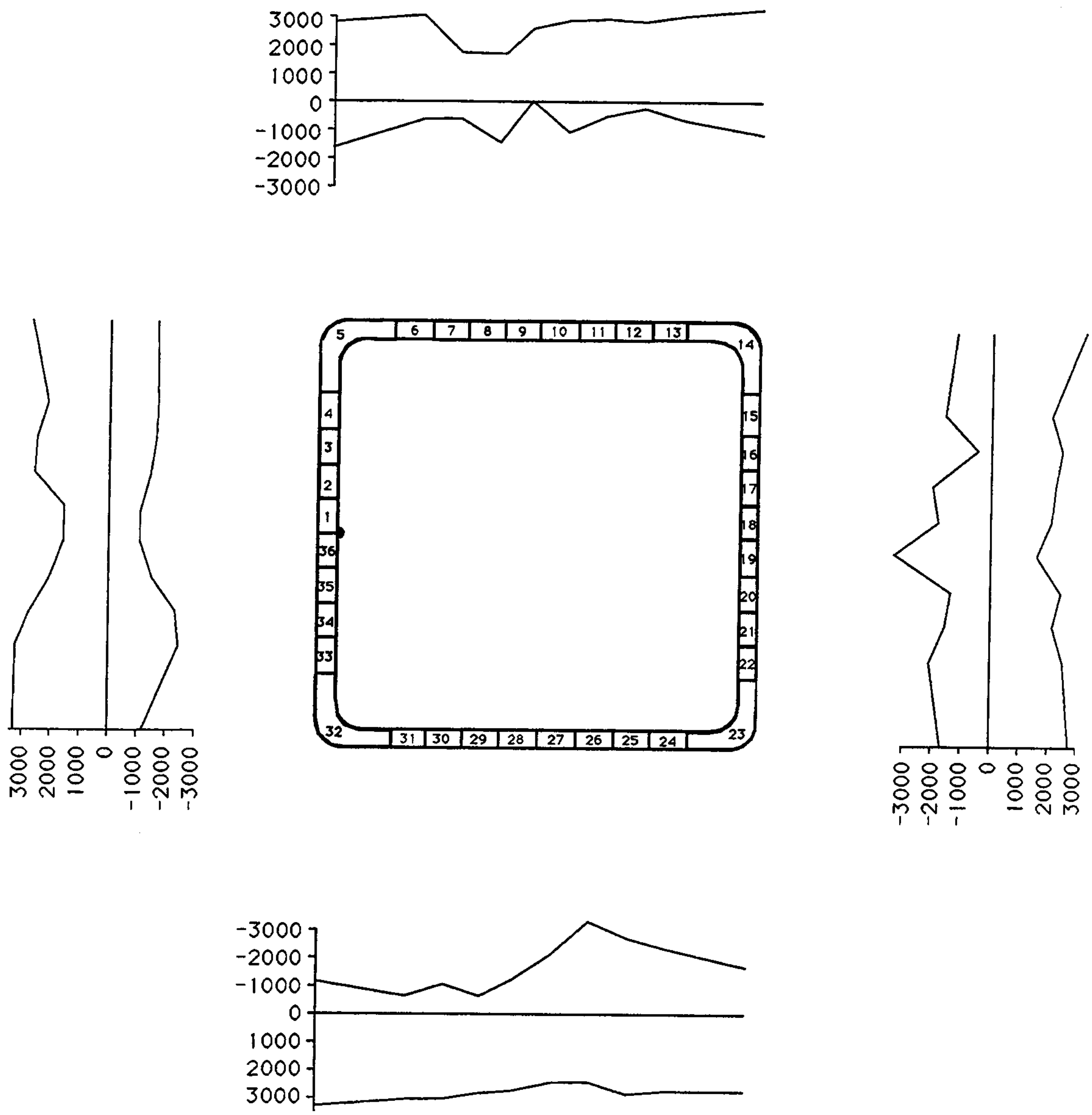

Figure 2.8 Through-thickness Residual Strain Distribution, Section 2

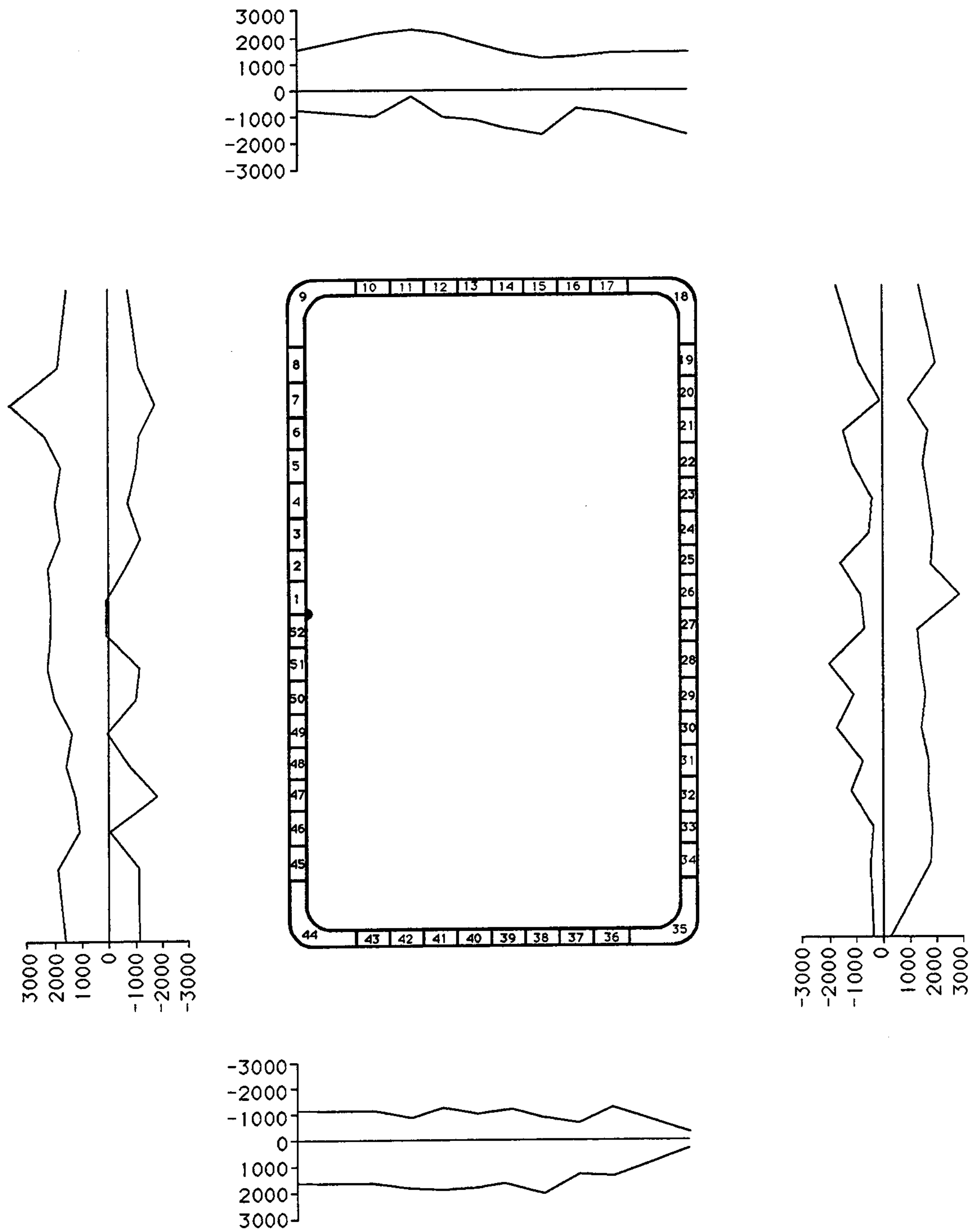

Figure 2.9 Through-thickness Residual Strain Distribution, Section 3

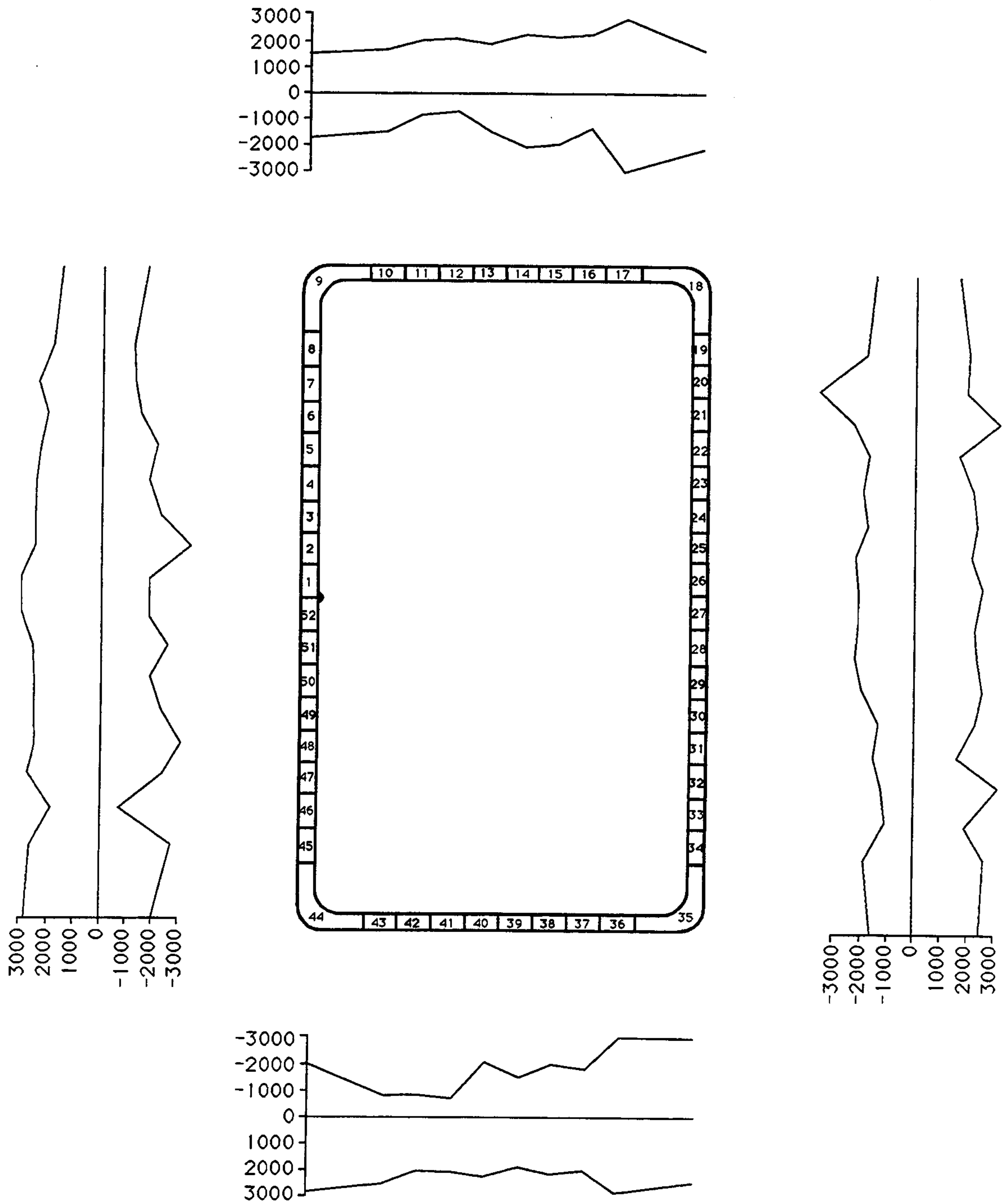

Figure 2.10 Through-thickness Residual Strain Distribution, Section 4

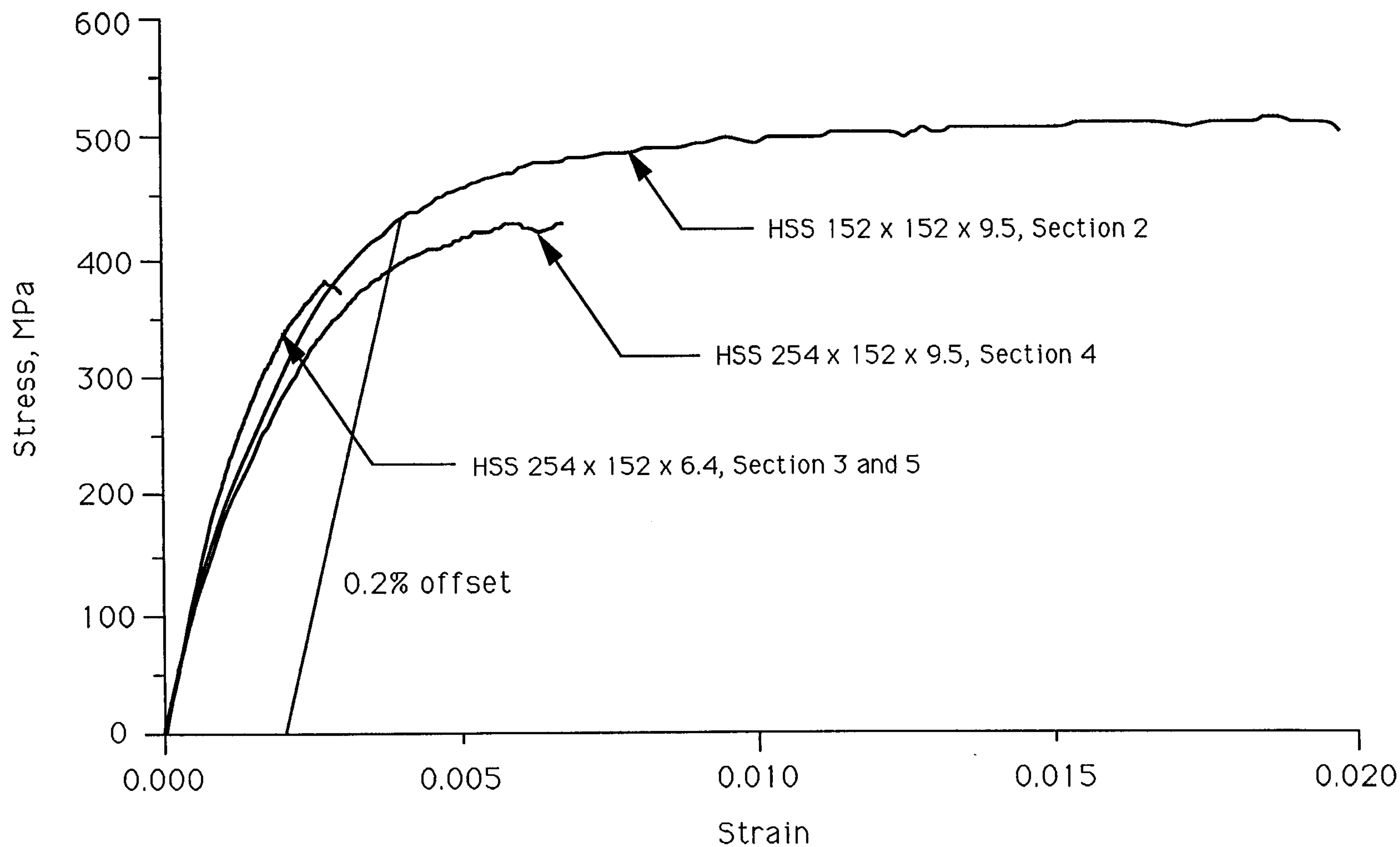

Fig. 2.11 Stress-strain Curve, Steel Stub Column

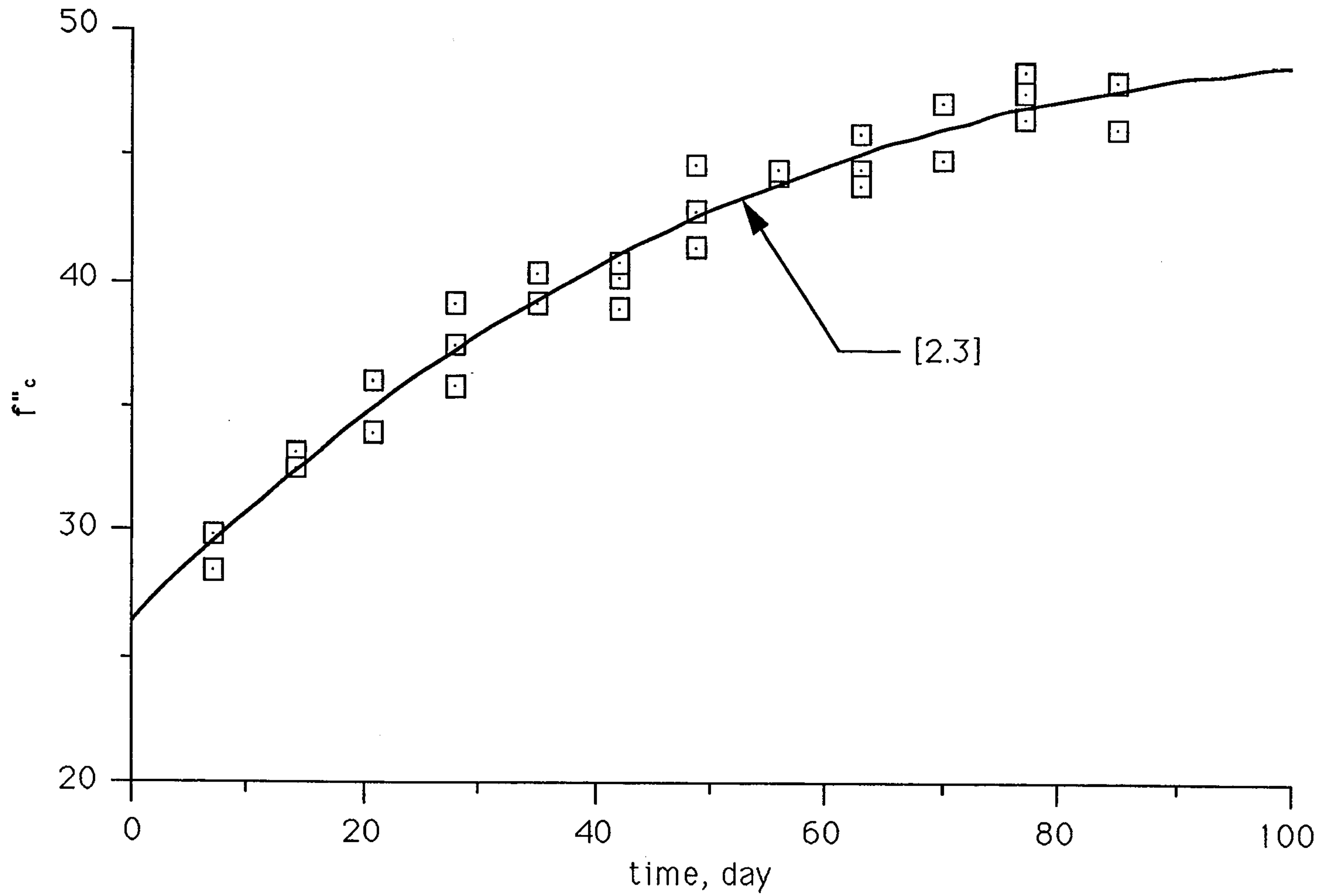

Fig. 2.12 Concrete Strength with Time

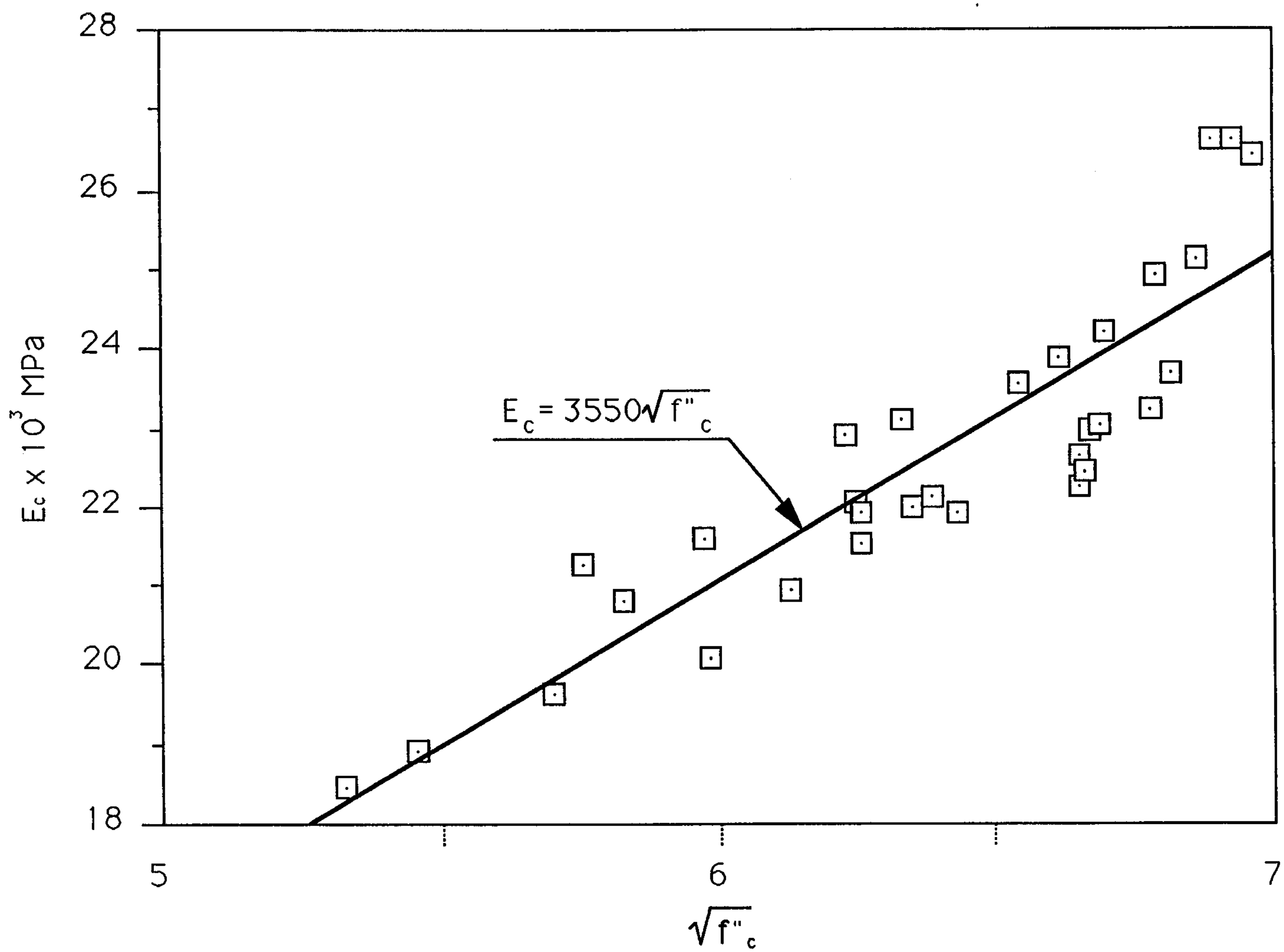

Fig. 2.13 Modulus of Elasticity Versus $\sqrt{f''_c}$

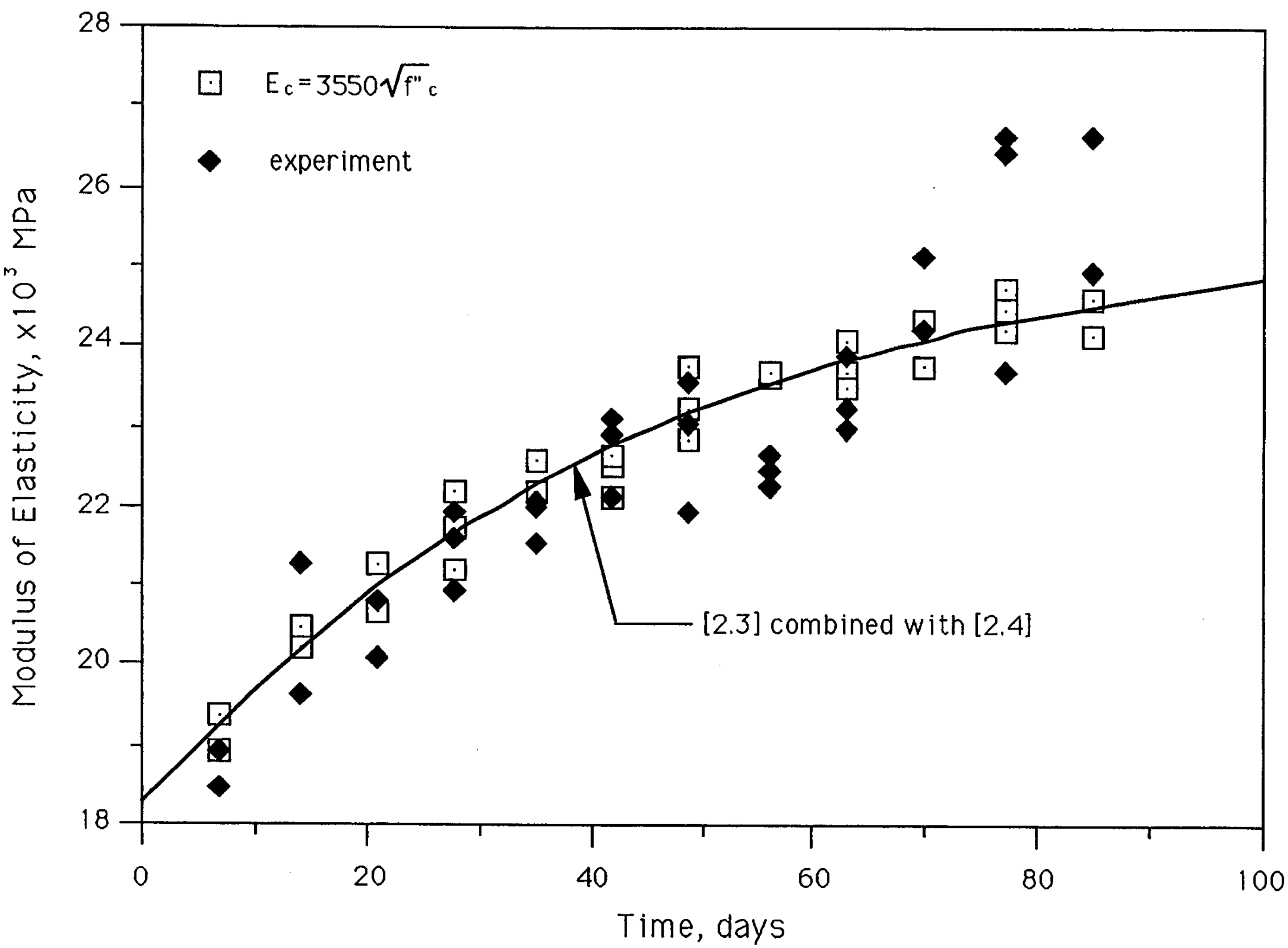

Figure 2.14 Modulus of Elasticity of Concrete

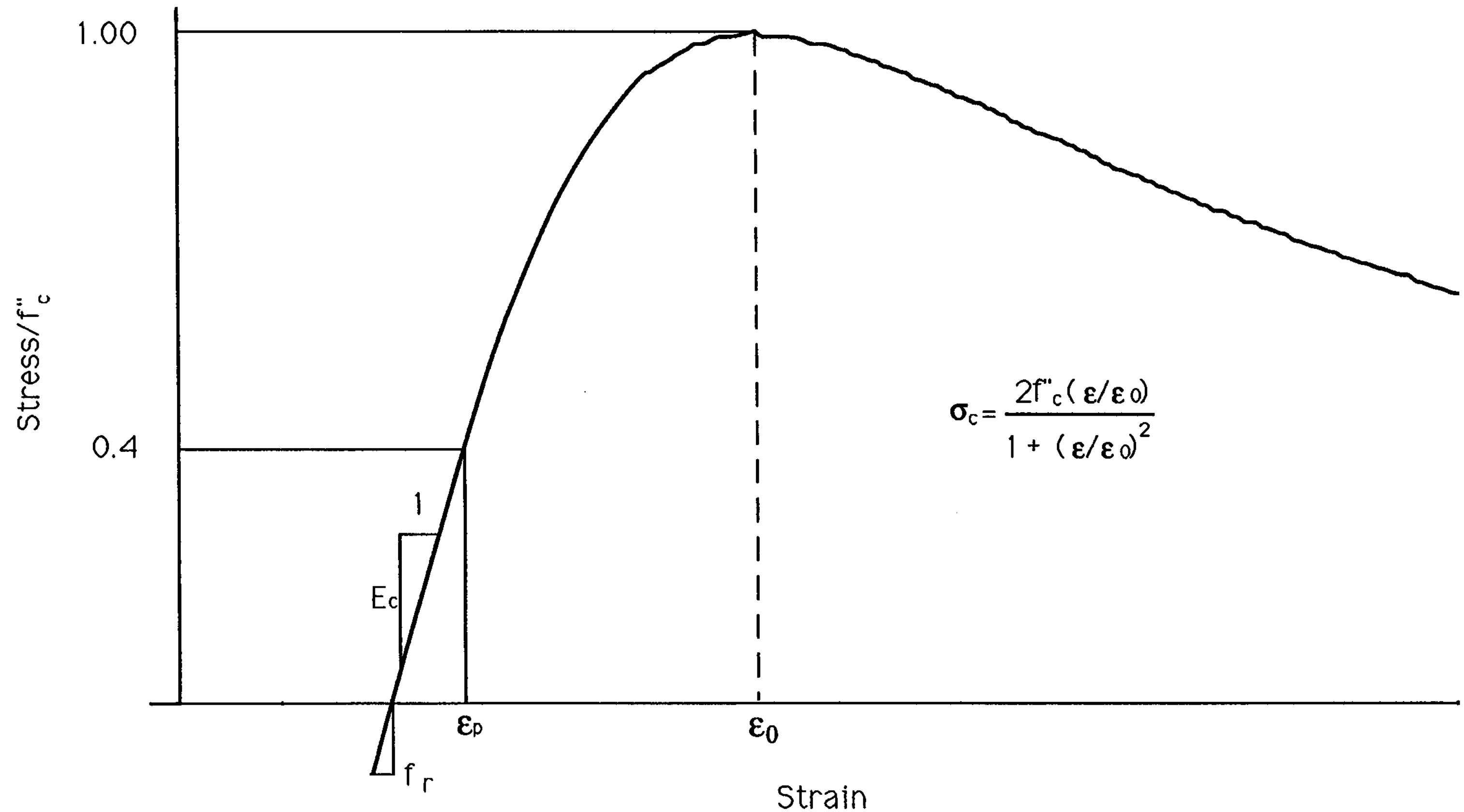

Fig. 2.15 Idealized Stress-strain Curve for Concrete

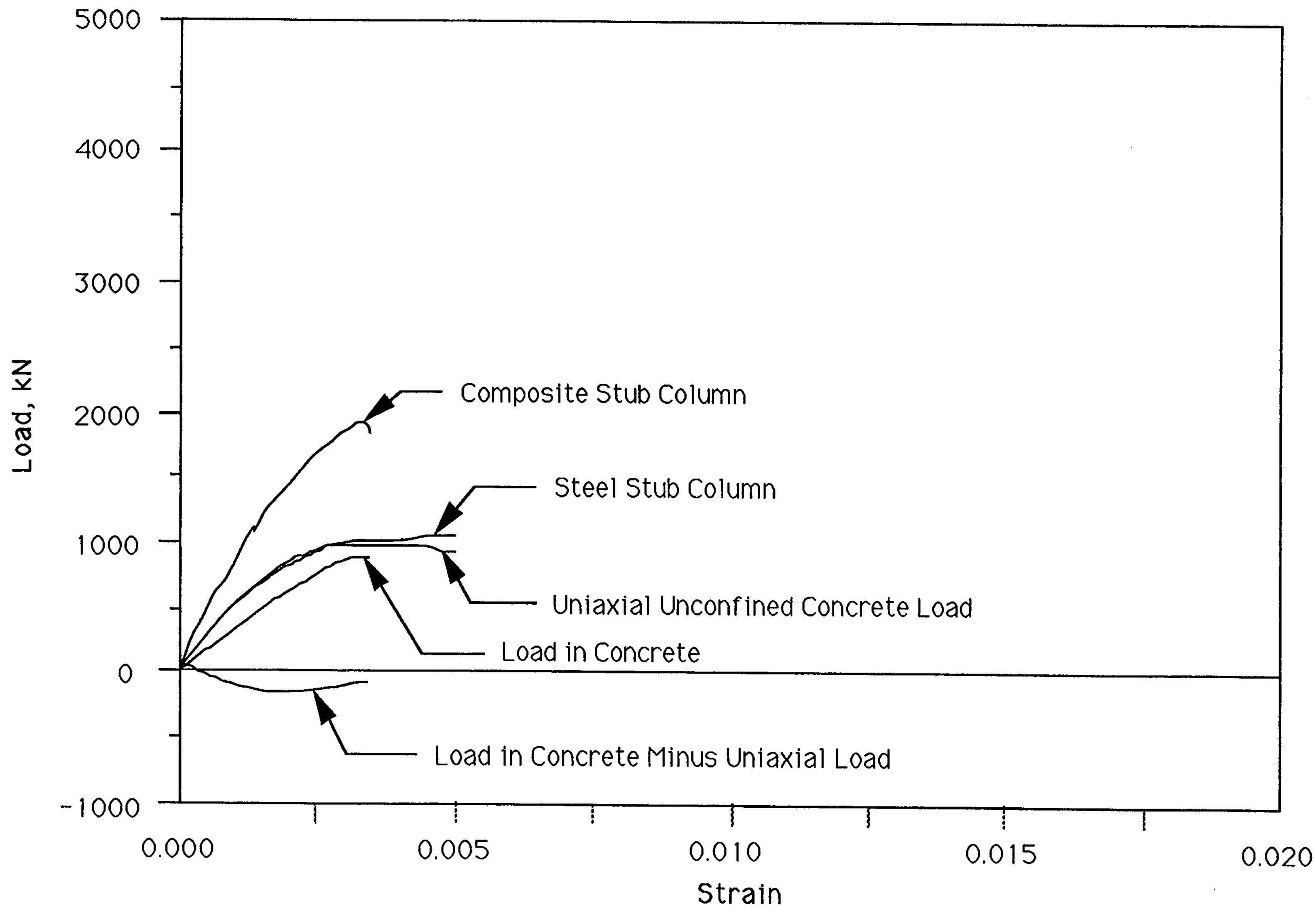

Figure 2.16 Load-strain Curve, Stub Column, Section 1

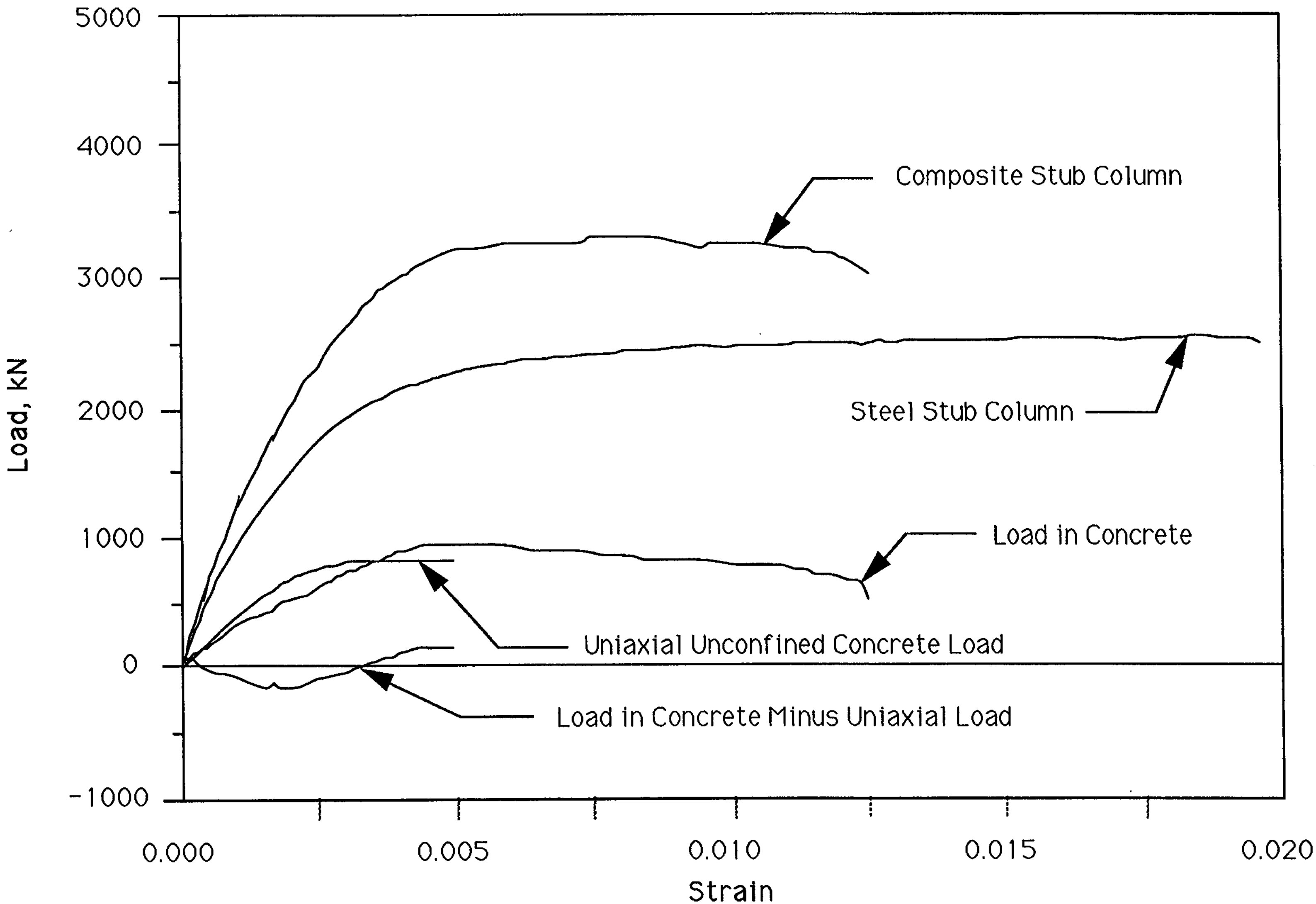

Figure 2.17 Load-strain Curve, Stub Column, Section 2

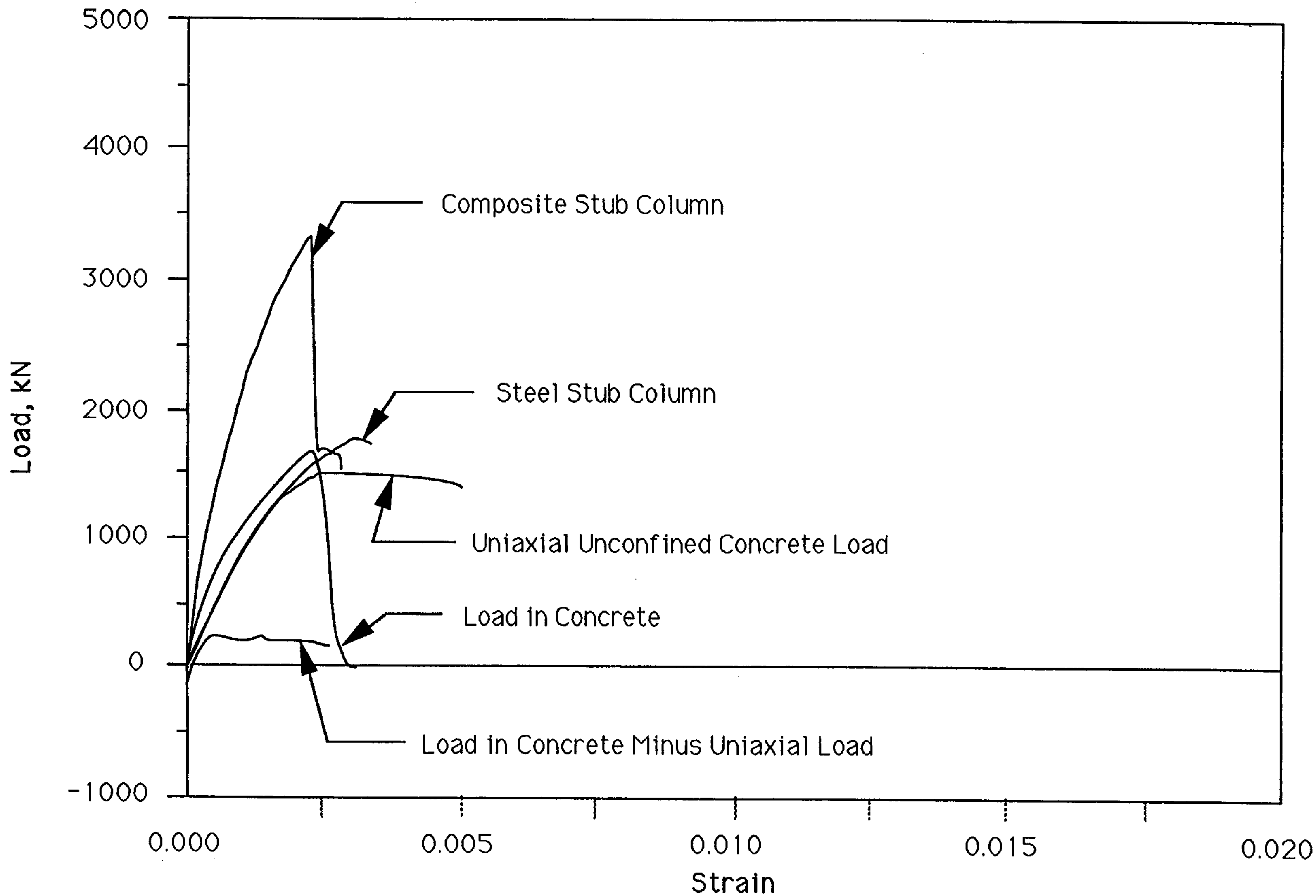

Figure 2.18 Load-strain Curve, Stub Column, Section 3

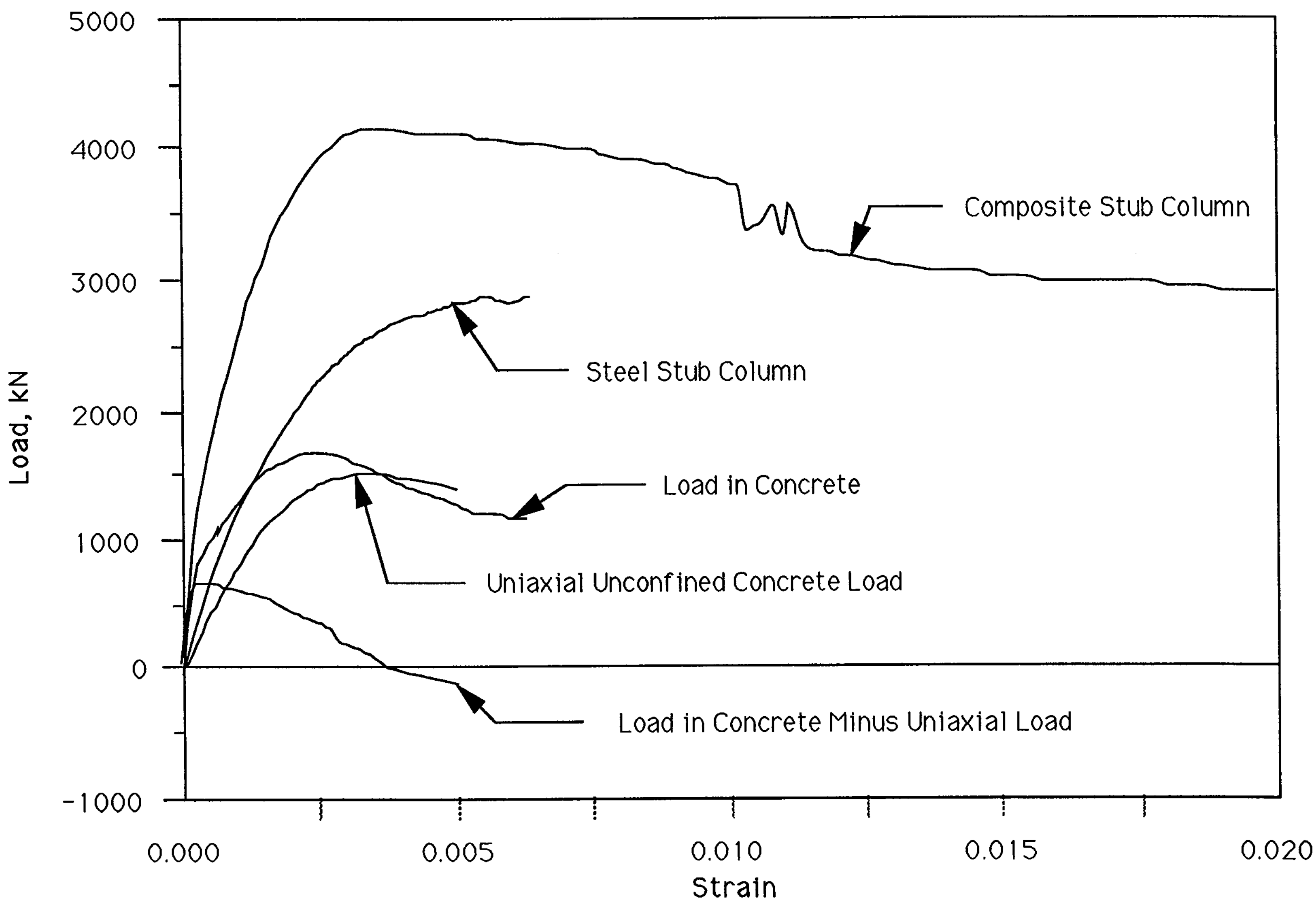

Figure 2.19 Load-strain Curve, Stub Column, Section 4

Chapter 3. Flexural Tests

3.1 General

The results of 12 flexural tests on concrete-filled hollow-structural sections are presented and analyzed together with 5 such tests on hollow structural sections made for comparative purposes. The flexural behaviour and effect of varying shear-span/depth ratios are discussed. Models are developed to predict the flexural resistance and compared to the test results.

3.2 Performance of Knife Edge and Rollers

As shown in Fig. 2.1, knife edges and roller assemblies were provided at each load and reaction point to allow rotation and longitudinal translation to occur so that simply supported tests were indeed performed without rotational or translational resistant at the load and reaction points.

In Fig. 3.1, for steel beam 2, is a typical plot of the measured deflection at the centre line versus the calculated deflection based on measured properties of the steel section and assuming no rotational restraints were provided. For the initial portion of the figure the measured values are not less than the calculated values indicating that there was no rotational or translational restraint.

Figs. 3.2 through 3.6 give the change in the shear-span versus the curvature in the constant moment region. The change in the shear-span is taken as the sum of the average outward movement of the reaction points and the average inward movement of the load points. The curvature was obtained as the sum of the average of the strains of the five gauges mounted on the top flange of the steel section plus the five values on the bottom flange all divided by the depth of the section.

With some anomalies, the change in shear-span versus curvature curves exhibit similar characteristics. There exists a roughly linear increase in shear-span with curvature until high curvatures are obtained when the shear-span change becomes more rapid. This is attributed to the increased deflections that occur when the steel top flange finally buckles without an increase in steel strain and therefore curvature.

For Section 1, Fig. 3.2, in both tests CB12 and CB15 significant changes in curvature occured with little change in the shear-span, which suggests that some restraint against movement of the load or reaction points occured. Dirt in the roller assemblies could be the cause. For Section 5, Fig. 3.6, a similar phenomenon occured for test CB51. Be that as it may, the measured shear-span changes were used to compute the bending moment in the constant moment region. No direct comparison between the steel beam and composite beam tests are made as the test situations are different.

3.3 Overall Behaviour

3.3.1 Moment-curvature Diagrams

The overall flexural behaviour is presented in the form of moment-curvature diagram in Figs. 3.7 through 3.11 for beam Sections 1 through 5 respectively. In each figure, the diagram for the steel beam is given as well as those for the composite beams.

3.3.2 Steel Beams

The data for steel beam 1 are taken from Kennedy and MacGregor (1984). In each case the M-ϕ diagram resembles the stress-strain diagram for the steel cross section with an initial elastic portion followed by inelastic behaviour with gradually decreasing stiffness until, in general, the maximum moment is reached asymptotically.

For SB2 (Fig. 3.8) failure occured due to local buckling under one of the load points. To prevent this in subsequent tests, internal stiffeners were positioned at the loads and reactions. The general mode of failure was downward buckling of the steel top flange in the constant moment region accompanied by outward buckling of the walls. Based on the yield strengths and section classification of Table 2.4 and the cross-sectional properties of Table 2.5 the predicted moment capacities are given in Table 3.1 together with the test strengths. The significant difference of the test moment to the yield moment for Section 1, designated as a Class 3 section in bending, is attributed to the fact that the section almost falls in Class 2. It therefore could be expected to have a moment approaching that of a Class 2 section of 55.3 kNm (ZF_y) reducing the test/predicted ratio to 1.177 in line with the ratios for the sections capable of reaching M_p. Secondly, for all the sections the cold-formed stress-strain curve is not flat at the yield value and therefore, provided local buckling does not occur, the moment developed will be greater than that assuming the maximum stress is the yield value.

Even Section 5, designated as a Class 4 section in bending, just greater than the Class 3 limit, was capable of exceeding the yield moment.

The upper portion of Table 3.2 compares experimental values of the flexural stiffness of the steel beams to those calculated from the measured moduli of elasticity and moments of inertia. The mean value is 0.992 with a coefficient of variation of 0.029.

3.3.3 Composite Beams

The moment-curvature diagrams for the composite beams of a given cross section in each of Figs. 3.7, 3.9, 3.10 and 3.11 follow each other closely. There is an initial elastic response, then inelastic behaviour with gradually decreasing stiffness, until the maximum moment is reached asymptotically. In general, failure occured when an upward buckle of the top flange of the steel cross section developed in the constant moment region. Subsequent examination, when the section of the steel in the failure region was cut from the beam, indicated that the concrete was crushed in the compression zone in this region and the concrete in the tension zone was severely cracked.

The initial stiffness of the composite sections are somewhat greater and the maximum moments are substantially greater than those of the corresponding hollow structural sections. Furthermore, the maximum curvatures of the composite sections are also significantly greater than that of the steel sections alone.

In Table 3.2, are given the initial flexural stiffness (the slope of the M-ϕ curve) as determined experimentally together with the value predicted from the uncracked fully transformed composite section properties using a modular ratio based on the concrete modulus of elasticity found from [2.4]. The test/predicted values are also given as well as the ratio of the stiffness of the composite section to the steel section alone.

The mean value of the test/predicted or experimental/predicted ratio for the composite beams based on an uncracked section is 0.810 with a coefficient of variation 0.063. This means that the flexural stiffness of the composite beams, even for moments not exceeding 20%, of the maximum values is significantly less than that based on the uncracked section. Cracking reduces the stiffness substantially.

The initial stiffness of the composite beams, as given in Table

3.2, is on the average 1.12 times that predicted for the steel beams alone with a coefficient of variation of 0.063. This means that a conservative design approach would be to use the flexural stiffness of the steel beams alone as a measure of that of the composite sections.

Table 3.3 compares the test moment resistance of the composite beams with that of the steel beams. It is recognized that during the course of the tests, the concrete gained strength and therefore this is reflected in these strength ratios. The average overall ratio of the strength of the composite beams to the steel beams is 1.231 with a coefficient of variation of 0.085. In general, the value is greater when the HSS walls are thinner resulting in a greater proportion of concrete to steel.

The moment-curvature diagrams show that filling the hollow structural sections with concrete enhances significantly their rotational capacity. Excluding three beams-CB22, CB41 and CB45- where the maximum curvature obtained was compromised by rotational or deflection limits as noted in their corresponding moment-curvature diagrams, the ratio of the curvature of the composite beams to that of the steel has a mean value of 3.4 with a coefficient of variation of 0.22. The enhancement of the curvature obtained is due to the larger strains the steel can undergo before buckling occurs. The steel top flange is forced to buckle upwards and as well is restrained torsionally at the flange-side wall (web) junction, because the web cannot rotate inwards.

3.4 Load Transfer from Steel to Concrete

3.4.1 General

The enhanced flexural behaviour of the composite sections relative to the steel sections means that the concrete contributes to the compression portion of the internal resisting couple of the cross section. As the concrete below the neutral axis is severely cracked at ultimate load and as no mechanical means of transfer was provided the compressive force in the concrete must be transfered to it from the steel, within the shear-span, solely by friction and whatever adhesion may have existed.

One model for the participation of the concrete is the tied-arch model shown in Fig. 3.12. Friction between the steel and the concrete is required to transfer the horizontal component of the compressive force in the inclined concrete strut to the steel tension tie. The strut also carries part of the transverse shear. The friction is enhanced when the normal forces, due to the loading and reaction points, through the steel to the concrete.

3.4.2 Moment-curvature Relationship Versus Shear-span

In Fig. 3.7 for Section 1, Fig. 3.9 for Section 3, Fig. 3.10 for Section 4 and Fig. 3.11 for Section 5 are plotted moment-curvature diagrams for shear-span/depth ratios ranging from 1.03 to 5.05. In each of these figures, the moment-curvature diagram is seen to be independent of the shear-span/depth ratio. The same maximum moment was reached for a given cross section and the same M-ϕ path was followed irrespective of the shear-span/depth ratio.

Reducing the shear-span by 5 times means that only 1/5 of the distance is available to develop the same compressive force in the concrete. Yet apparently this force was developed without any difficulty.

3.4.3 Slip Between Steel and Concrete

Figs. 3.13 through 3.24 give the slip measured between the steel and concrete at various locations for the 12 composite beam tests. The location of the gauges measuring slip are shown in Fig. 2.2. They are identified on Figs. 3.13 to 3.24 as top, middle and bottom gauges depending on their relative vertical location on the side of the test specimen and as west or east gauges as related to their position along the length of the specimen.

In no case did any appreciable slip occur. The slip remained relatively small until the maximum moment was reached when slips, generally of the order of 0.5 to 1 mm, were recorded as given in Table 3.4. The high readings of 3.9 mm and 2.1 mm for tests CB13 and CB15 respectively are considered to be accidental readings as in the first case the LVDT was bumped and in the second a supporting plate kicked out. Within the constant moment region the "slips" could be attributed to relative moment between the steel and the concrete when the steel top flange buckled and the concrete finally crushed. In a few cases "negative" slips were recorded when the neutral axis migrated above the slip measurement points.

3.4.4 Strain Distribution in Steel and Concrete

From both the 16 electrical resistance strain gauges mounted on the steel, five on each flange surface and three on each side, and from the demec gauges mounted on the concrete, three on each side, strains can be estimated independently at the level of the top and bottom flange surfaces using least squares best fit linear strain distributions. These data are plotted on Figs. 3.25 to 3.36. In all cases close correspondence is obtained between the strain at these levels based on the measured steel and concrete strains.

3.4.5 Conclusions

All three of the independent observations cited above: (i) the virtually identical moment-curvature relationships for a given composite cross-section irrespective of the shear-span, (ii) the negligible slips that were reached before the maximum moments were reached and even the very small relative movements then, and (iii) the close correspondence between the steel strains on the flange surfaces and those deduced from the concrete strain measurements, lead to the conclusion that no degradation of the moment capacity arose due to load transfer problems without mechanical anchorage between the steel and the concrete. No special provisions are necessary, even with a/d ratios as low as one, to achieve composite action.

3.5 Strain Distribution Across Depth

3.5.1 Strain Distribution

Figs. 3.37 and 3.38 show strain distributions across the depth of the steel beams at maximum moment. For Section Classes 3 and 4, beam Sections 1 and 5 respectively, the maximum strains reached are relatively small, approximately 5 700 and 4 000 $\mu\varepsilon$ respectively, and are about the same in tension and in compression. Section 3, although just barely a Class 1 section, had similar maximum strains. For Sections 2 and 4, stocky Class 1 sections, the maximum strains are significantly larger reaching up to 12 000 $\mu\varepsilon$ in tension and compression.

In each of Figs. 3.39 to 3.50, for the 12 composite beams the distribution of strains across the depth of the section is shown for two different levels of moment. The maximum moment on the cross section and a moment about one-fifth of this value. In each case the least squares best fit linear distribution is also shown.

The following observations are made:

The measured strains vary considerably from the best fit straight lines. In fitting these lines, correlation coefficients as low as 0.820 with a mean value of 0.953 with a coefficient of variation 0.053 were obtained as given in Table 3.5.

The neutral axis is seen to rise with increasing moment.

The maximum strains obtained are very large. Top strains vary from about 7 400 $\mu\varepsilon$ for Section 5, a Class 4 section in bending, to over 26 300 $\mu\varepsilon$ for Section 4, the very stocky Class 1 section with the least width-thickness ratio. Bottom strains are very large varying from about 16 600 to 29 600 $\mu\varepsilon$. The larger bottom strains occur, of course, because more of the steel must be in tension to balance the compressive force in the concrete. These strain are tabulated in Table 3.5 The mean value of the tensile strain is about 14 000 $\mu\varepsilon$ and of the compressive strain is about 23 000 $\mu\varepsilon$.

A comparison of the steel strains reached by the composite beams to those of the steel beams alone shows significant differences. Tensile strains are much greater simply due to the fact that the tensile force in steel must balance the compressive force in the steel and concrete. For the steel sections most prone to buckle the compressive strains reached in the composite beams are appreciably enhanced as the presence of the concrete modifies the buckling behaviour. The increase in compressive strains for the very compact Class 1 sections in bending (Sections 2 and 4) is relatively small.

3.5.2 Movement of Neutral Axis with Moment

Figs. 3.51 to 3.55 show the movement of the neutral axis with moment for each of the sections tested.

The variation of the position of the neutral axis for the steel beams alone is relatively small until buckling finally occurs consistent with a downward shift. Prior to this the variation is seen to be related to the presence of residual stresses causing non-symmetric yield and changing load-carrying capacity.

The curves of the movement of the neutral axis for the composite sections are all very similar and consist of up to 5 distinct parts.

For very small moments the positions of the neutral axis is unchanged, but soon cracking of the concrete occurs and the position shifts rapidly upward about 5 to 15 mm, depending on the depth of section, as the cracks increase in length.

There follows a very gradual upward shift as the moment increases substantially. In this region, steel strains in general do not exceed the yield strain (about 4 000 $\mu\varepsilon$ by the 0.2% offset method) while the concrete is straining more and more inelastically.

Subsequently, the strain increases very substantially and the neutral axis shifts again rapidly upward with a small increase in moment. This portion corresponds on the moment-curvature diagram, first to the knee and then to the plateau which is reached asymptotically. The moment corresponding to the maximum height of the neutral axis is termed the penultimate moment and is the moment that exists before local effects such as flange buckling occur.

The final portion of the curve occurs when the top flange of the steel buckles in compression reducing its load carrying capacity and the neutral axis shifts downward.

The entire curve resembles the shape of the back of a brontosaurus.

3.6 Moment Resistance of Composite Section

3.6.1 General

The moment resistance achieved by the composite section depends on the strains developed in the steel and the concrete and the effective stress-strain relationships for the two materials. From the experimental data presented two values of moment at or near the maximum moment were deemed of interest. The penultimate moment, corresponding to the maximum height of the neutral axis, is considered to be the best moment for establishing the position of the neutral axis as it is not affected by subsequent local effects. The ultimate or maximum moment is considered to be the best measure of the moment resistance. The penultimate and maximum moments are tabulated in Table 3.6 together with their ratios. The mean ratio of the penultimate moment to the maximum moment is 0.984 with a coefficient of variation of 0.013.

Also tabulated in Table 3.5 is the position of the neutral axis corresponding to the penultimate moment. Using this position and assuming alternately that the bottom and top strain for the maximum moment are correct two other limiting strain distributions can be plotted as shown in Fig. 3.39 to 3.50 by the dashed lines. These limiting strain distributions are seen in all cases with the exception of the strain distribution for beam CB41, to fall within the range of measured strains. It is therefore considered valid, within the ratios of width-thicknesses used in these tests, to base the contribution of the steel and concrete on the measured position of the neutral axis at the penultimate moment and to use the average top and bottom steel strains of 14 000 and 23 000 $\mu\varepsilon$ at the maximum moment. Fig. 3.56 shows the variation of steel stress with strain for four cross sections determined as the weighted average of the tensile coupon values. It is seen that there is little variation in the stress level within this range and indeed for the entire range of strains at maximum moment of 7 400 to 26 300 $\mu\varepsilon$. The mean stress at these two strain levels was therefore used for both tension and compression.

3.6.2 Contribution of Concrete to the Moment Resistance

The contribution of the concrete to the moment resistance was back calculated from the assumptions based on the observed behaviour as follows:

(i) the position of the neutral axis was taken as that determined from the best fit linear strain distribution of the 16 steel strains at the penultimate moment.

(ii) the steel, both in compression and in tension, was considered to have a rectangular stress block at an average stress intensity corresponding to strains of 14 000 and 23 000 $\mu\varepsilon$. From Fig. 3.56 these are 446 MPa for Section 1, 490 MPa for Section 2, 462 MPa for Section 3 and 440 MPa for Section 4.

(iii) The force in the concrete is deduced as the difference of the tensile force and compressive force in the steel, i.e., $C_c = T_s - C_s$

(iv) the ratio of the maximum stress intensity in the concrete to the unconfined compressive strength at the time of testing is deduced from

[3.1] $$k_3 = C_c/0.85f''_c A_c$$

which implies that the concrete force is assumed to be developed from a rectangular stress block extending 0.85 of the distance to the neutral axis.

For the calculated values of k_3 tabulated in Table 3.6 the mean value is determined to be 1.014 with a coefficient of variation of 0.131. A value of 1.00 for k_3, suggesting that the full unconfined strength of the concrete is developed, rather than 0.85 of it as used in the reinforced concrete ultimate strength design of beams, appears appropriate.

Table 3.6 gives the predicted moment resistance based on the calculated value of k_3 and also the ratio of the maximum test moment divided by this prediction. The mean value of the ratio is 1.015 with a coefficient of variation of 0.020. These values indicate exceptional agreement of the predicted values to the test values.

3.6.3 Research Model

Based on the mean value of k_3 = 1.014 with the very small coefficient of variation of 0.020, a value of k_3 = 1.00 is considered appropriate for establishing a research or design model. The other factors for the research model were the concrete cylinder strength at the time of testing, giving a concrete force $C_c = 0.85f''_c A_c$ and a steel stress, both in compression and in tension, taken as the average of that at 14 000 and 23 000 $\mu\varepsilon$. The use of a steel stress corresponding to these high strain levels, based on these test results, is valid for sections with nominal b/t ratios of 36.0 or less in grade 350 steel, and therefore for all the sections listed in the handbook (CISC, 1991) except HSS 305 x 203 x 6.4, HSS 203 x 152 x 4.8, HSS 203 x 102 x 4.8 and HSS 305 x 305 x 6.4. The position of the neutral axis is determined such that horizontal equilibrium is satisfied.

Resisting moments calculated on this basis are tabulated in Table 3.6 under the heading "Research". The ratio of test/predicted moments has a mean value of 1.016 with a coefficient of variation reaches of 0.025.

The results again indicate exceptional agreement of the predicted values to the test values. This suggests that the model, based on tests with a wide variation of the concrete area to that of the steel, is generally applicable to concrete-filled hollow structural sections.

3.6.4 Design Model

Designers will not know, a priori, the steel stresses at the elevated strains found to exist at the maximum test moment. Therefore a model of the flexural resistance appropriate for design would be based on the specified minimum yield strength of the steel and the 28 day cylinder strength of the concrete with the neutral axis again established to satisfy equilibrium.

To check the adequacy of this model based on the test results the specified yield strength is replaced by the measured yield strength and the 28 day cylinder strength by the measured cylinder strength at the time of testing. Table 3.6 gives value of the predicted design moment based on the yield strength from the steel stub column tests and ratios of the maximum test moment to this predicted moment.

The mean value is now found to be 1.188 with a coefficient of variation 0.0337. The mean value of the test/predicted ratio is increased by 17% although the coefficient of variation is still quite low. The increase in the ratio is directly attributable to the use of the yield strength for the steel rather than the stress levels at high strains. The high mean value would not be disadvantageous in design because a resistance factor derived on this basis together with the ratios for the variation of the yield strength and cross-sectional properties to the minimum specified values and their associated coefficients of variation would give the desired reliability levels.

3.6.5 Effects of Proportions of Steel and Concrete and of Shear-span/Depth Ratios

In Table 3.7 is tabulated the ratios of the compressive area of the concrete to that of steel, A_c/A_s, the ratio of the shear-span to depth, a/d, and the ratio of the test moment to the predicted moment, M_t/M_p. As all of the test/predicted moment ratios are essentially one, M_t/M_p is seen to be independent of both the A_c/A_s and the a/d ratios which vary from 3.07 to 5.63 and 1.03 to 5.05 respectively.

Table 3.1 Ratio of Test to Predicted Moment

Section		Class	F_y, MPa	S (mm^3)	Z (mm^3)	M_y, kNm	M_p, kNm	M_t, kNm	$\frac{M_t}{M_y \text{ or } M_p}$
Number	Designation								
1	152 x 152 x 4.8	3	389	121.6×10^3	142.2×10^3	47.3		65.1	1.376
2	152 x 152 x 9.5	1	432		261.3×10^3		112.9	133.0	1.178
3	254 x 152 x 6.4	1	377		398.7×10^3		150.3	155.8	1.037
4	254 x 152 x 9.5	1	394		558.7×10^3		220.1	244.2	1.109
5	152 x 254 x 6.4	4	377	248.5×10^3		93.9		110.5	1.177
μ									1.175
V									0.107

Table 3.2 Flexural Stiffness

Section		Predicted, $\times 10^{12}$ Nmm^2	Experimental, $\times 10^{12}$ Nmm^2	Experimental / Predicted	Experimental / Steel, Predicted
Number	Beam				
1	SB1	1.957	2.019		1.032
2	SB2	3.486	3.435		0.985
3	SB3	8.609	8.462		0.983
4	SB4	11.898	11.401		0.958
5	SB5	3.918	3.924		1.002
	μ				0.992
	V				0.029
1	CB12	2.819	2.073	0.735	1.027
1	CB13	2.779	2.209	0.795	1.094
1	CB15	2.764	2.332	0.844	1.155
2	CB22	4.151	3.478	0.838	1.013
3	CB31	12.563	9.506	0.757	1.123
3	CB33	12.496	9.763	0.781	1.154
3	CB35	12.460	10.639	0.854	1.257
4	CB41	15.962	12.017	0.753	1.054
4	CB45	15.871	12.719	0.801	1.116
5	CB52	5.251	4.177	0.795	1.064
5	CB53	5.179	4.575	0.883	1.166
5	CB55	5.154	4.578	0.888	1.167
	μ			0.810	1.116
	V			0.063	0.063

Table 3.3 Moment Resistance of Composite Beam

Beam	Test Moment Resistance, kNm	Test Moment Composite / Test Moment Steel
CB12	73.6	1.131
CB13	75.1	1.154
CB15	71.3	1.095
CB22	146.5	1.102
CB31	210.7	1.352
CB33	210.7	1.352
CB35	207.6	1.332
CB41	283.8	1.162
CB45	282.2	1.156
CB52	144.7	1.310
CB53	146.7	1.328
CB55	142.9	1.293
μ		1.231
V		0.085

Table 3.4 Maximum Slip

Beam	Maximum Slip, mm
CB12	0.7
CB13	3.9
CB15	2.1
CB22	0.5
CB31	0.6
CB33	0.9
CB35	0.8
CB41	1.0
CB45	0.9
CB52	0.3
CB53	0.2
CB55	0.4

Table 3.5 Strains at Maximum Moment and Neutral Axis Position at Penultimate Moment

Beam	Strain at Top, $\mu\varepsilon$	Strain at Bottom, $\mu\varepsilon$	Correlation Coefficient	$\frac{\text{Distance from Top to N.A}}{\text{Beam Depth}}$
SB1	5700	5700	---	0.500
SB2	11800	11800	0.999	0.500
SB3	5300	5000	0.995	0.515
SB4	9700	10000	0.999	0.492
SB5	3900	3900	0.999	0.500
μ			0.998	0.501
V			0.002	0.017
CB12	13500	29600	0.942	0.301
CB13	12000	28000	0.990	0.299
CB15	11400	23600	0.992	0.323
CB22	14000	22100	0.992	0.387
CB31	15900	24800	0.971	0.361
CB33	14600	23700	0.927	0.351
CB35	13700	21900	0.946	0.353
CB41	26300	23200	0.820	0.388
CB45	17400	27900	0.991	0.366
CB52	7400	16900	0.960	0.305
CB53	11300	20900	0.913	0.313
CB55	7600	16600	0.989	0.313
μ	13800	23300	0.953	0.338
V	0.3583	0.1738	0.053	0.098

Table 3.6 Analysis of Moments

Test	Test Moment			N.A. Position from Top, mm	Calculated K_3	Predicted Moment			$\frac{\text{Maximum test Moment}}{\text{Predicted Moment}}$		
	Penultimate M_u, kNm	Maximum M_n, kNm	$\frac{M_u}{M_n}$			K_3 Calc.	Research K_3=1.00	Design K_3=1.00	K_3 Calc	Research K_3=1.00	Design K_3=1.00
CB12	72.5	73.6	0.985	45.9	1.012	72.7	73.63	63.53	1.012	1.000	1.159
CB13	72.9	75.1	0.971	45.5	1.139	72.8	72.17	63.13	1.031	1.041	1.190
CB15	70.3	71.3	0.986	49.3	0.946	71.7	71.97	62.89	0.994	0.991	1.134
CB22	145.2	146.5	0.991	59.0	1.157	139.7	137.2	123.08	1.049	1.068	1.190
CB31	202.0	210.7	0.959	91.4	0.862	209.7	212.4	176.16	1.005	0.992	1.196
CB33	207.8	210.7	0.986	88.9	0.986	211.5	211.7	175.63	0.996	0.995	1.200
CB35	205.2	207.6	0.990	89.4	0.984	211.1	211.3	175.31	0.983	0.983	1.184
CB41	273.7	283.8	0.964	98.1	0.986	275.0	275.2	248.67	1.032	1.031	1.141
CB45	279.4	282.2	0.990	92.5	1.323	280.5	274.7	247.98	1.006	1.027	1.138
CB52	1441	144.7	0.996	46.3	0.891	141.8	142.5	117.10	1.020	1.015	1.236
CB53	145.0	146.7	0.988	47.6	0.924	141.2	141.4	116.47	1.039	1.038	1.260
CB55	142.9	142.9	1.000	47.6	0.958	141.2	141.4	116.43	1.012	1.011	1.227
μ			0.984		1.014				1.015	1.016	1.188
V			0.013		0.131				.0.020	0.025	0.034

Table 3.7 Ratios of Compressive Area of Concrete to That of Steel, Shear-span to Depth and Test Moment to Predicted Moment

Section	Area(in compression), mm^2		$\frac{A_c}{A_s}$	a/d	$\frac{M_t}{M_p}$
	Concrete	Steel			
CB12	5116	1017	5.03	1.54	1.000
CB13	5706	1013	5.63	3.03	1.041
CB15	5183	1047	4.95	5.04	0.991
CB22	6618	2157	3.07	1.54	1.068
CB31	8728	1926	4.53	1.03	0.992
CB33	9684	1894	5.11	3.03	0.995
CB35	9720	1901	5.11	5.03	0.983
CB41	10007	2869	3.49	1.03	1.031
CB45	12579	2786	4.54	5.03	1.027
CB52	7321	1994	3.67	1.55	1.015
CB53	7839	2010	3.90	3.05	1.038
CB55	8135	2011	4.05	5.05	1.011

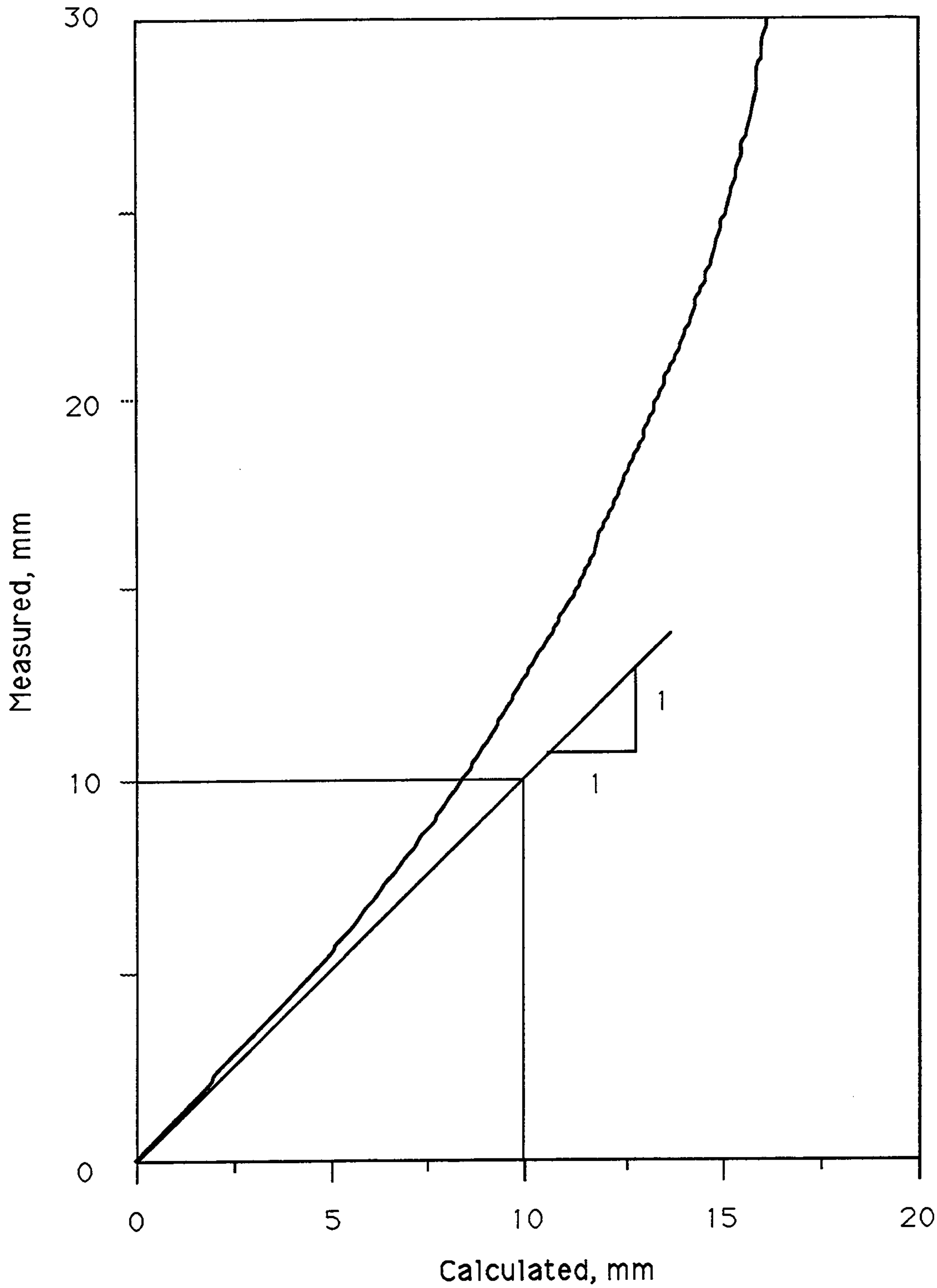

Figure 3.1 Measured Deflection-calculated Deflection

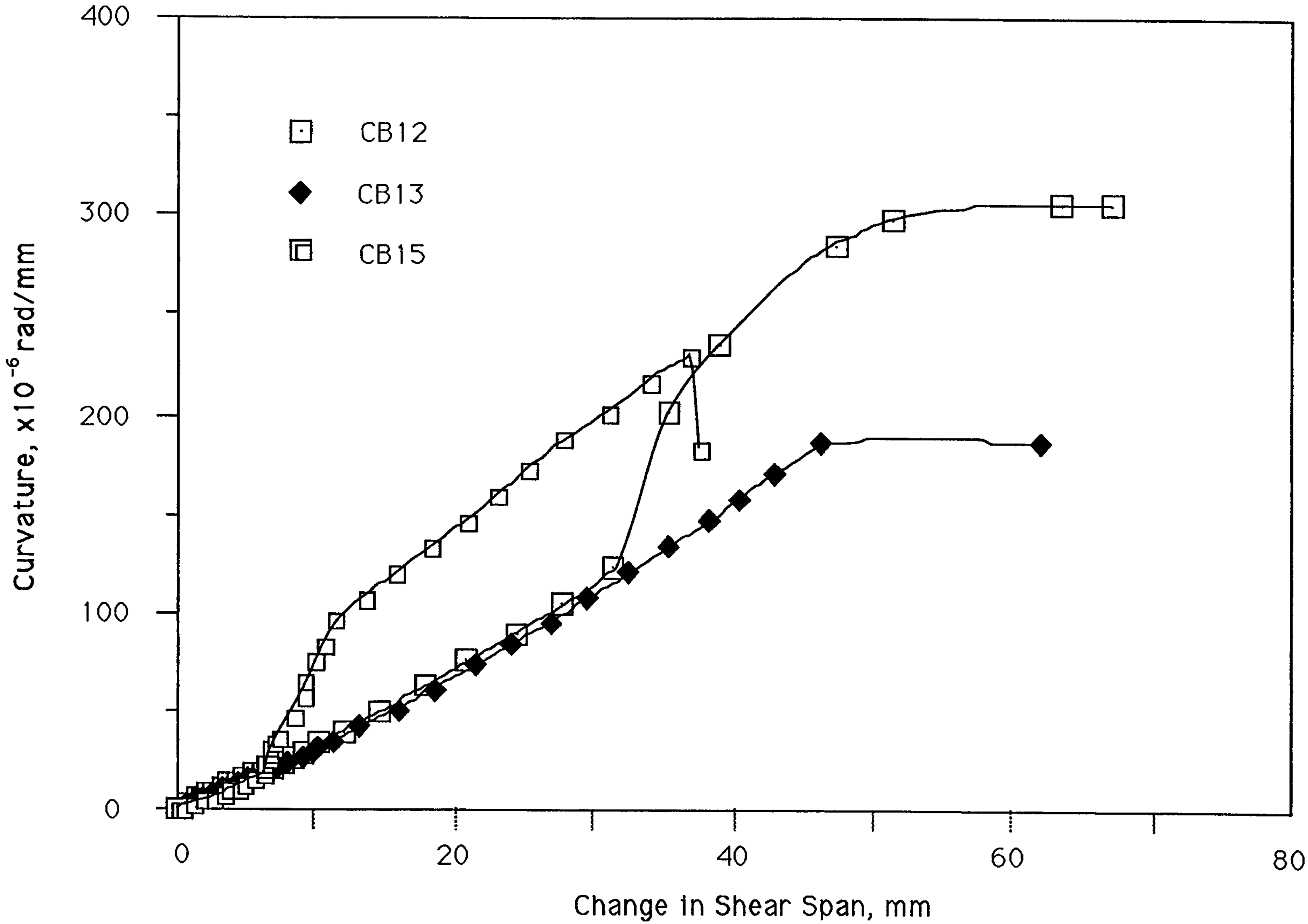

Figure 3.2 Curvature-change in Shear Span, Section 1

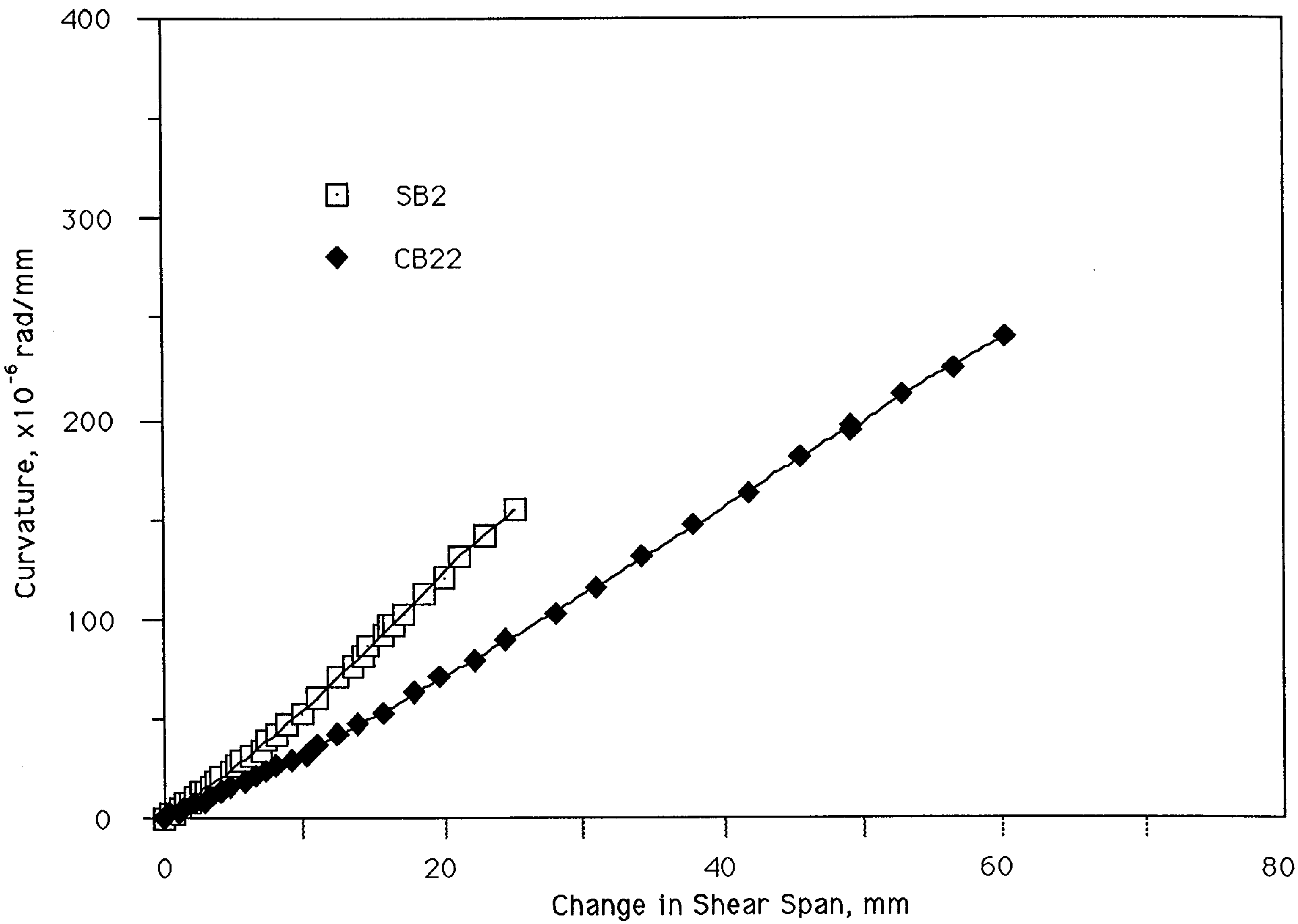

Figure 3.3 Curvature-change in Shear Span, Section 2

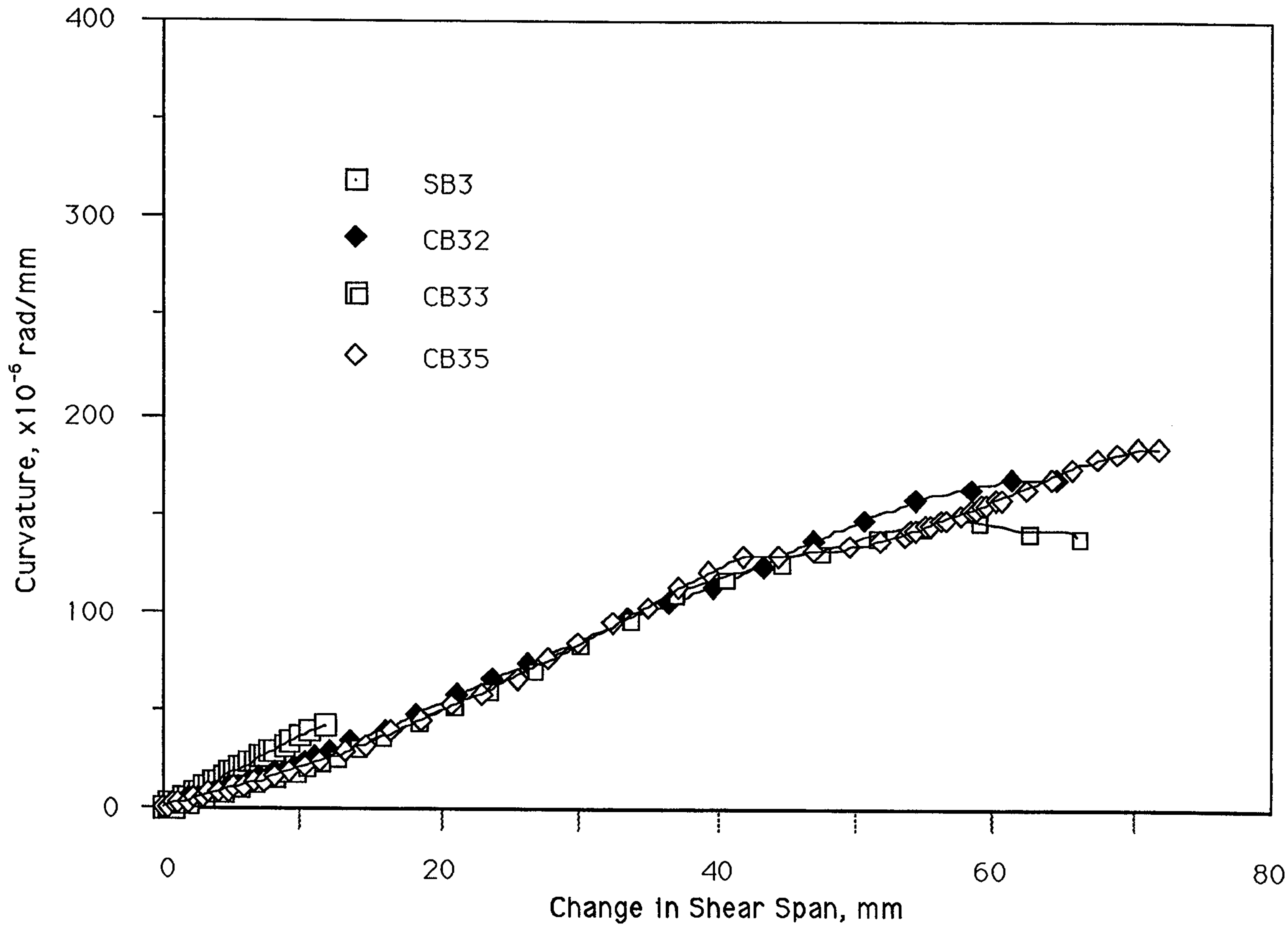

Figure 3.4 Curvature-change in Shear Span, Section 3

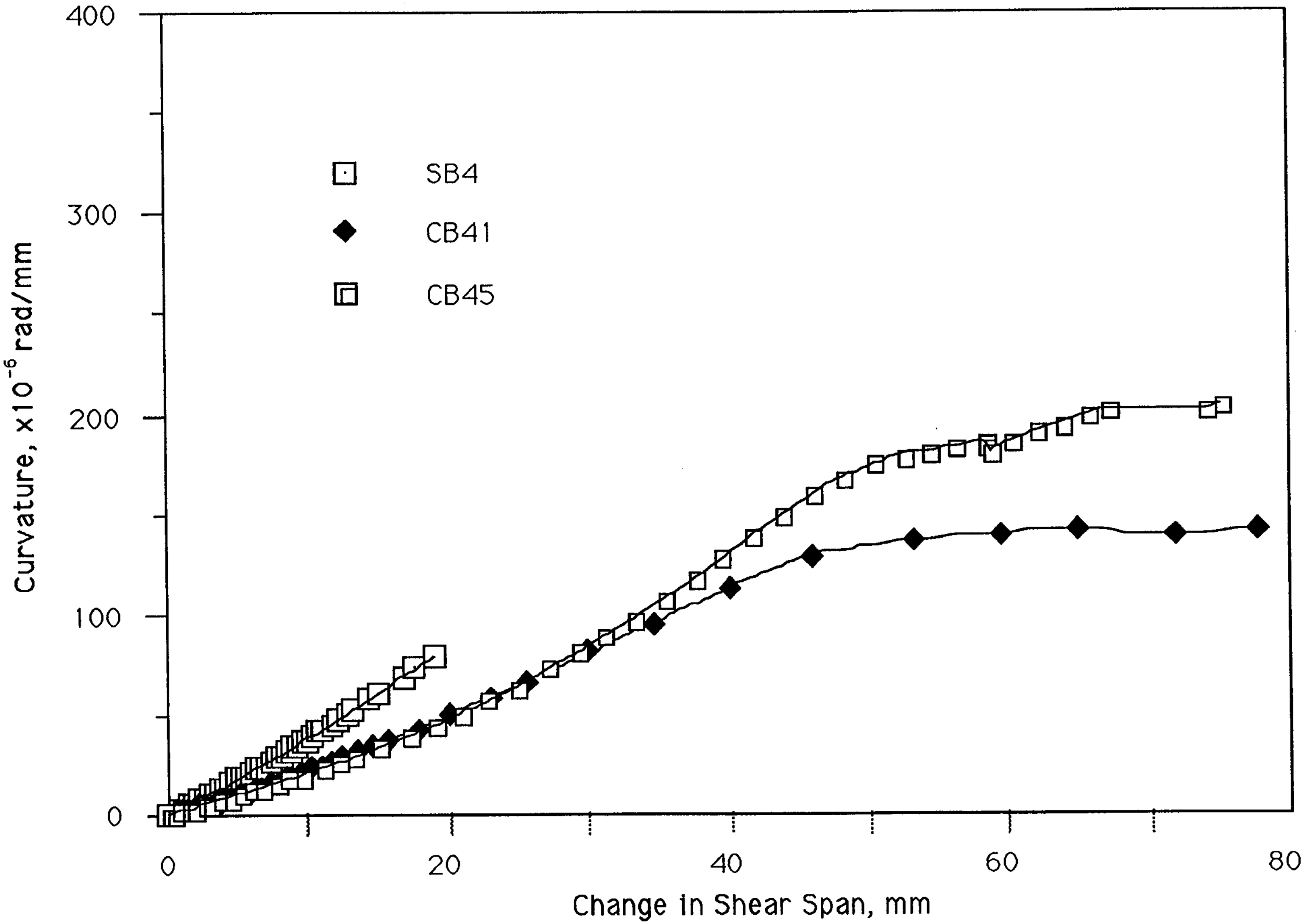

Figure 3.5 Curvature-change in Shear Span, Section 4

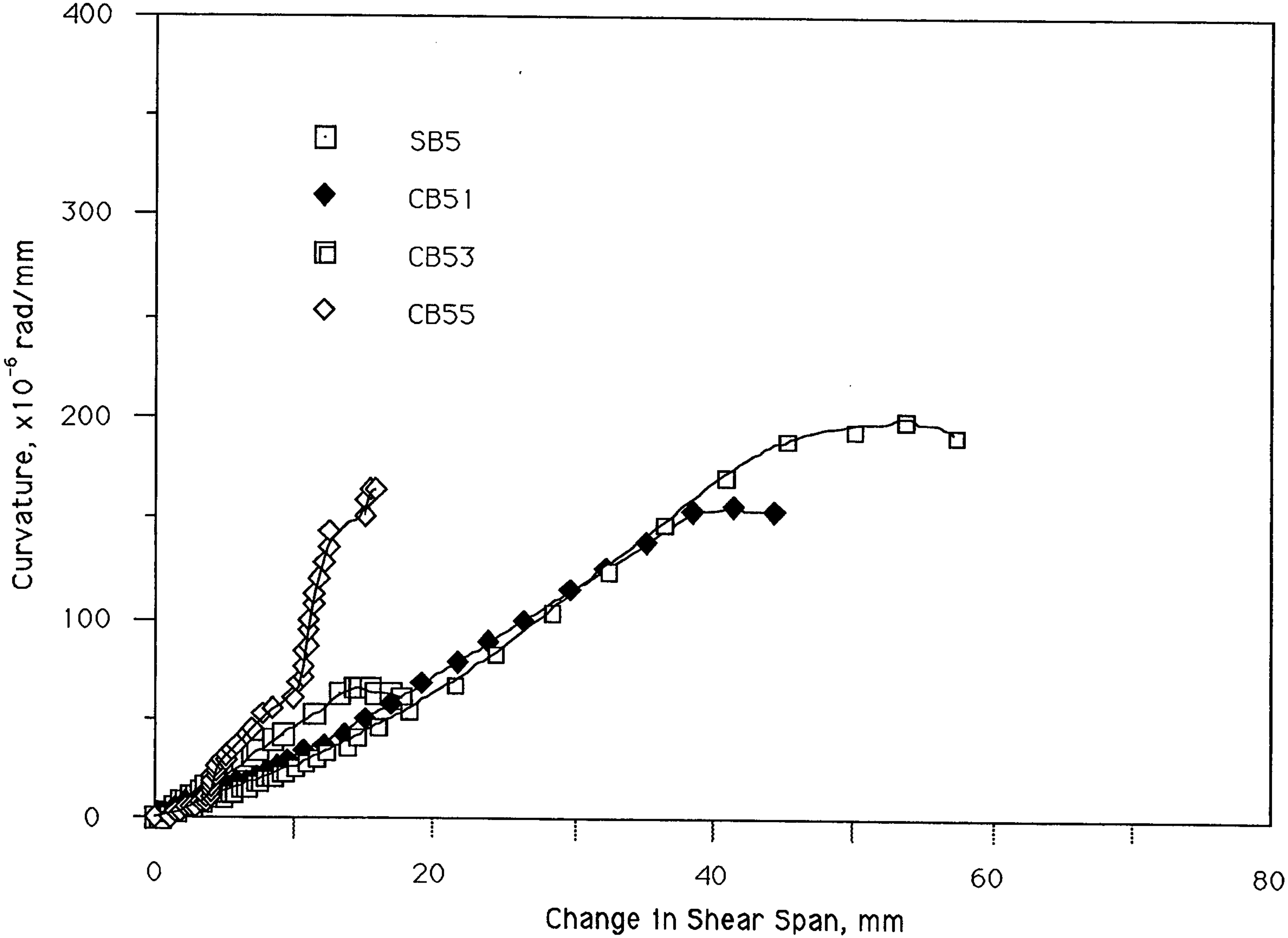

Figure 3.6 Curvature-change in Shear Span, Section 5

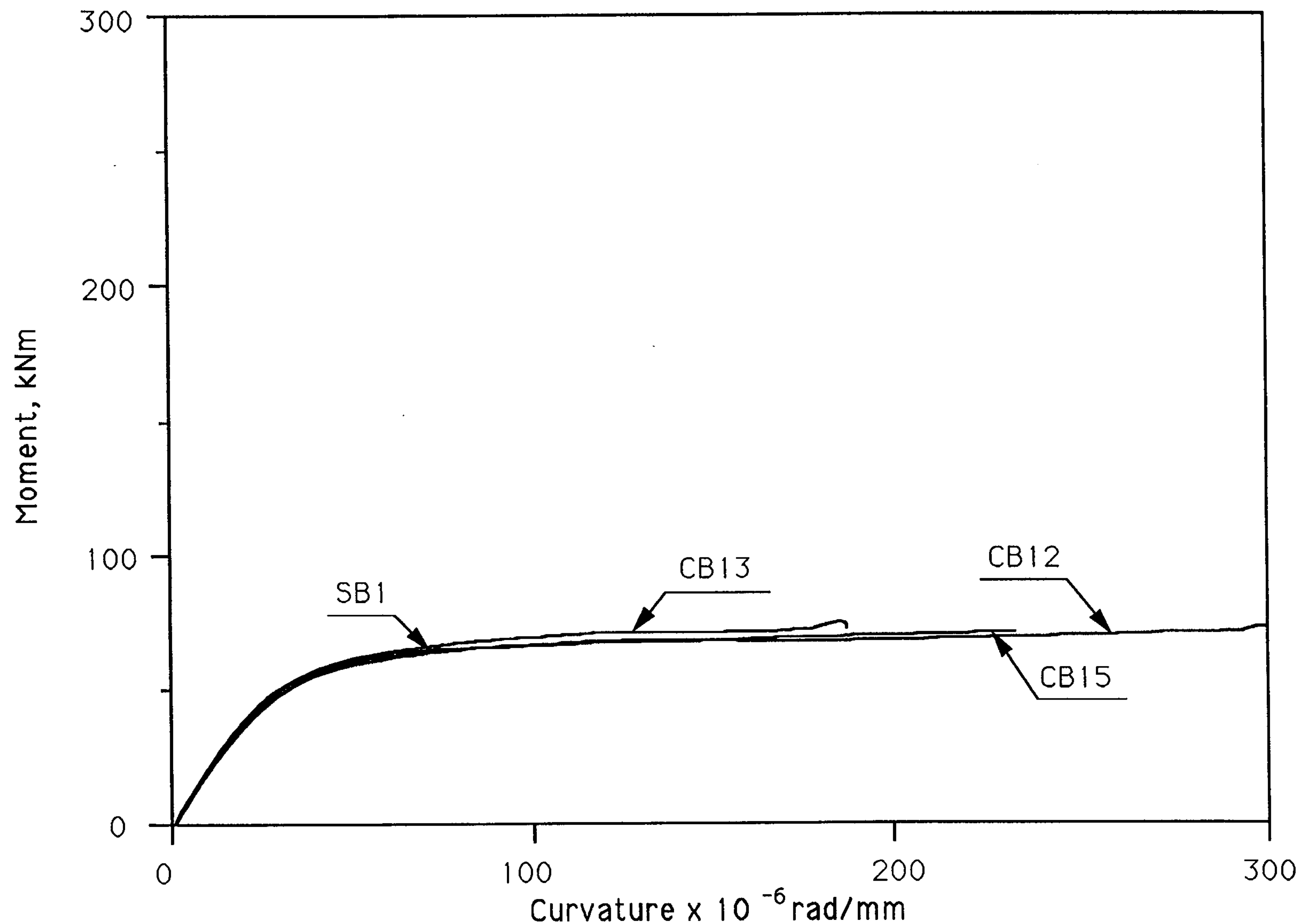

Figure 3.7 Moment-curvature Diagram, Section 1

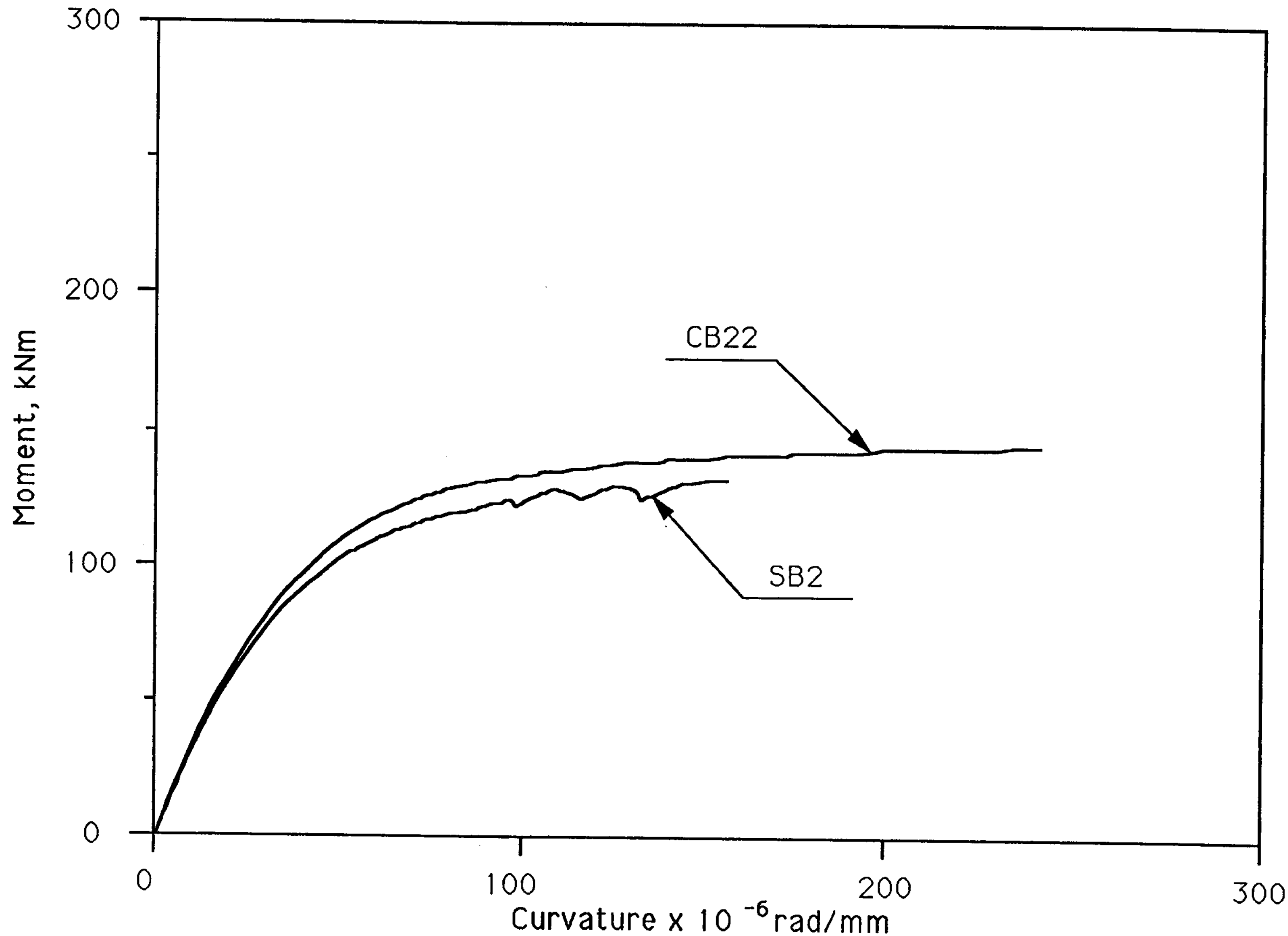

Figure 3.8 Moment-curvature Diagram, Section 2

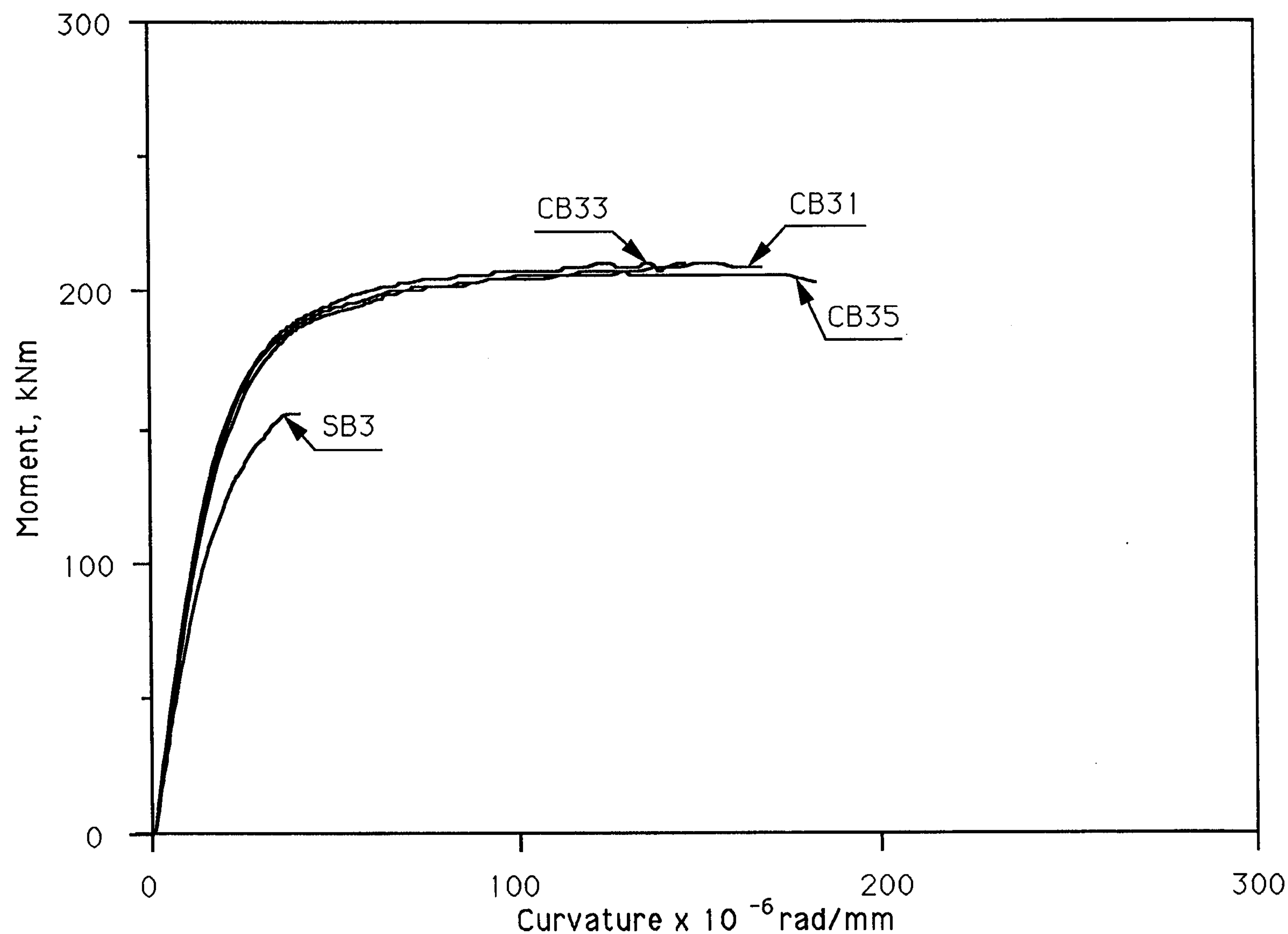

Figure 3.9 Moment-curvature Diagram, Section 3

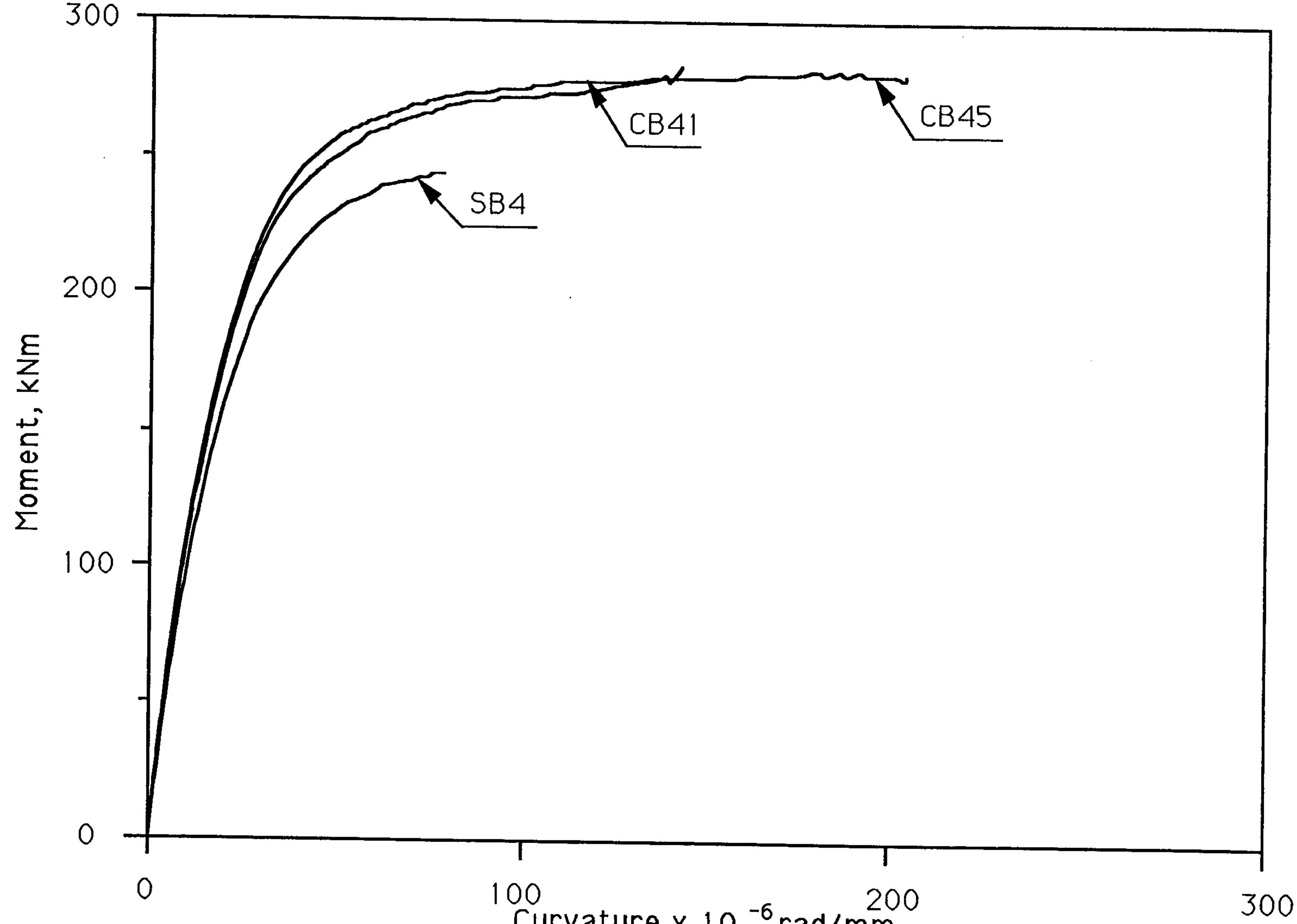

Figure 3.10 Moment-curvature Diagram, Section 4

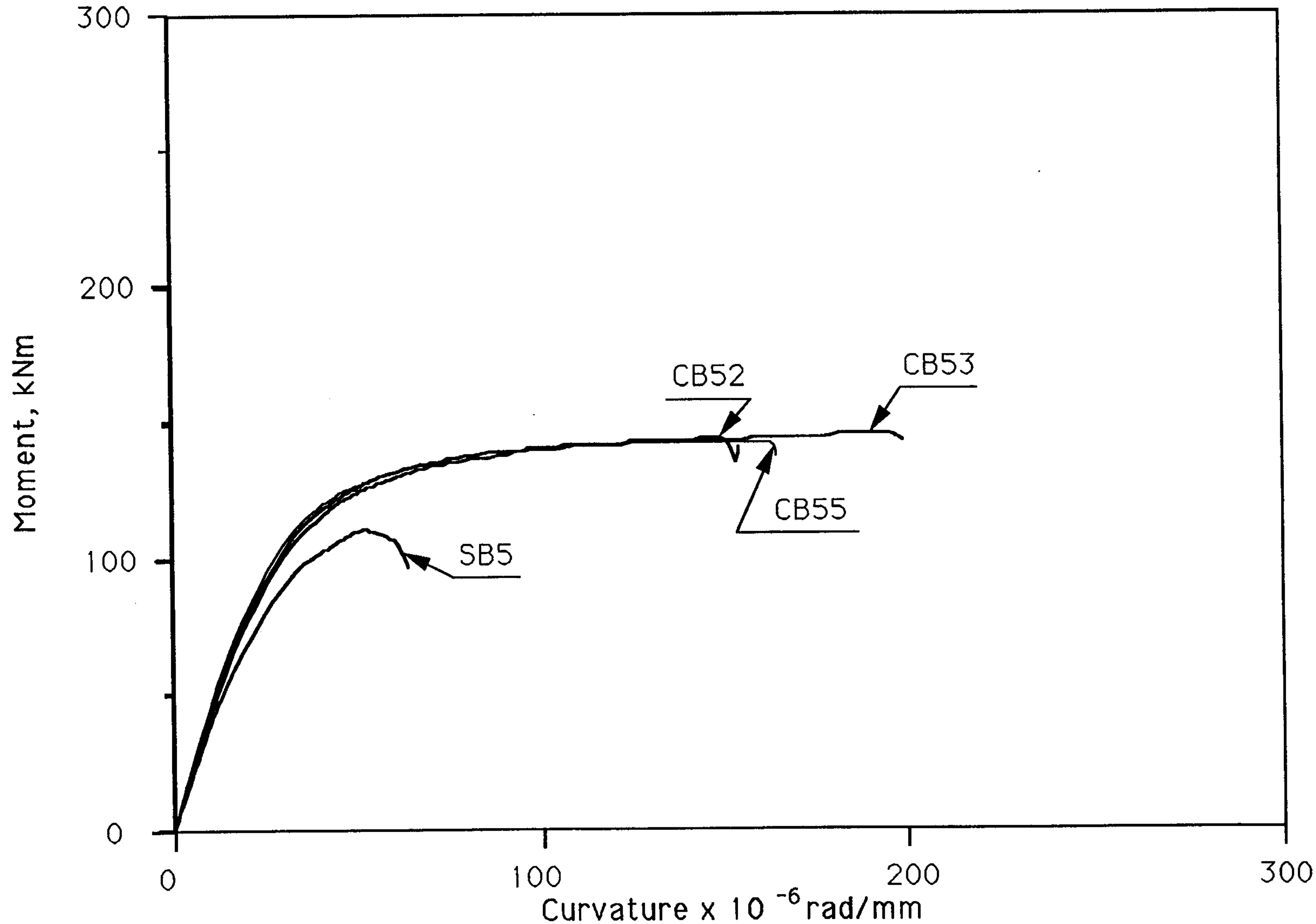

Figure 3.11 Moment-curvature Diagram, Section 5

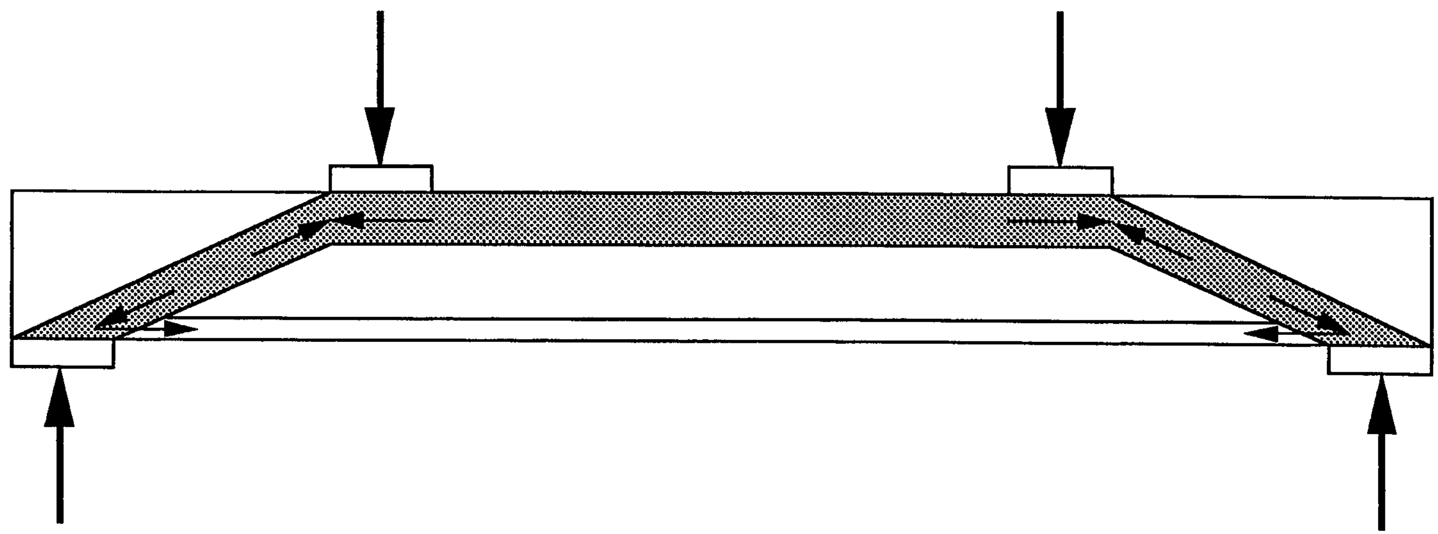

Figure 3.12 Tied-arch Model for Concrete

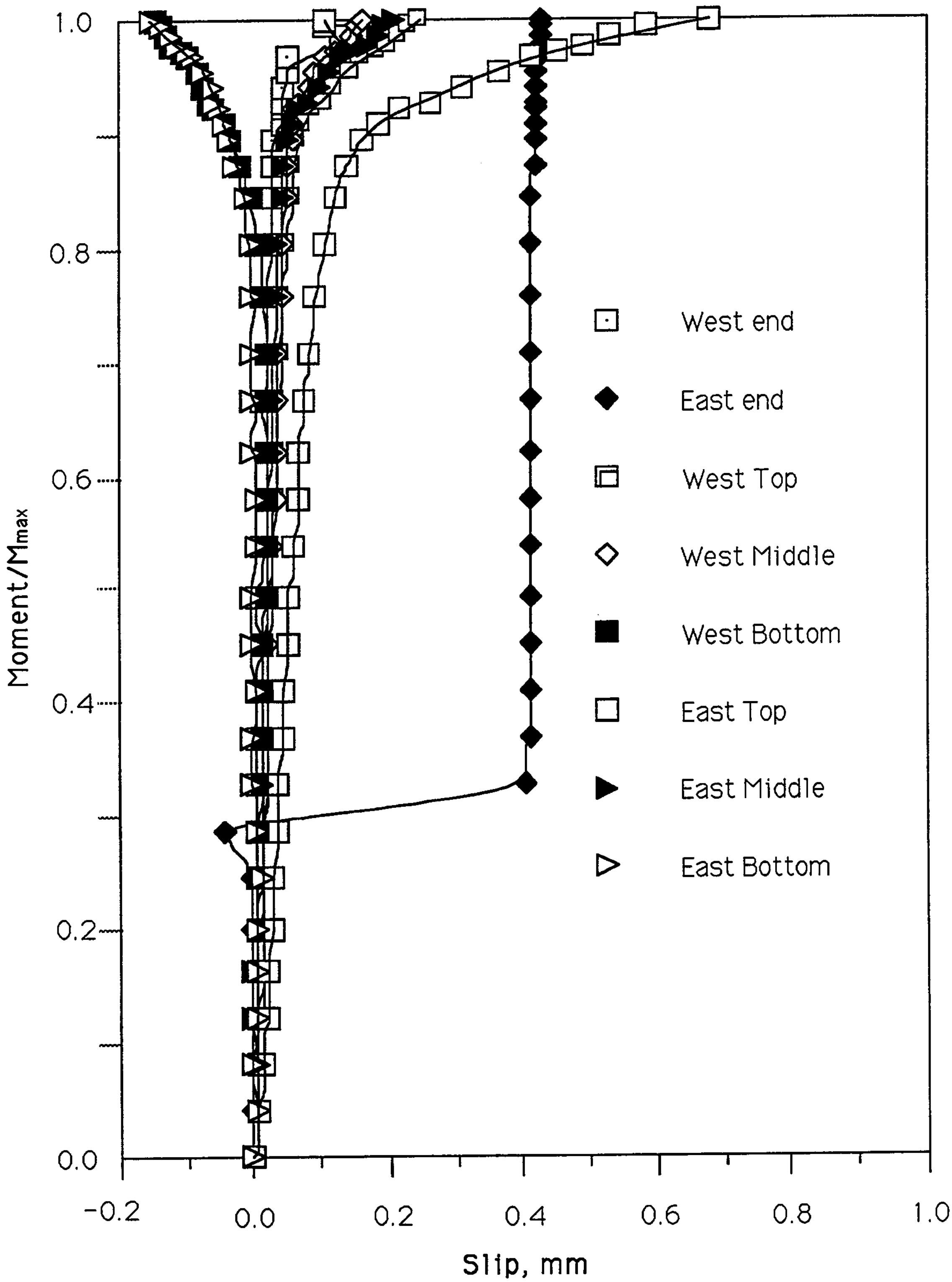

Figure 3.13 Steel/Concrete Slip, Beam CB12

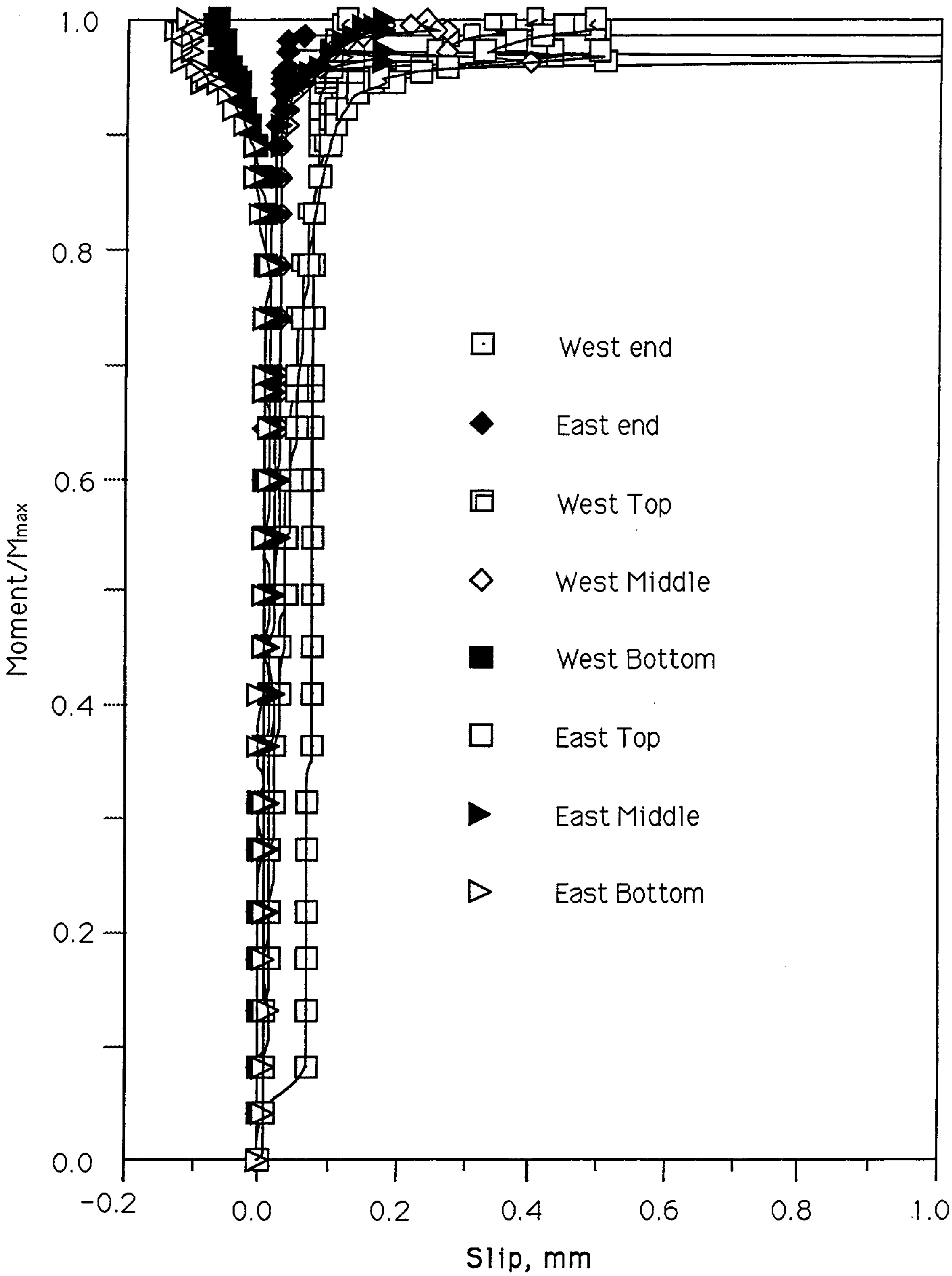

Figure 3.14 Steel/Concrete Slip, Beam CB13

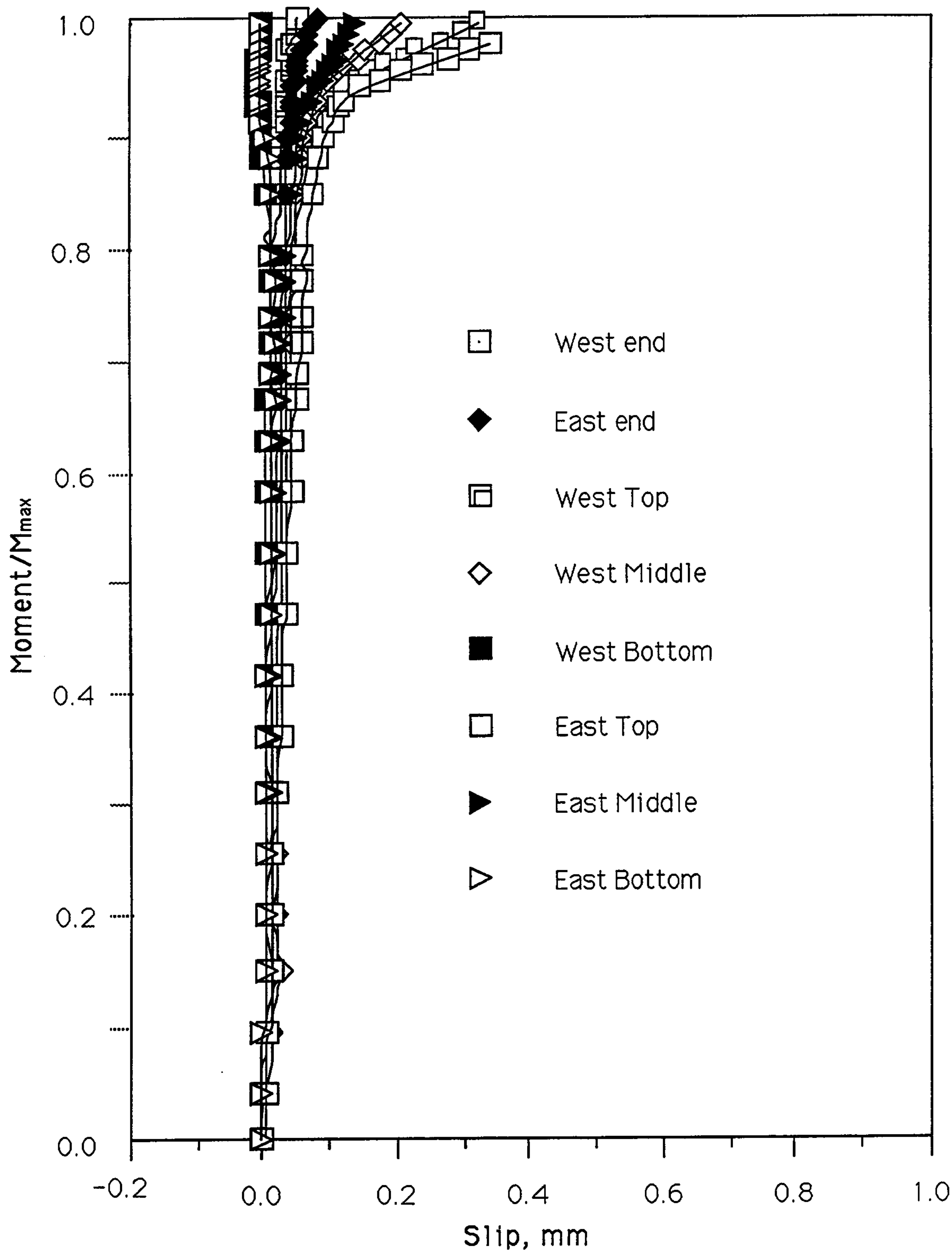

Figure 3.15 Steel/Concrete Slip, Beam CB15

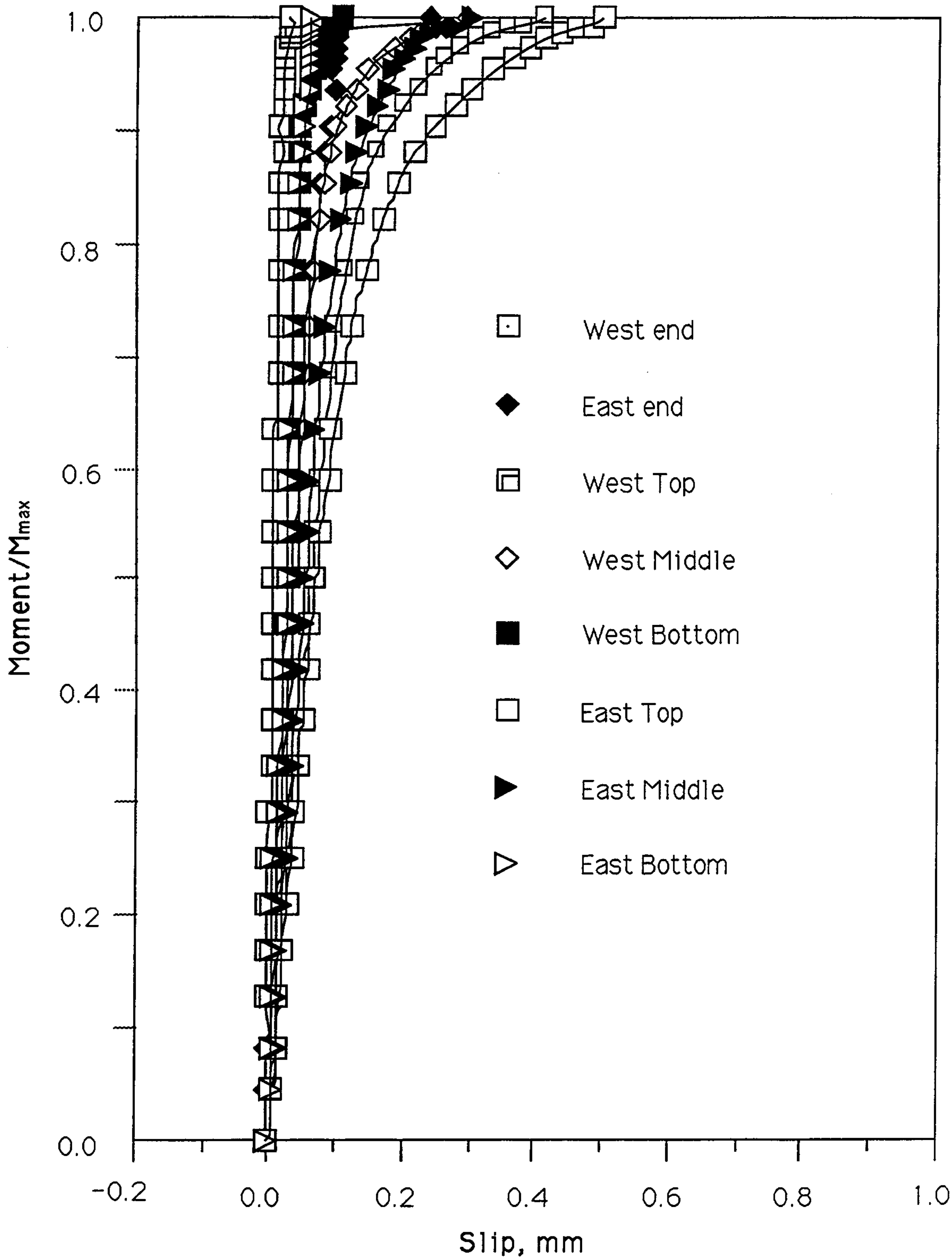

Figure 3.16 Steel/Concrete Slip, Beam CB22

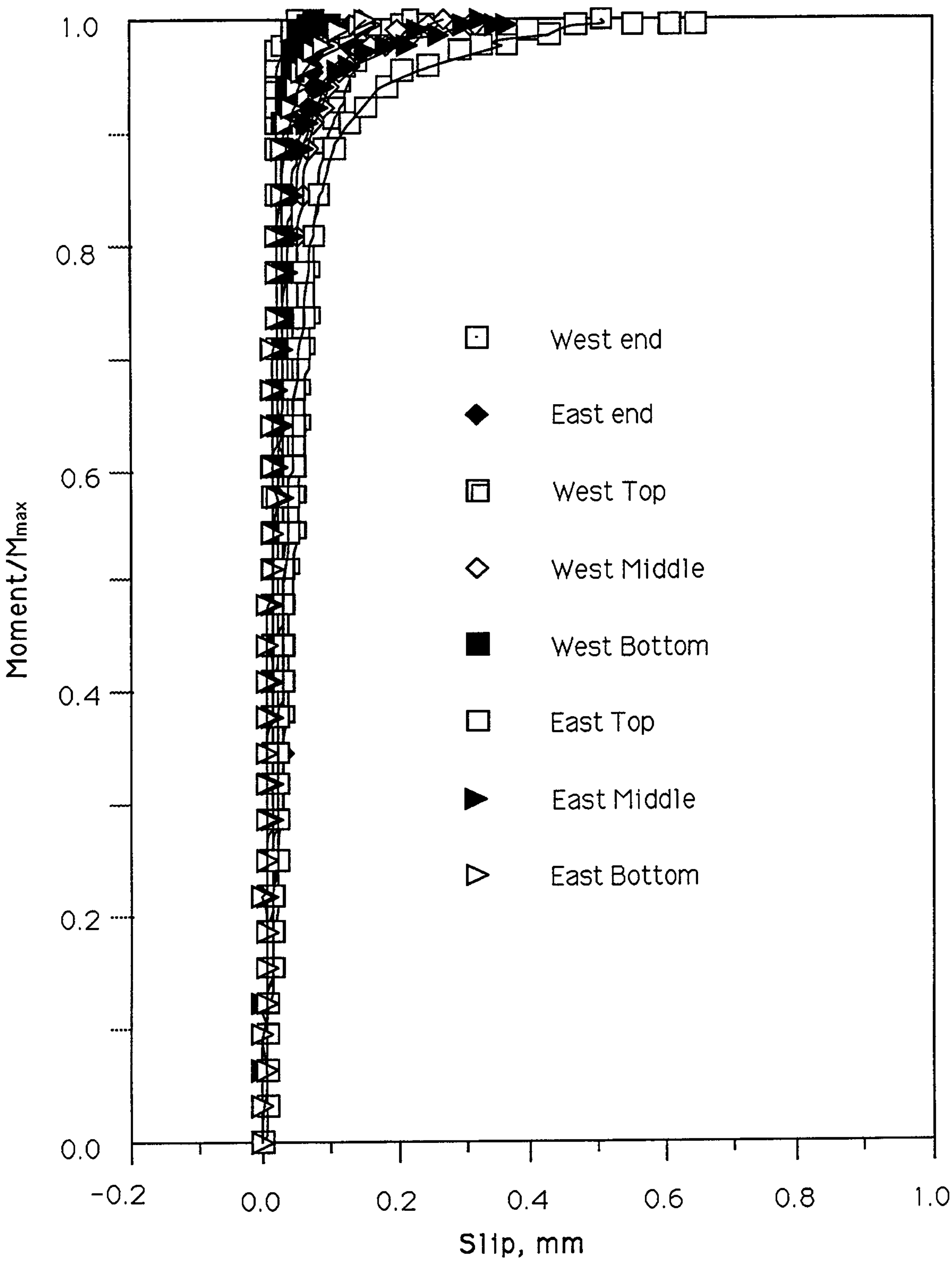

Figure 3.17 Steel/Concrete Slip, Beam CB31

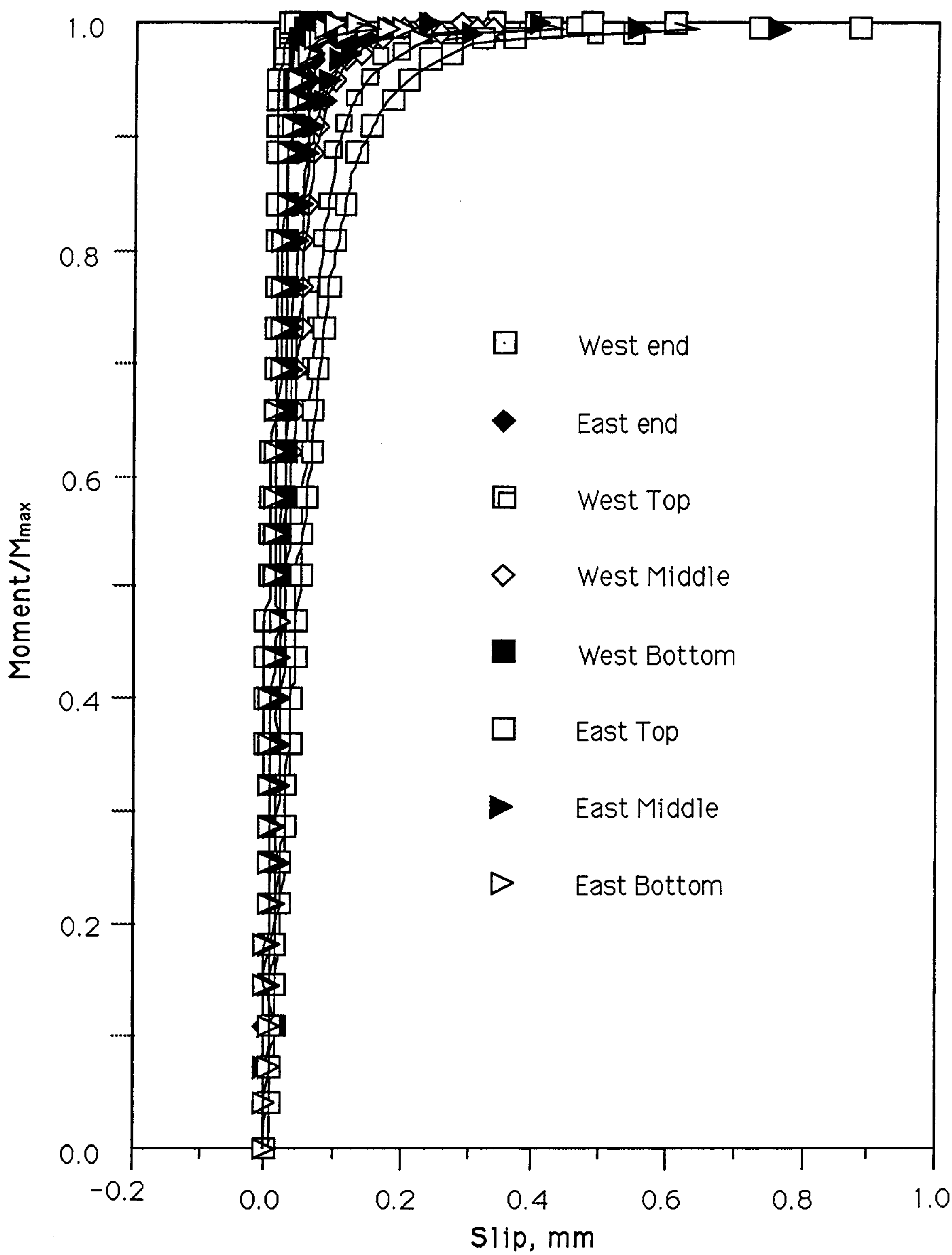

Figure 3.18 Steel/Concrete Slip, Beam CB33

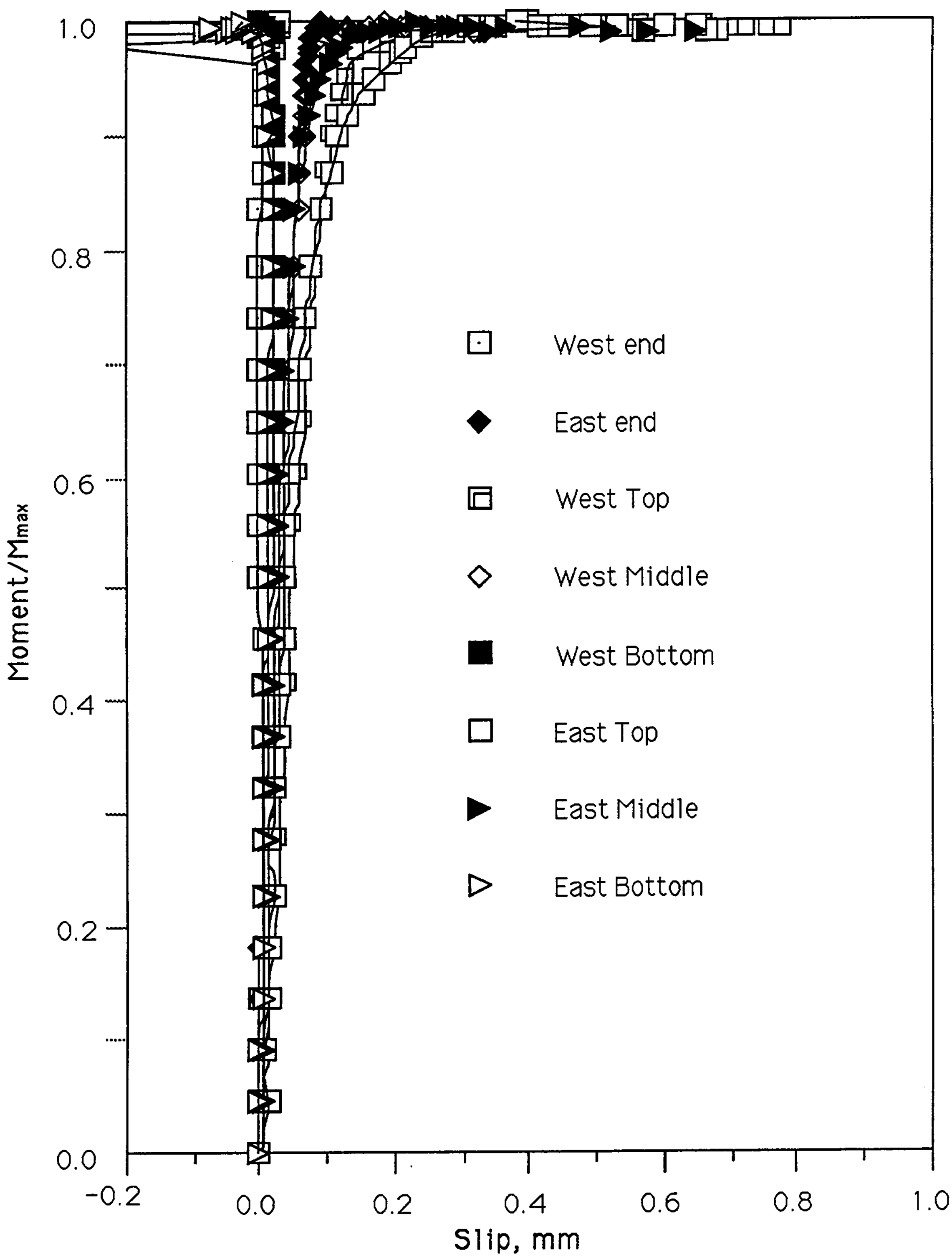

Figure 3.19 Steel/Concrete Slip, Beam CB35

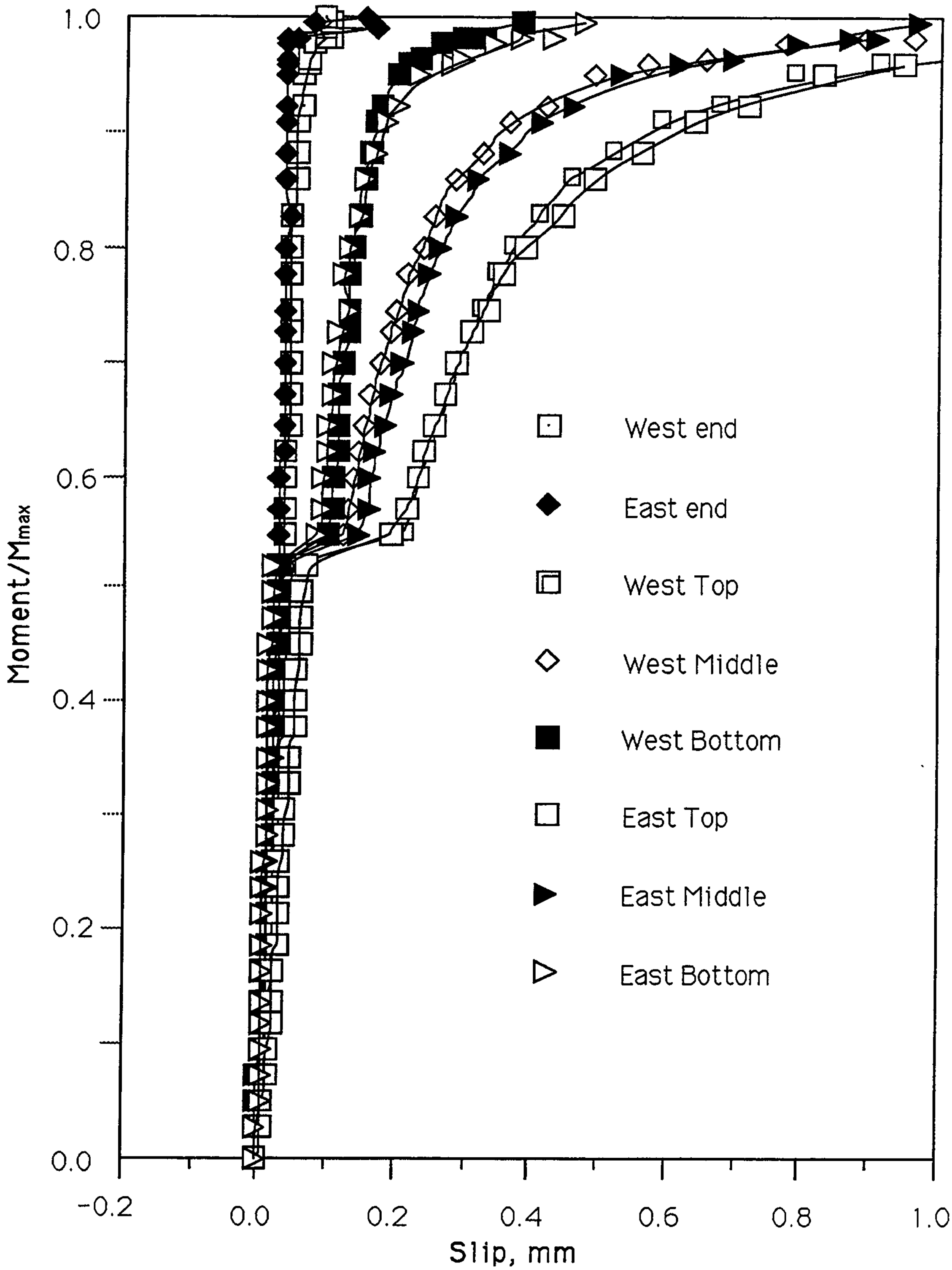

Figure 3.20 Steel/Concrete Slip, Beam CB41

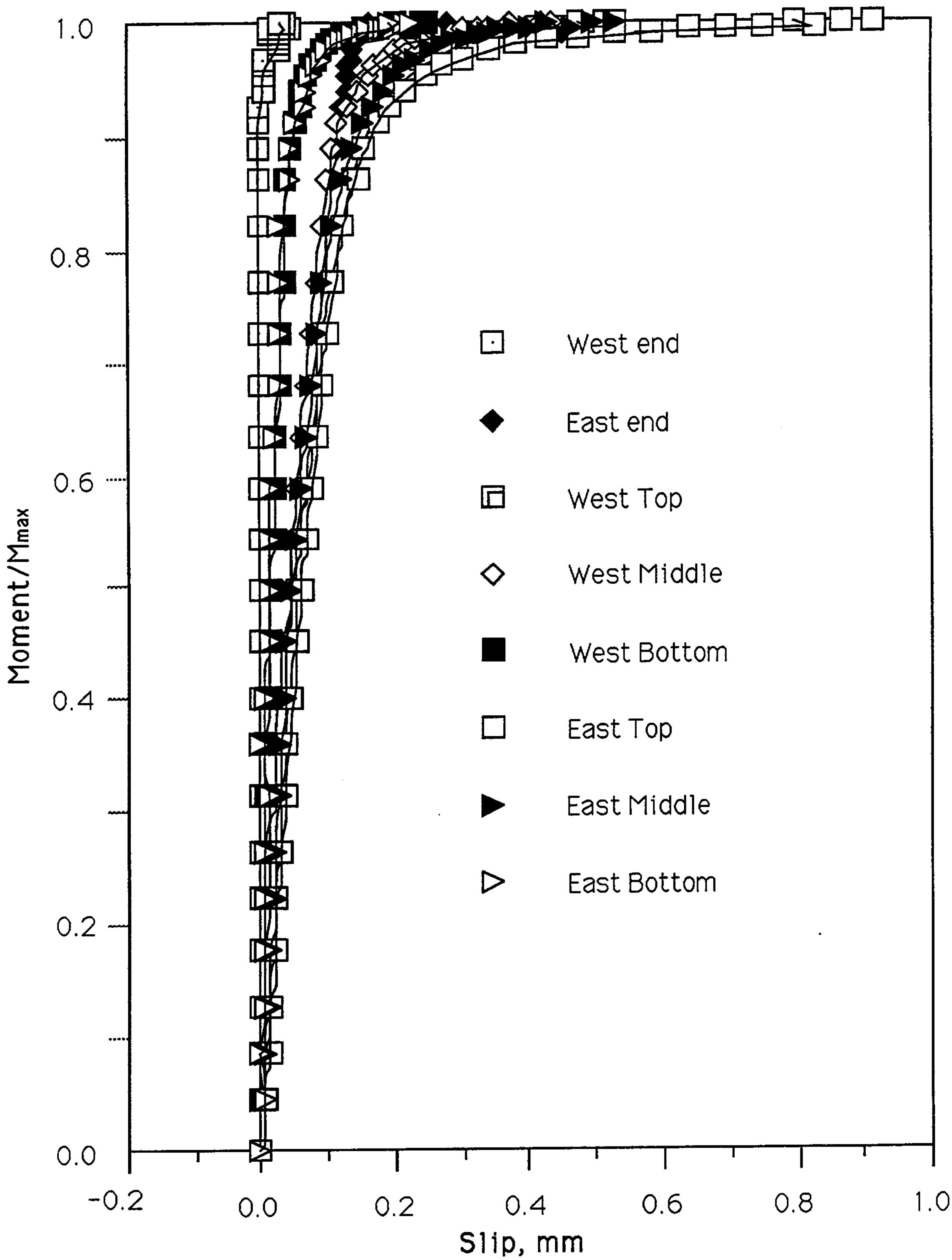

Figure 3.21 Steel/Concrete Slip, Beam CB45

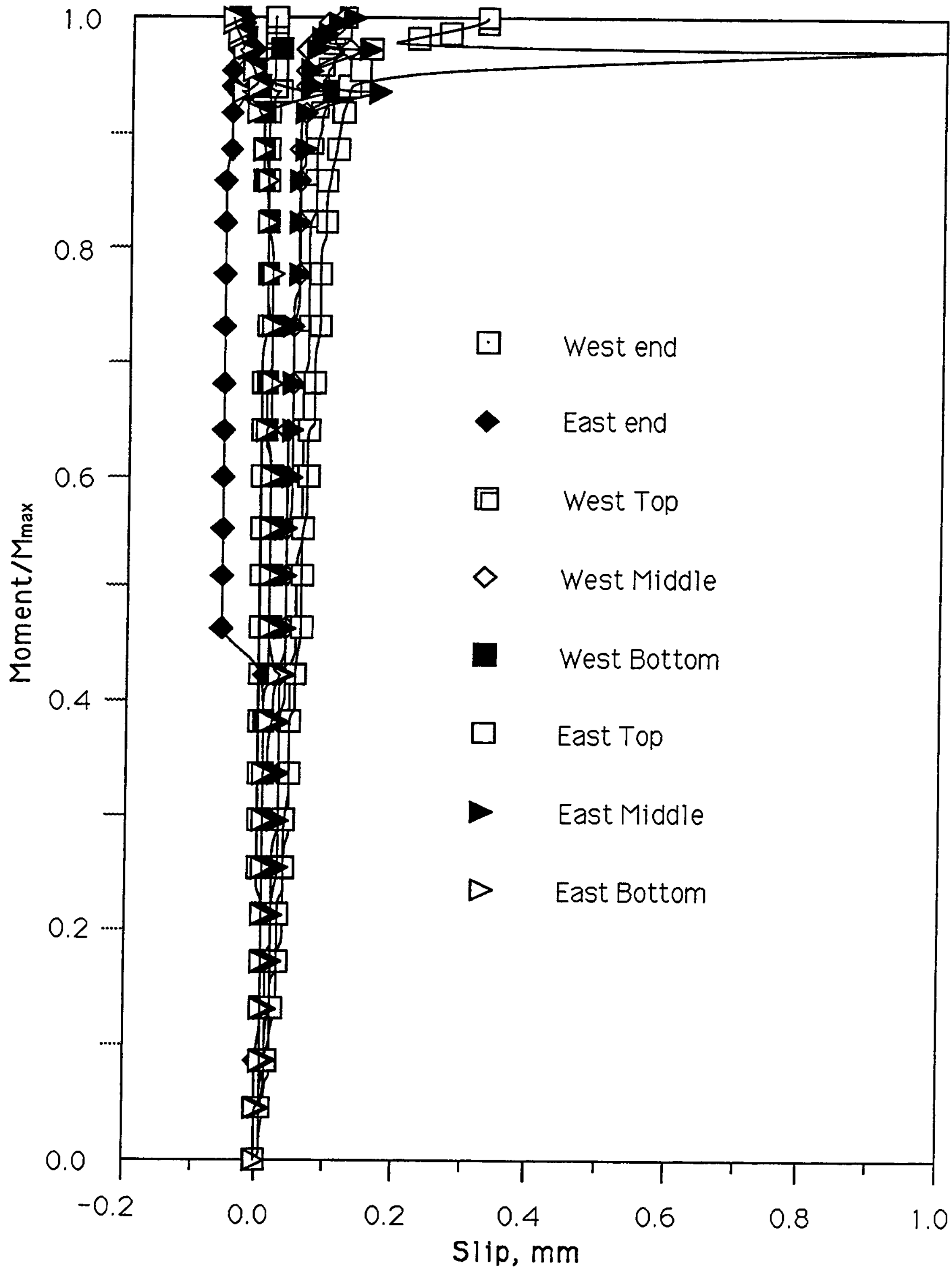

Figure 3.22 Steel/Concrete Slip, Beam CB52

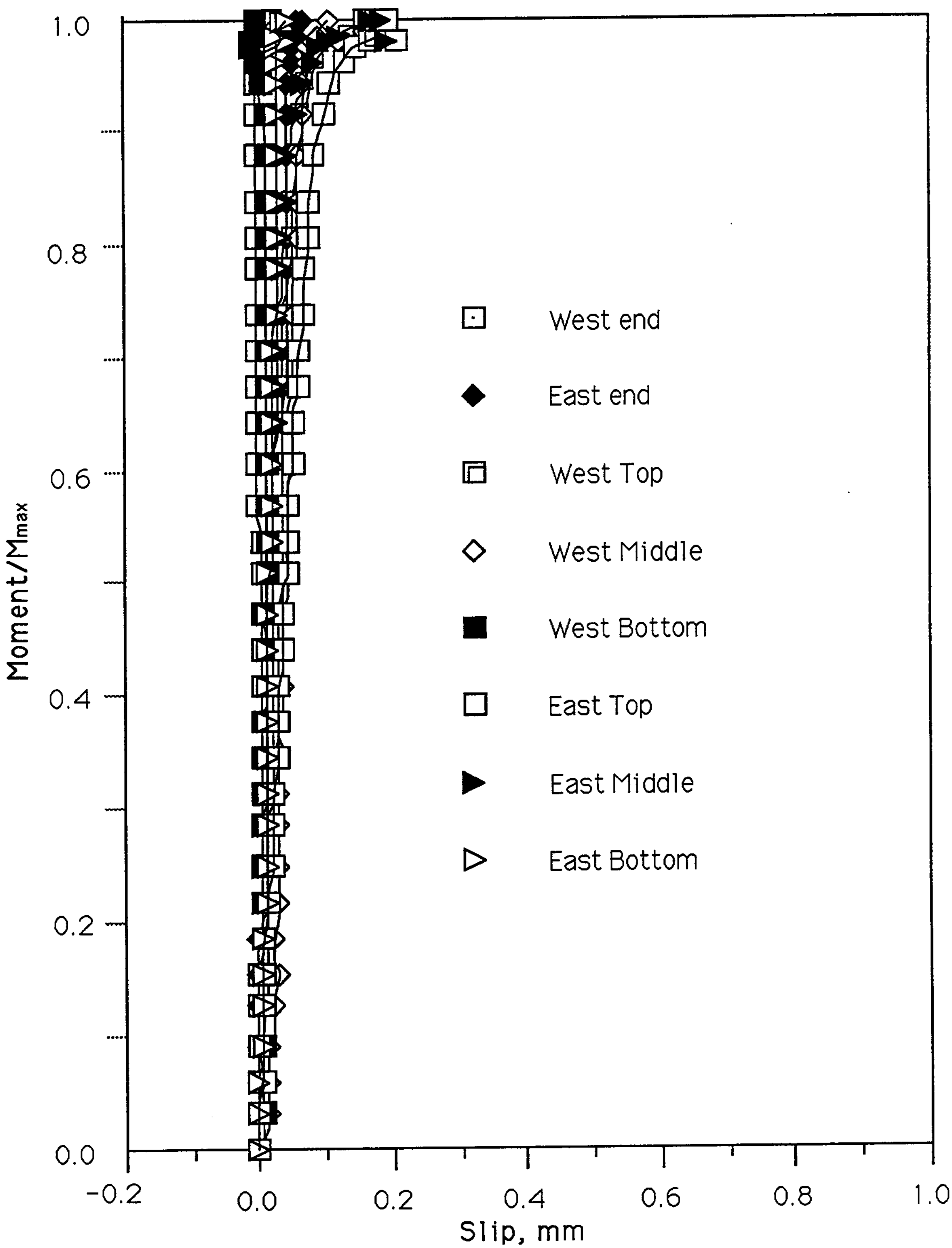

Figure 3.23 Steel/Concrete Slip, Beam CB53

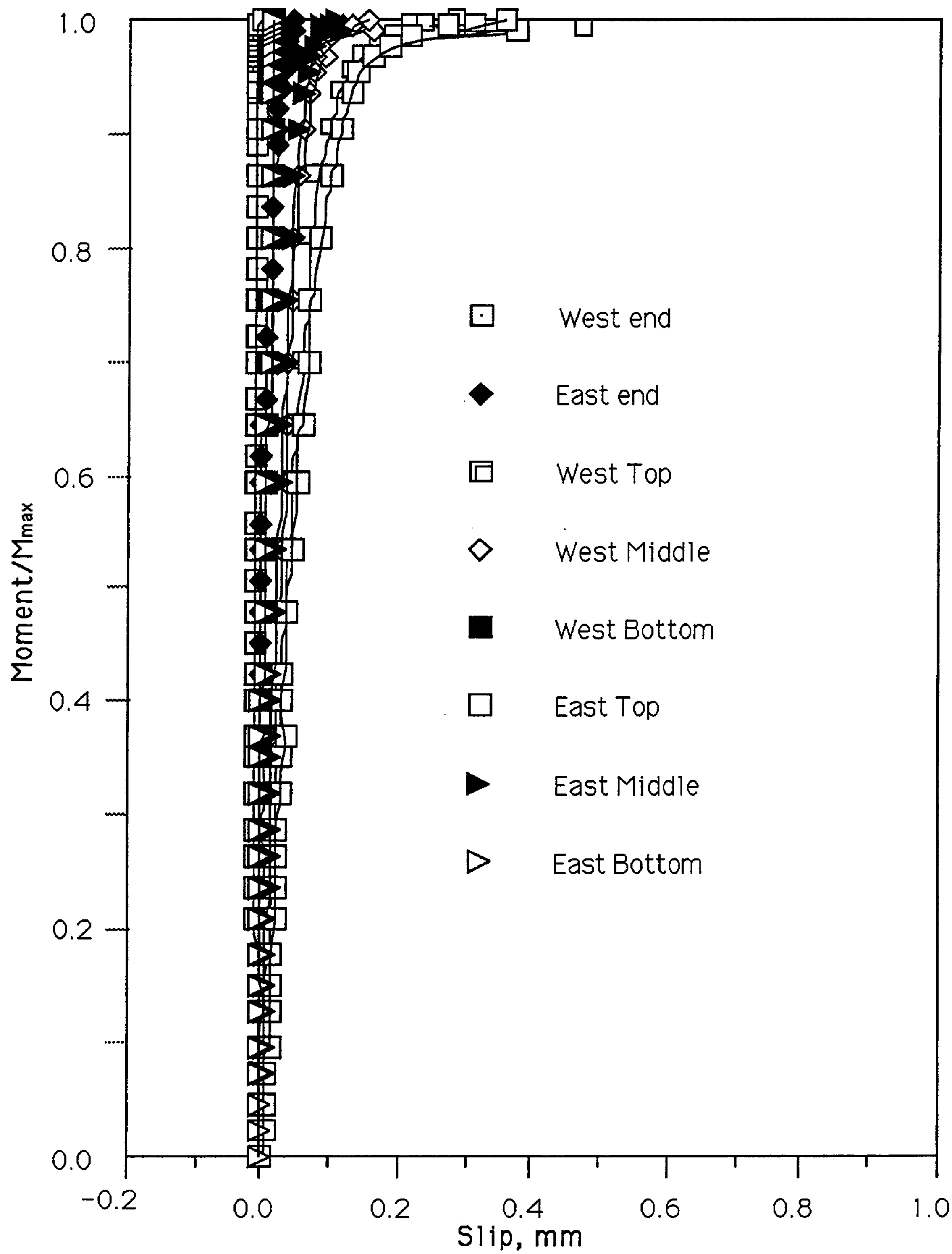

Figure 3.24 Steel/Concrete Slip, Beam CB55

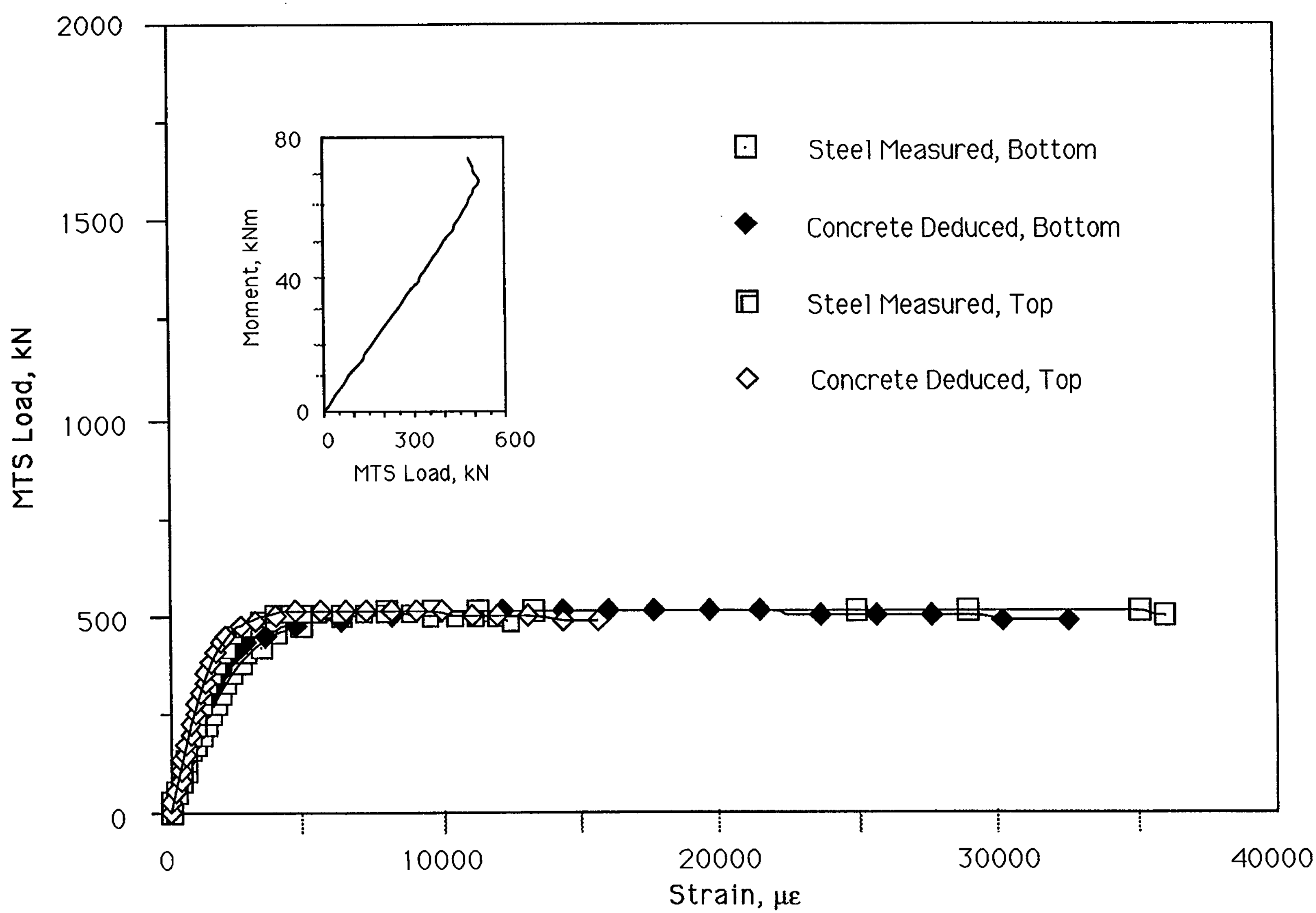

Figure 3.25 MTS Load versus Strain, Beam CB12

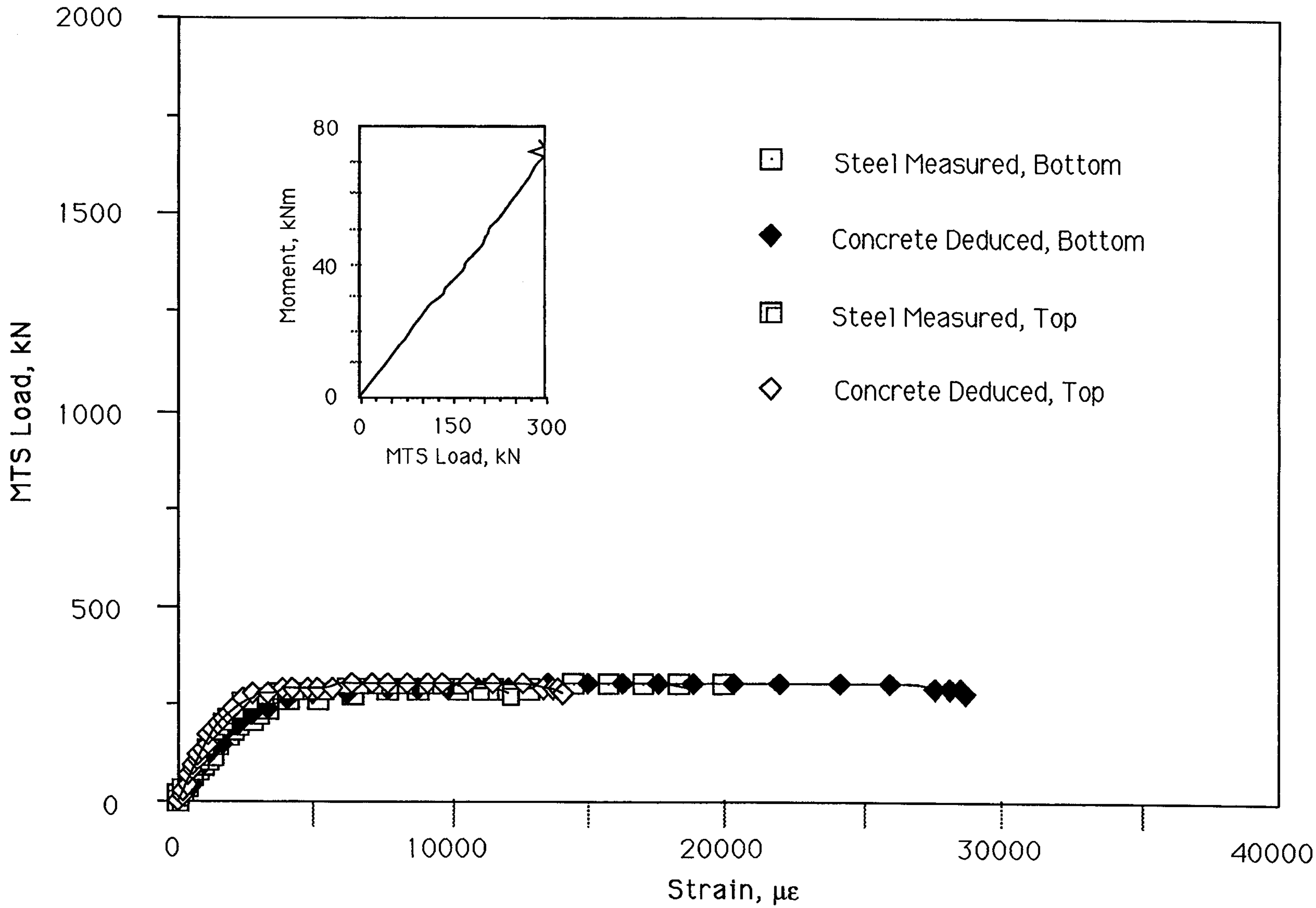

Figure 3.26 MTS Load versus Strain, Beam CB13

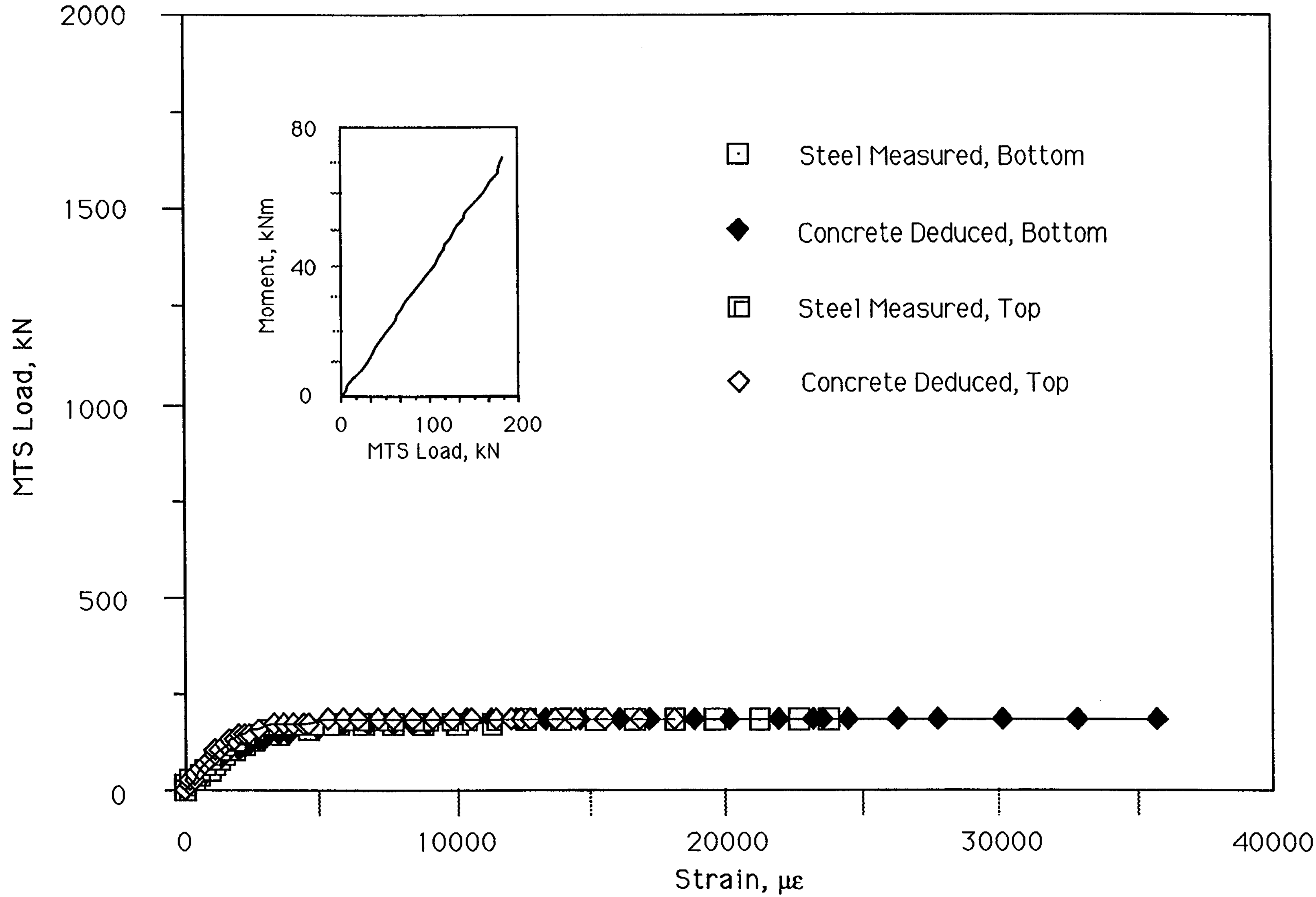

Figure 3.27 MTS Load versus Strain, Beam CB15

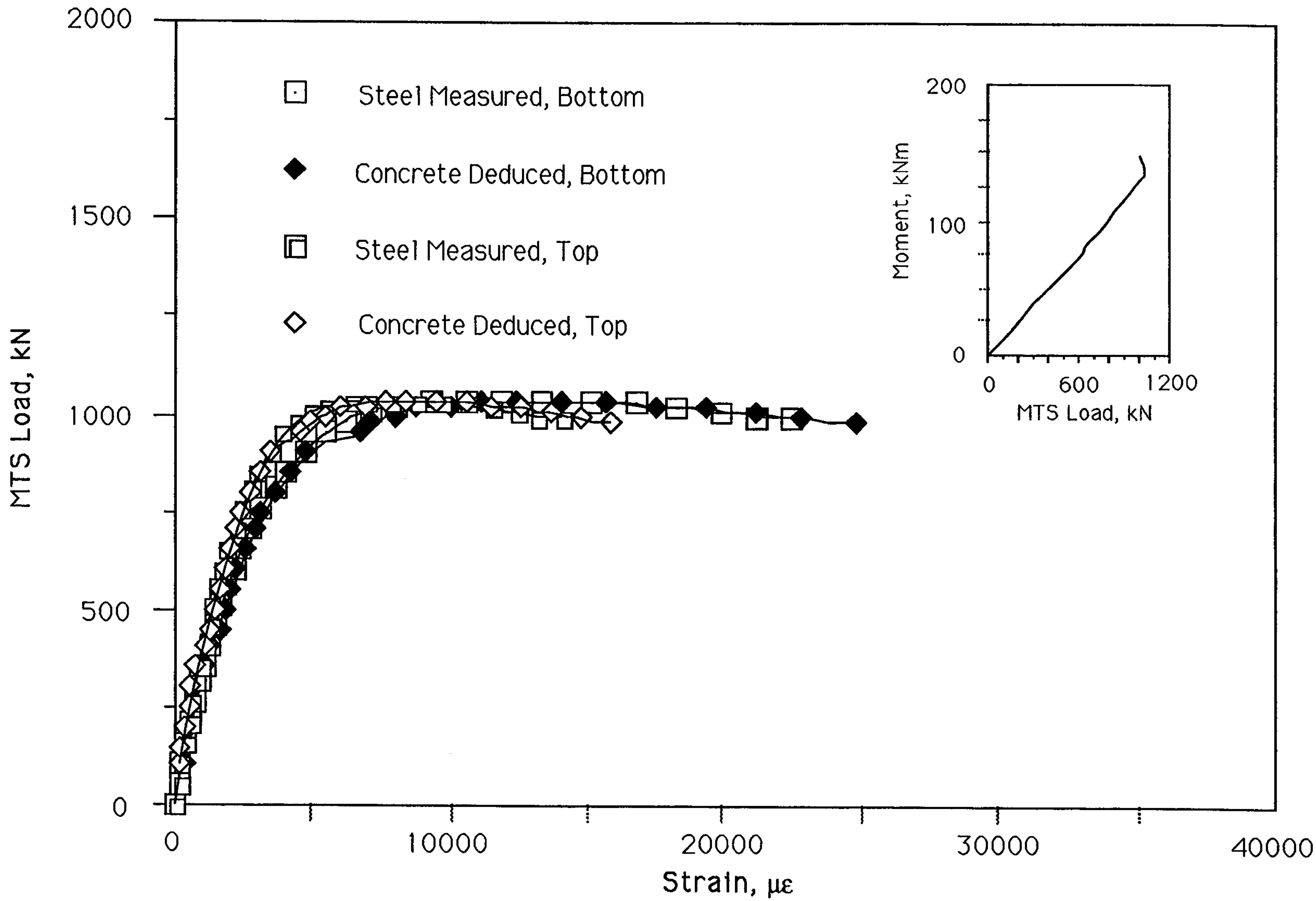

Figure 3.28 MTS Load versus Strain, Beam CB22

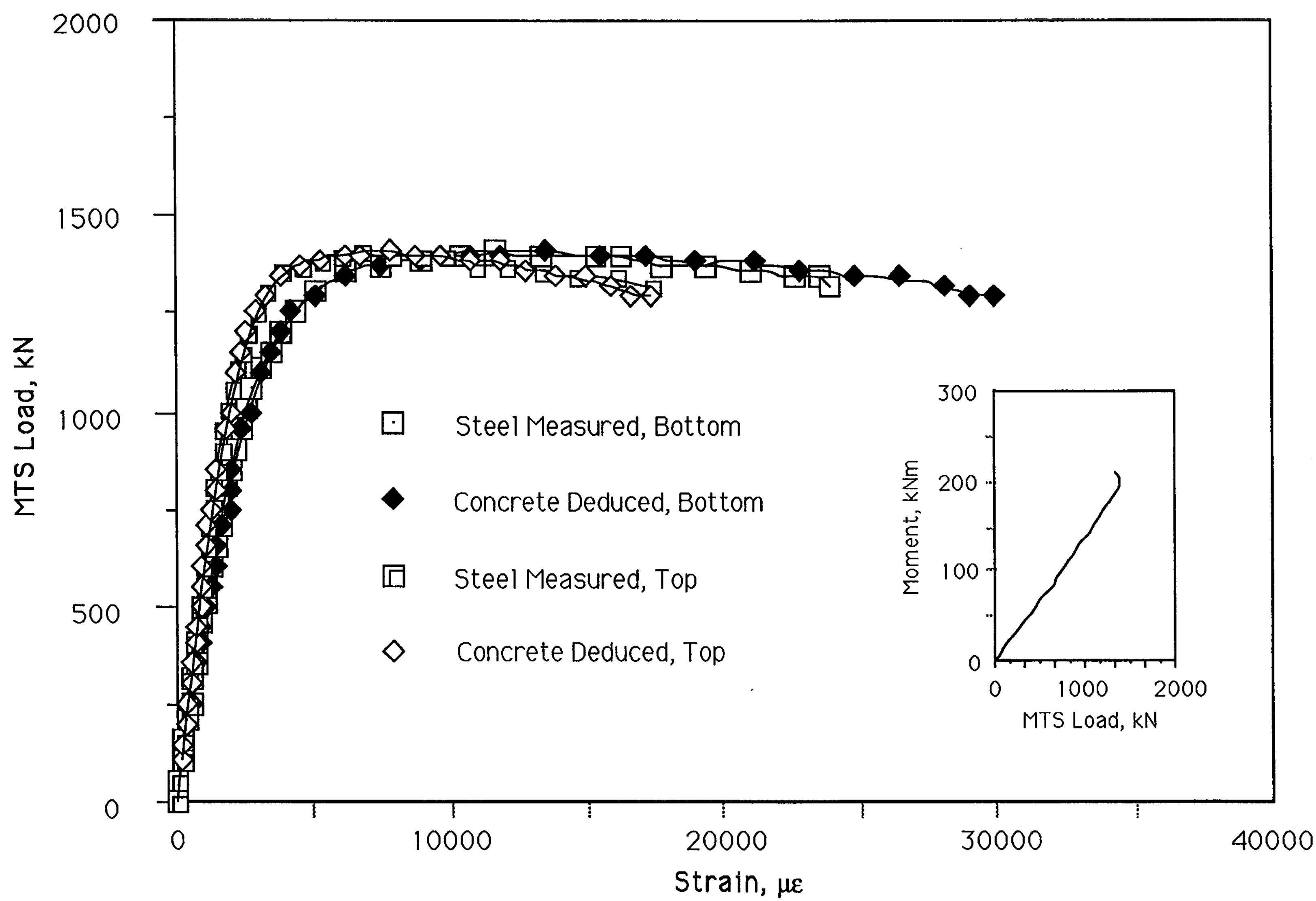

Figure 3.29 MTS Load versus Strain, Beam CB31

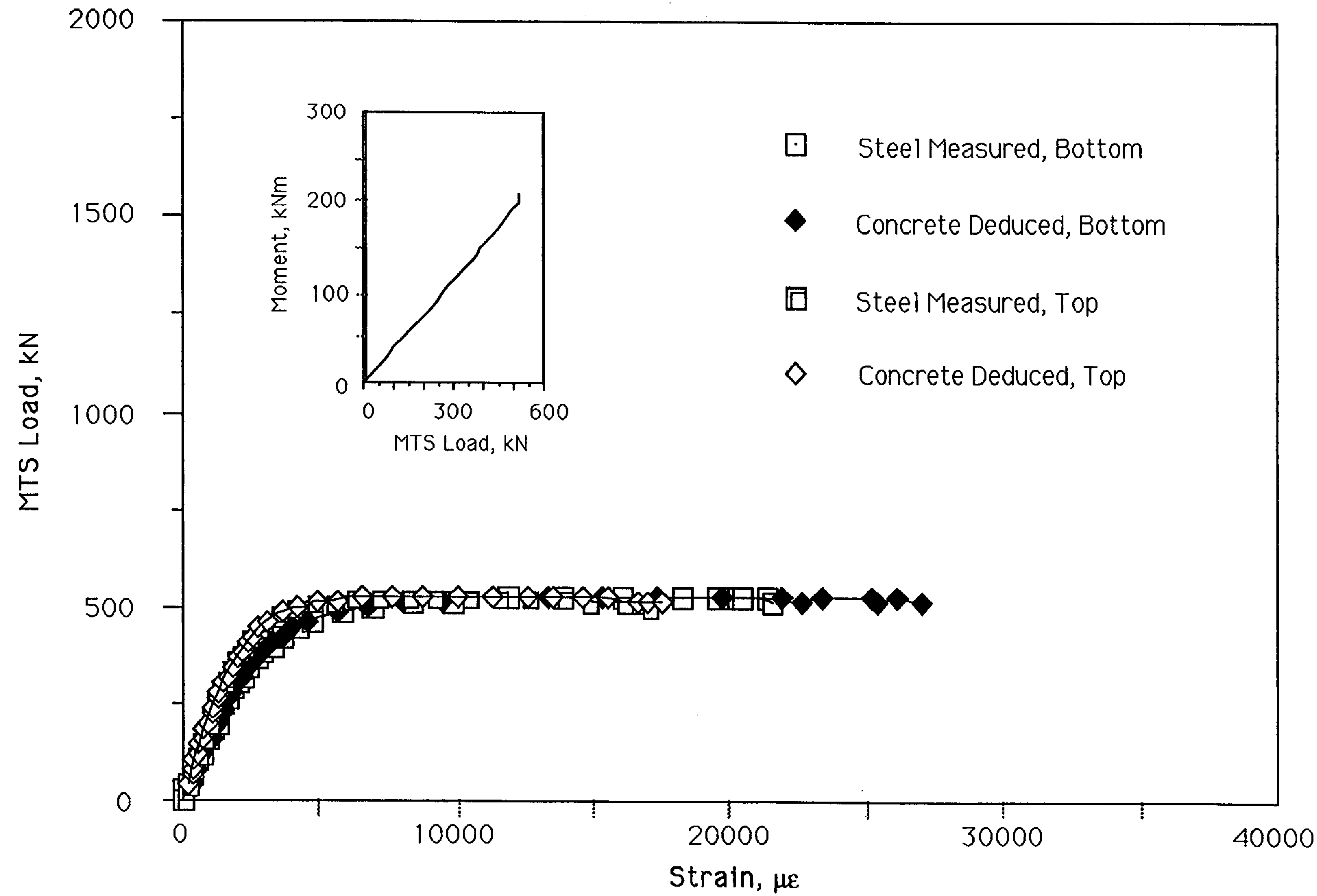

Figure 3.30 MTS Load versus Strain, Beam CB33

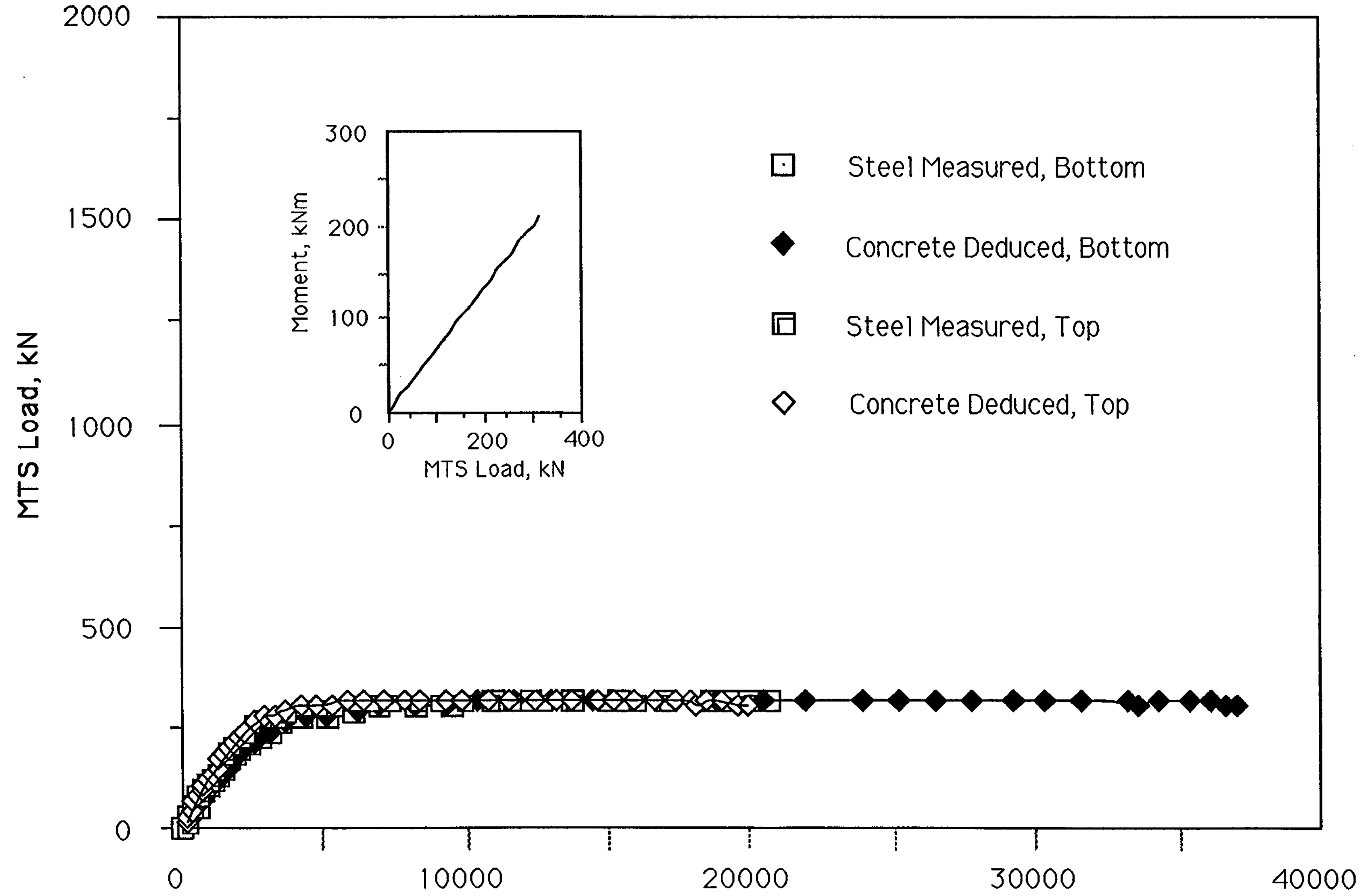

Figure 3.31 MTS Load versus Strain, Beam CB35

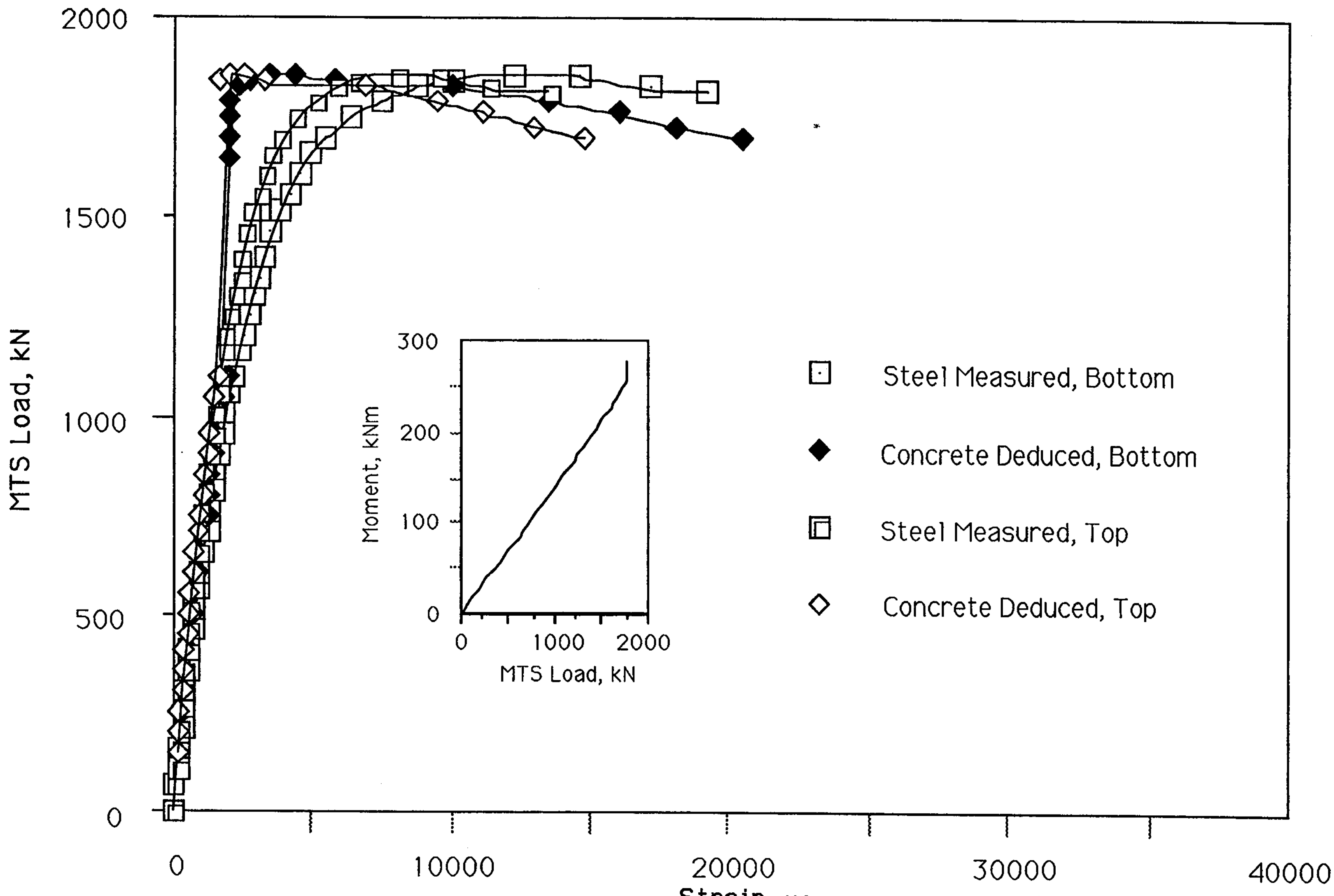

Figure 3.32 MTS Load versus Strain, Beam CB41

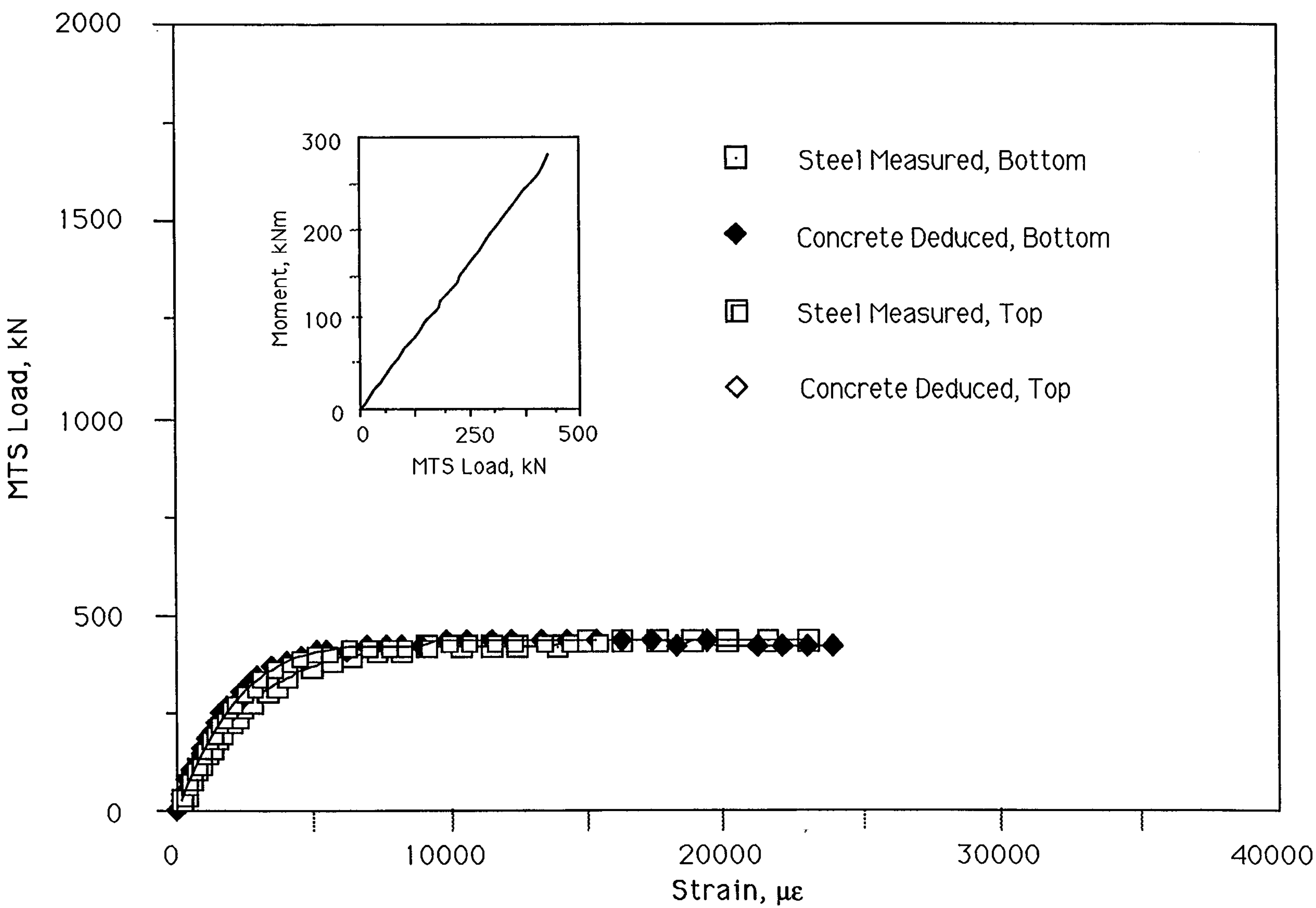

Figure 3.33 MTS Load versus Strain, Beam CB45

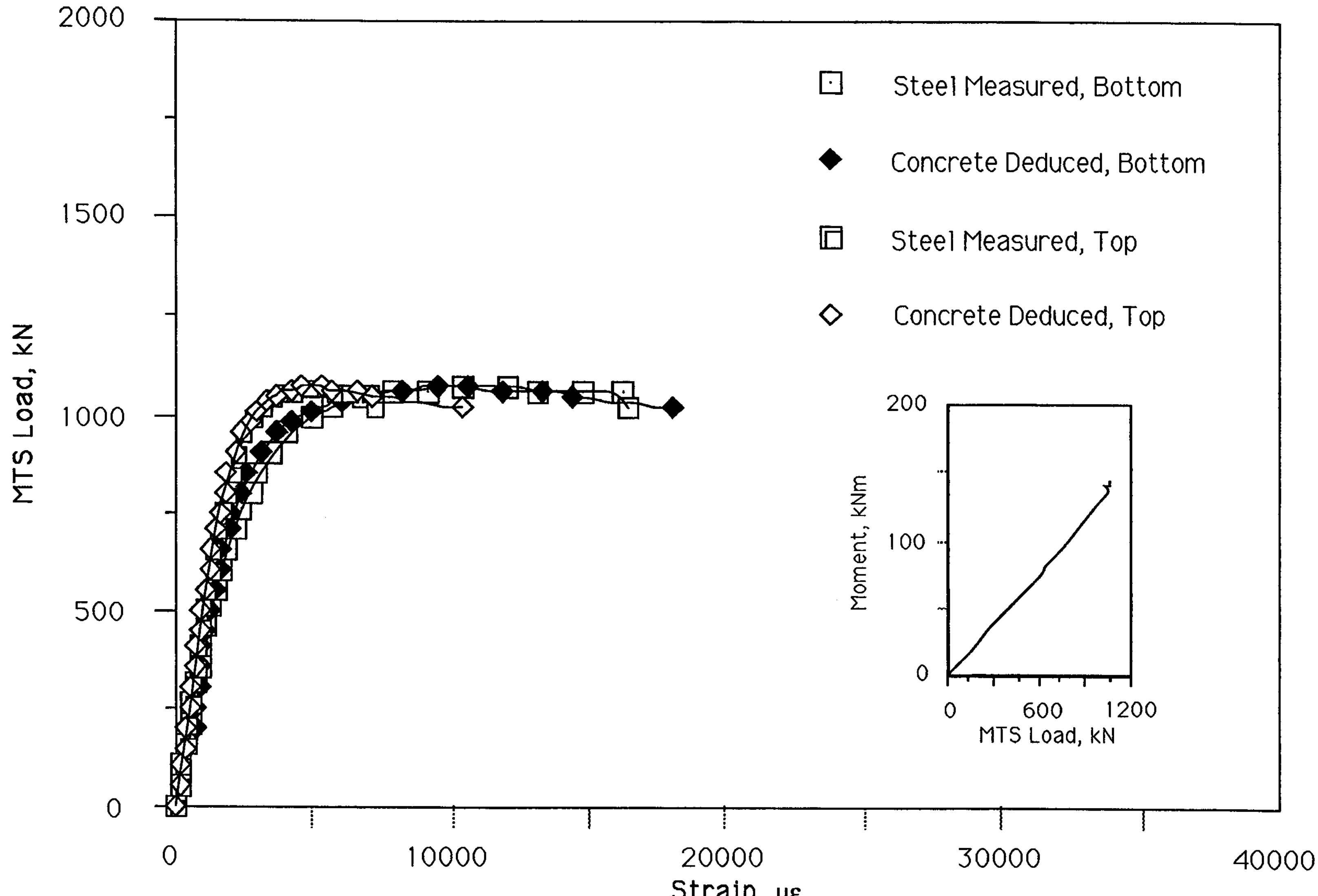

Figure 3.34 MTS Load versus Strain, Beam CB51

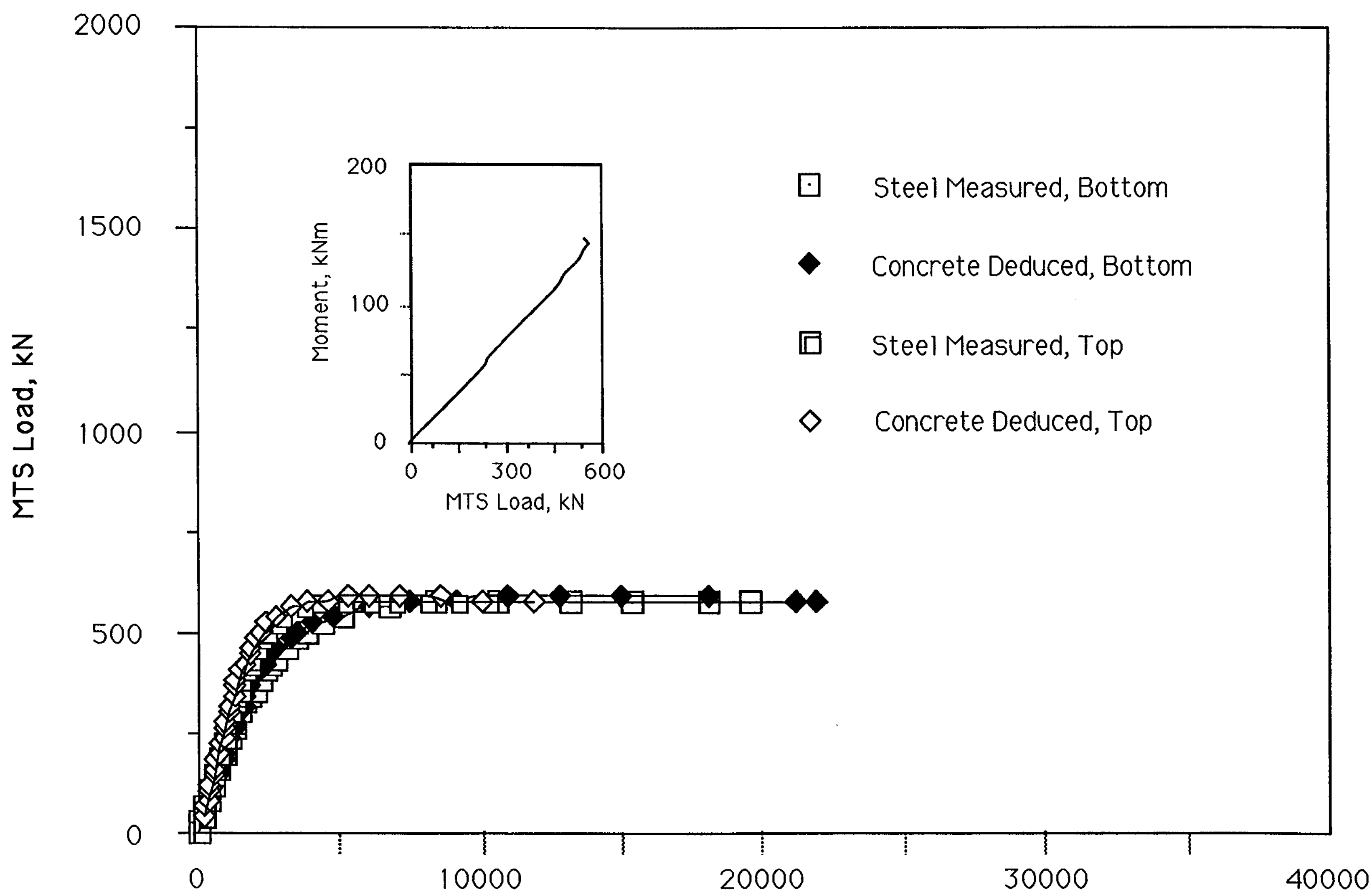

Figure 3.35 MTS Load versus Strain, Beam CB53

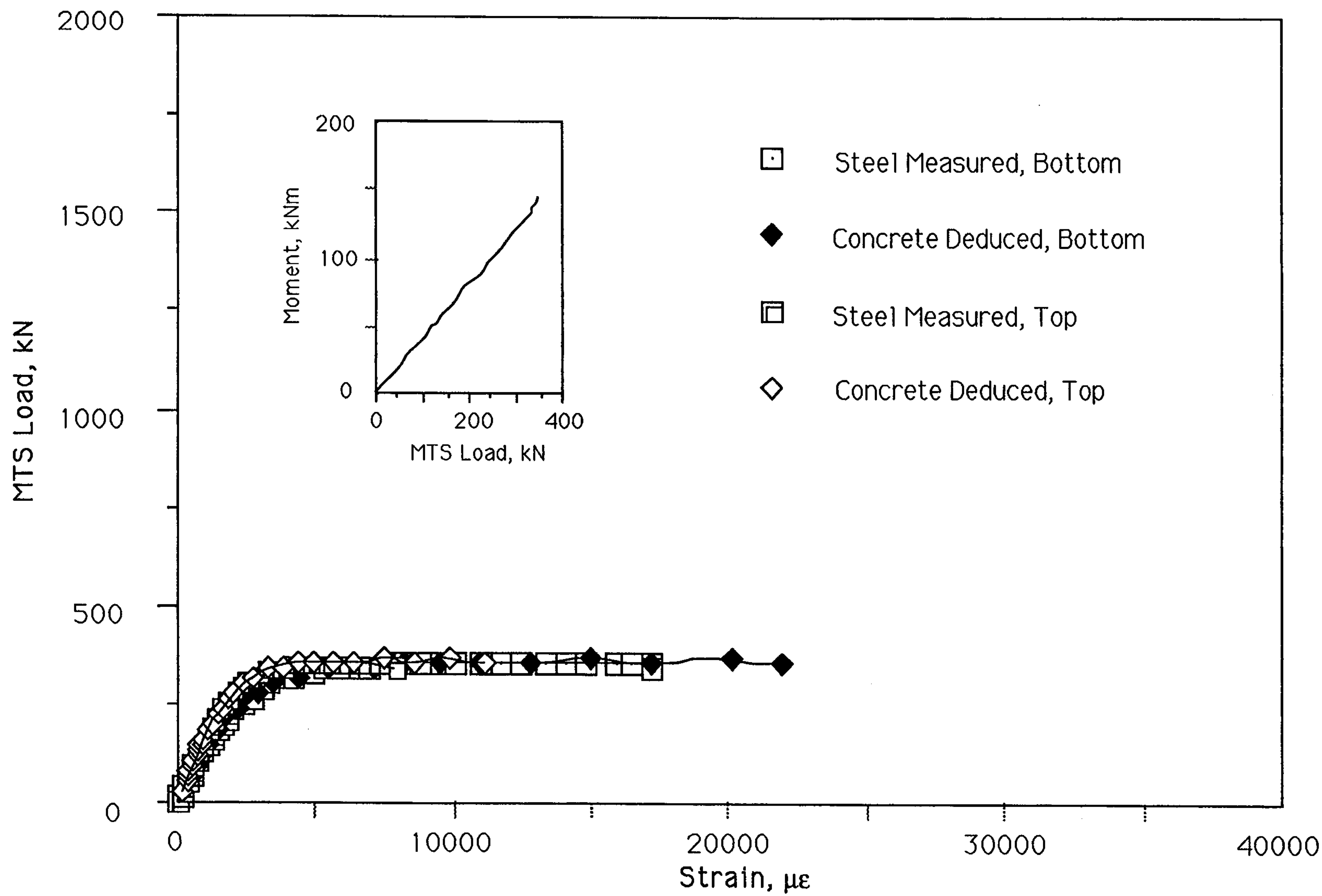

Figure 3.36 MTS Load versus Strain, Beam CB55

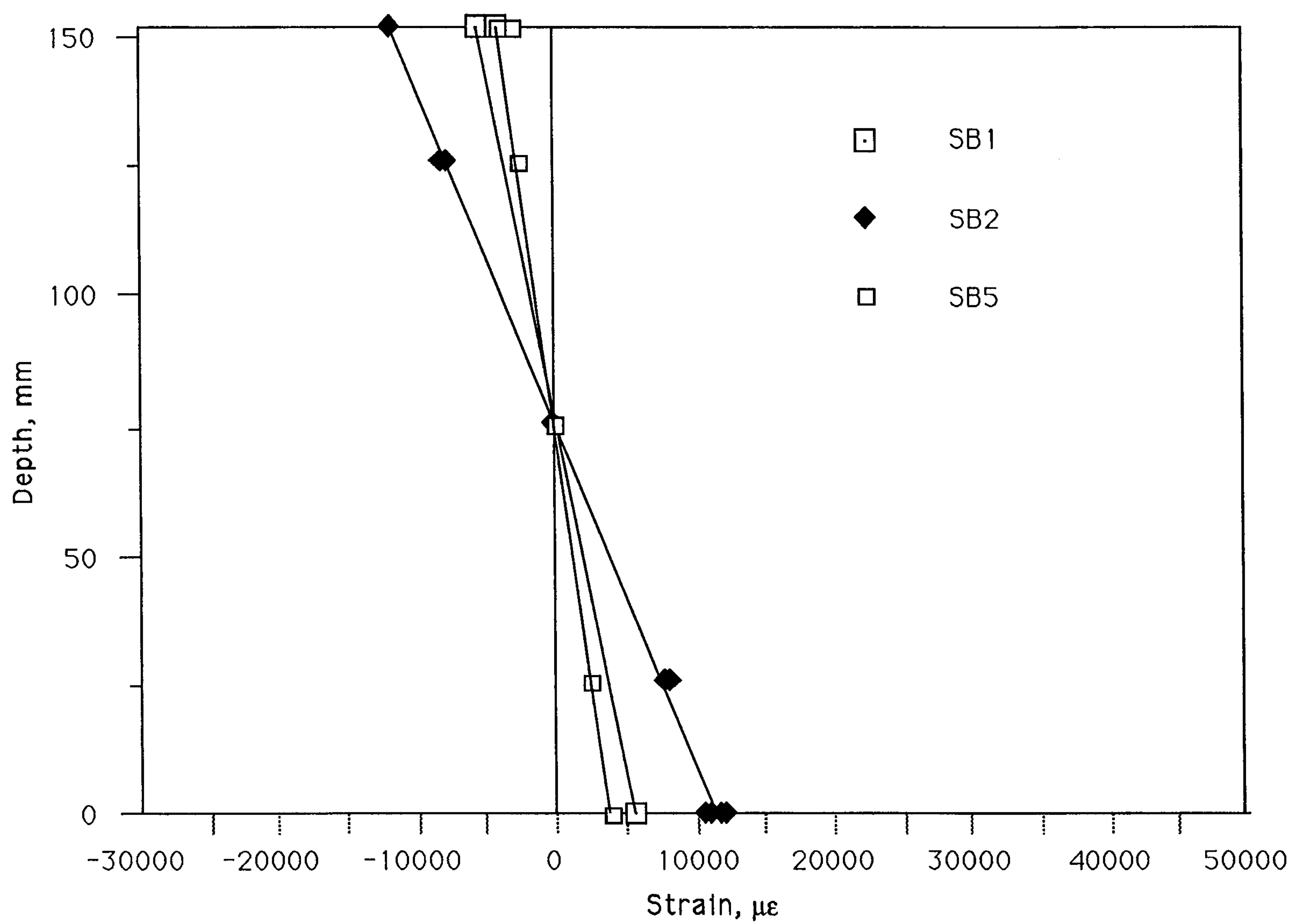

Figure 3.37 Strain Distribution Across Depth at Maximum Moment, Steel Beams 1, 2 and 5

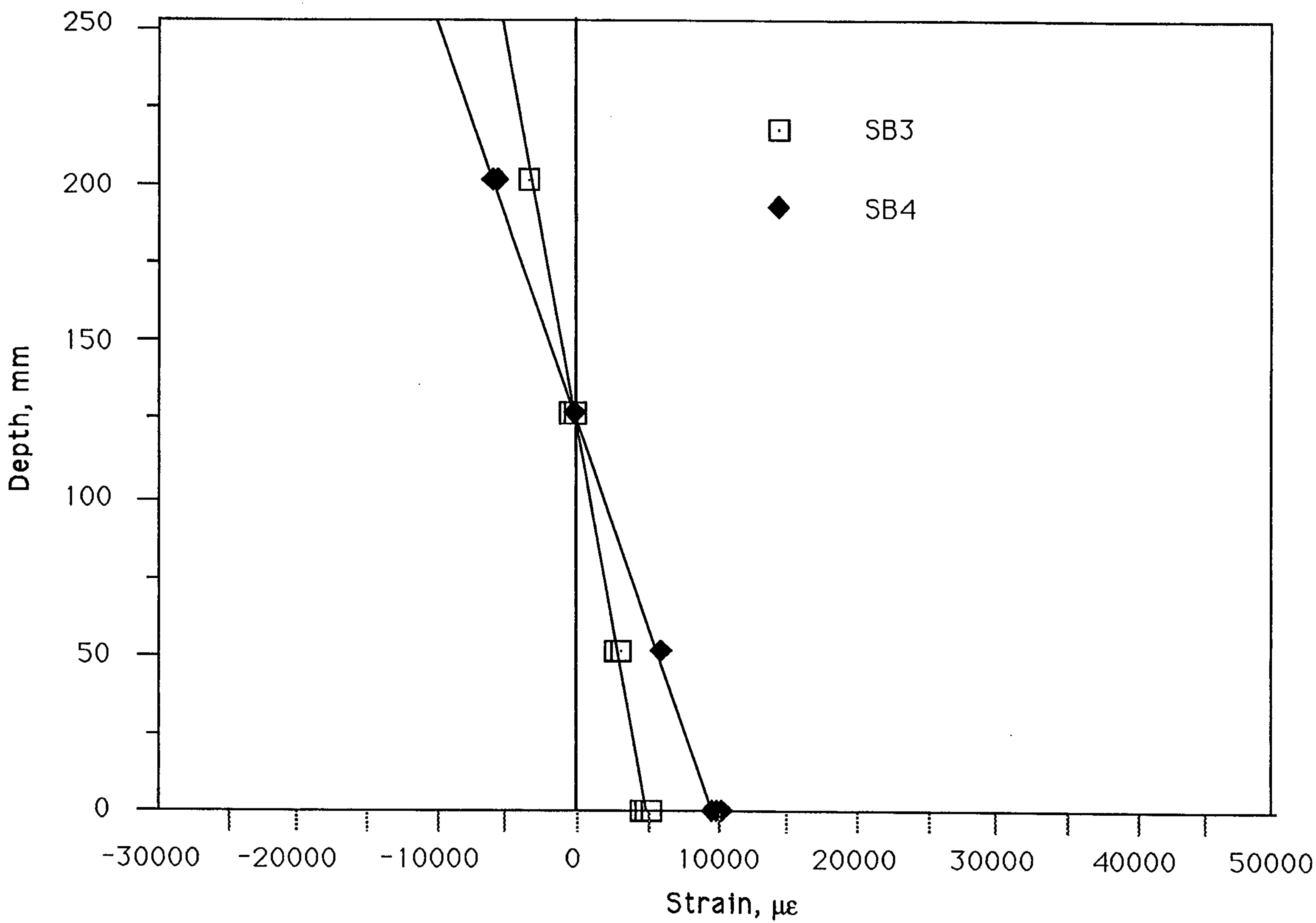

Figure 3.38 Strain Distribution Across Depth at Maximum Moment, Steel Beams 3 and 4

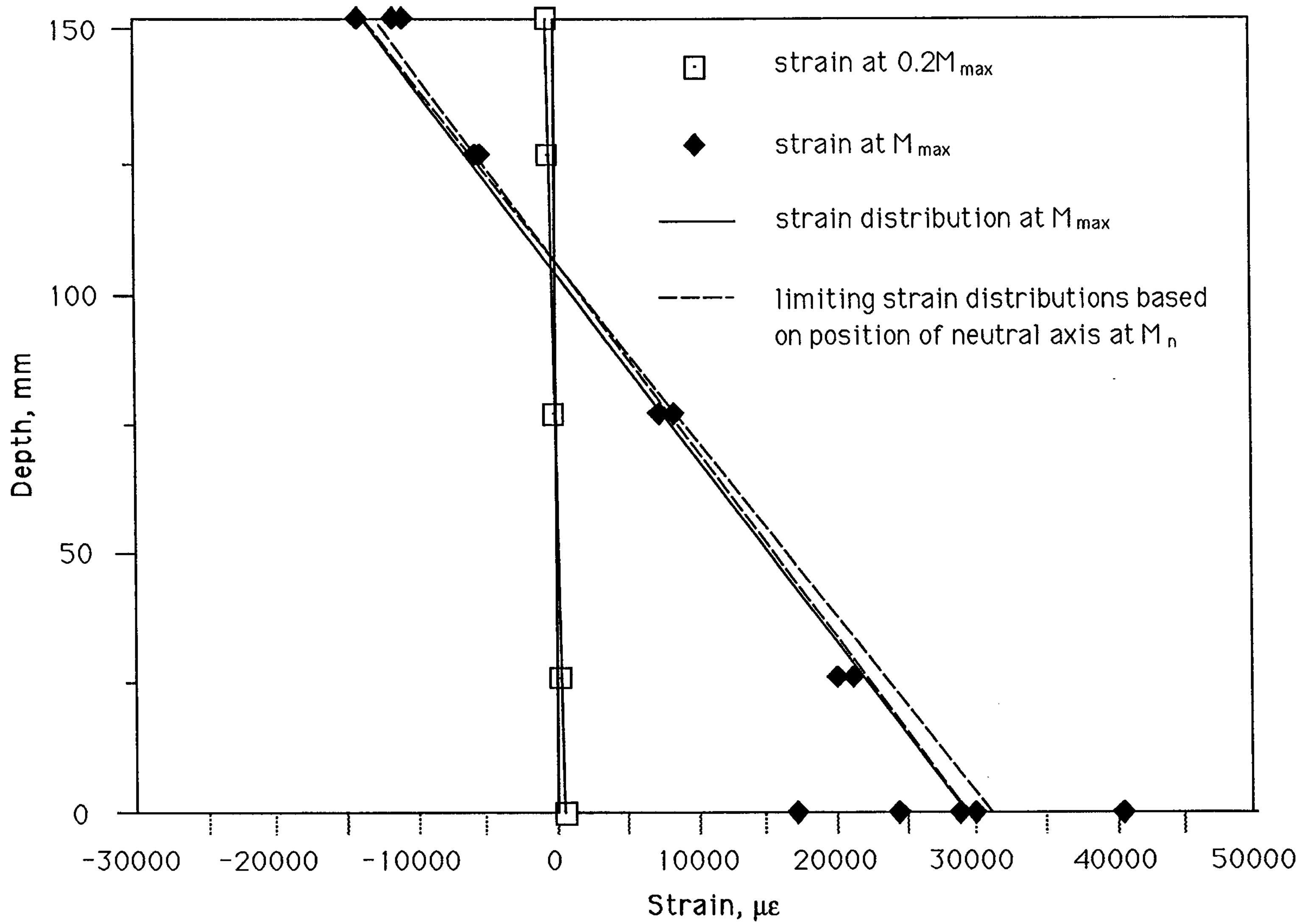

Figure 3.39 Strain Distribution Across Depth, CB12

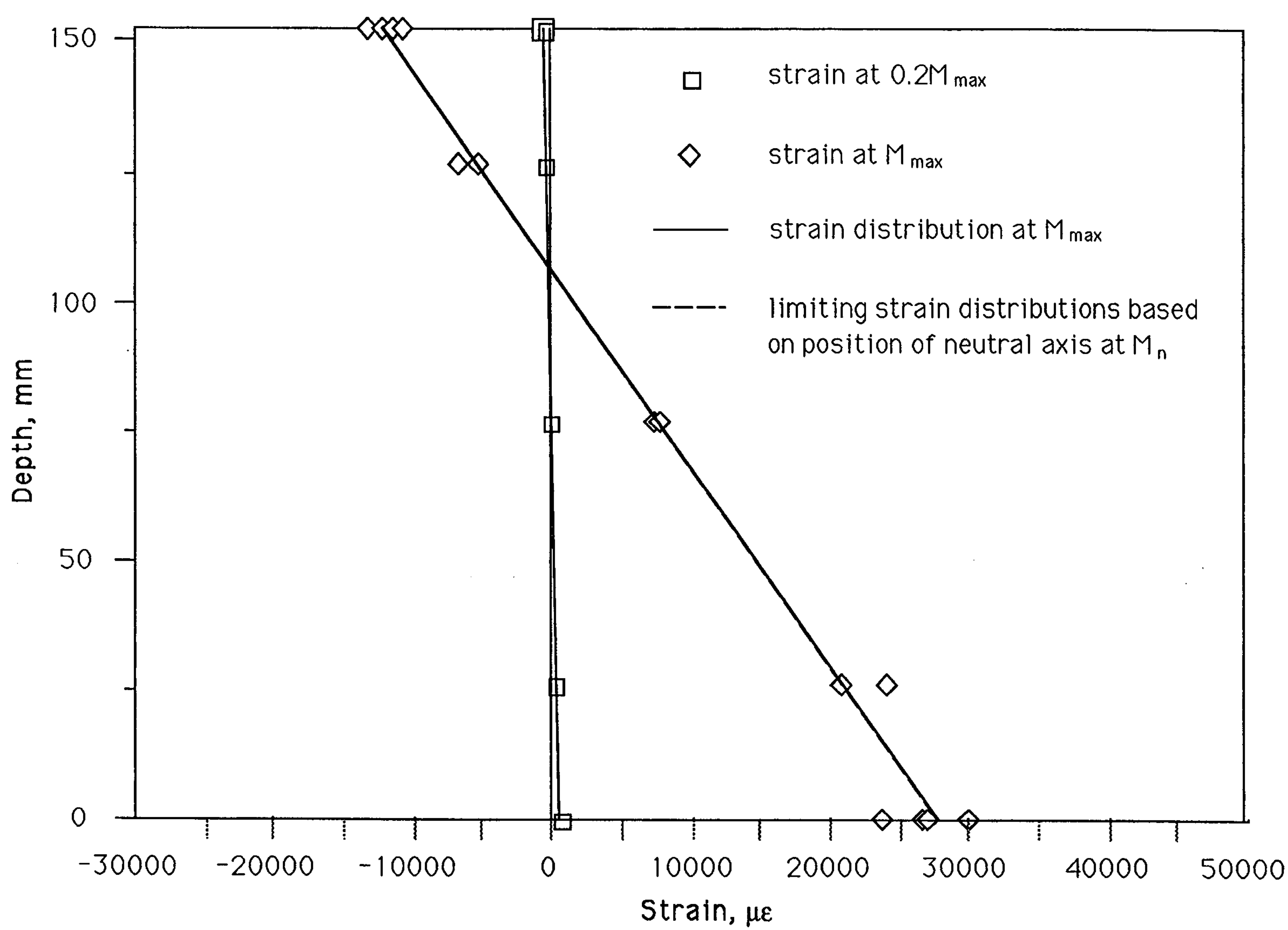

Figure 3.40 Strain Distribution Across Depth, CB13

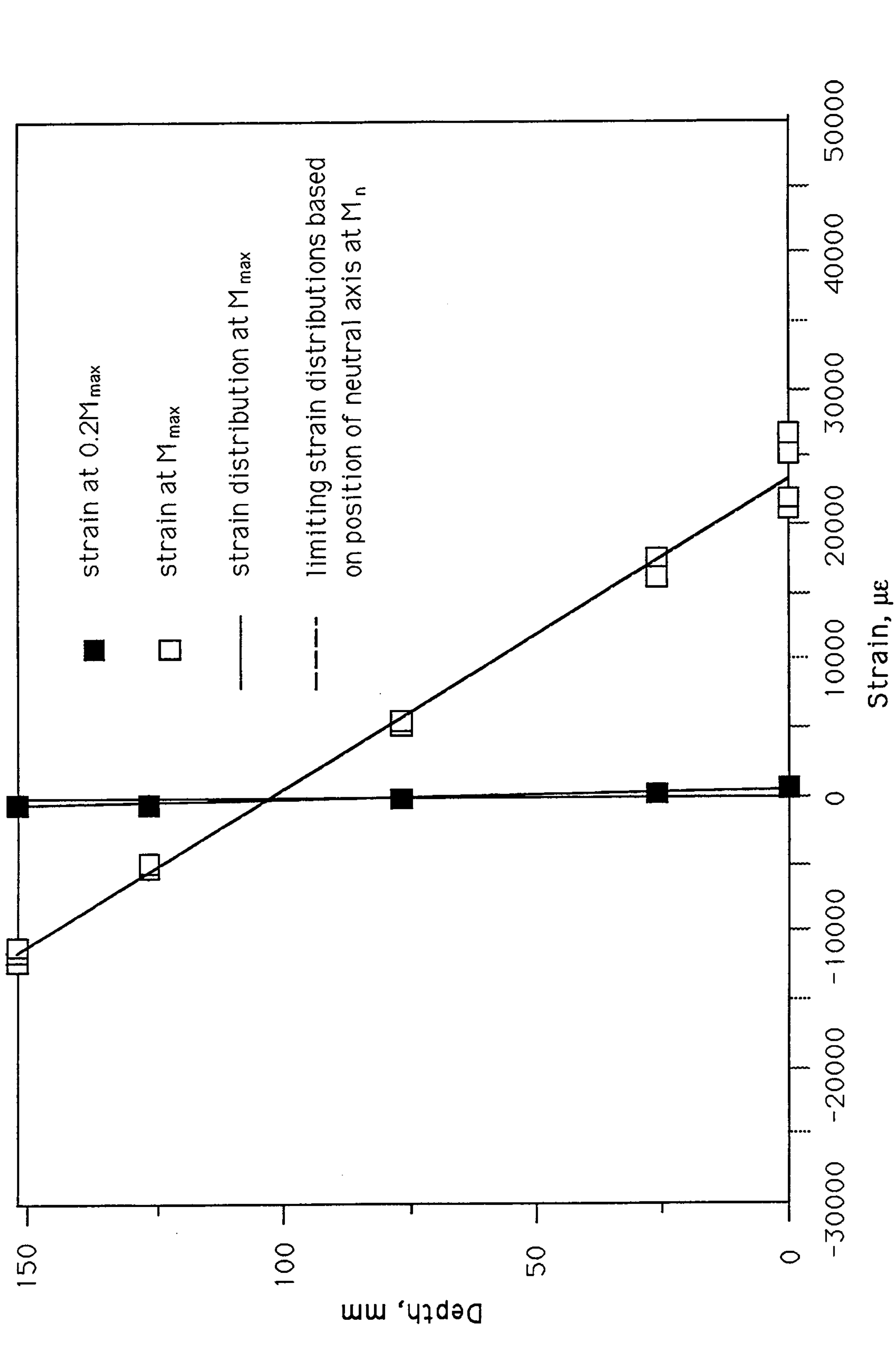

Figure 3.41 Strain Distribution Across Depth, CB15

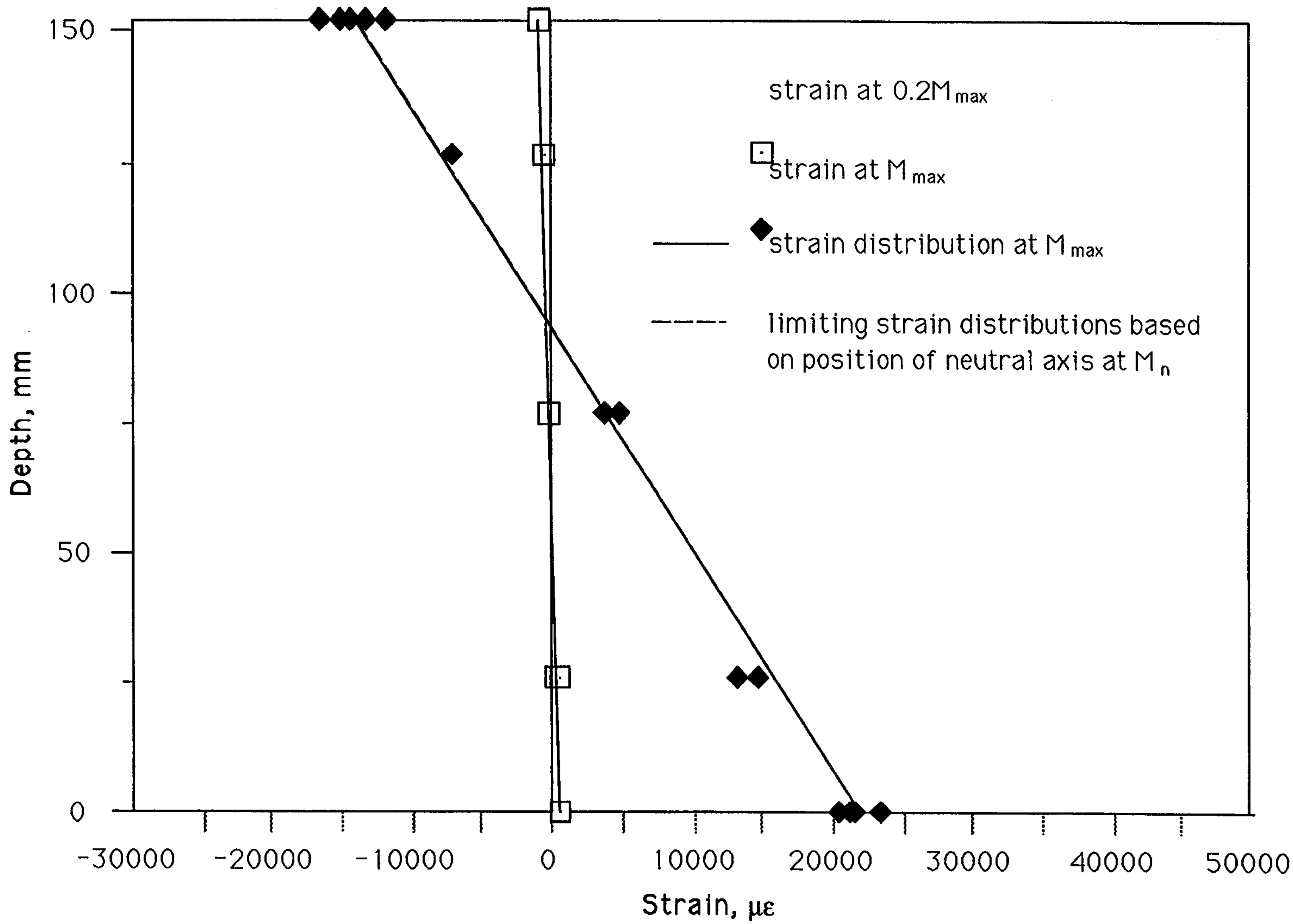

Figure 3.42 Strain Distribution Across Depth, CB22

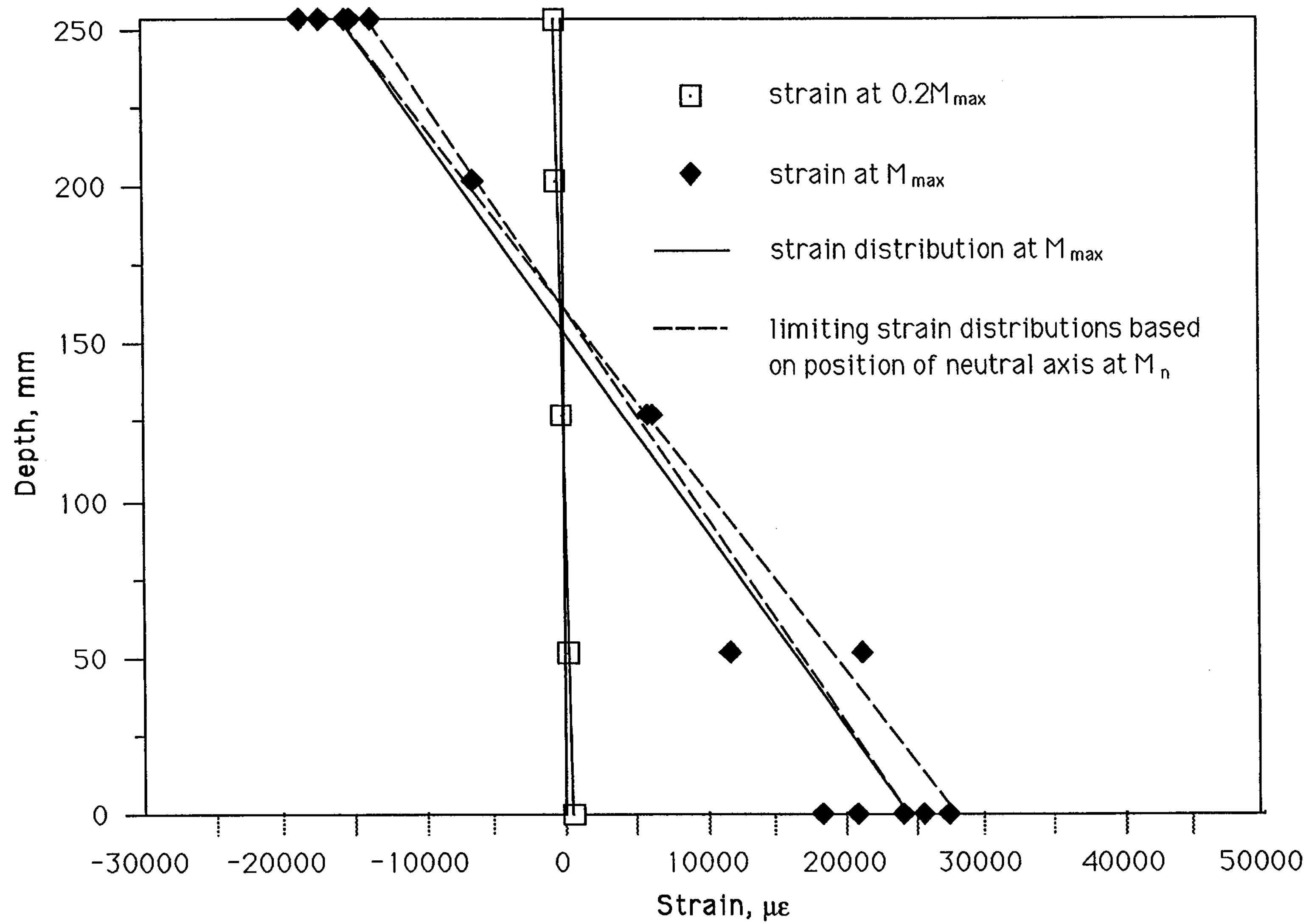

Figure 3.43 Strain Distribution Across Depth, CB31

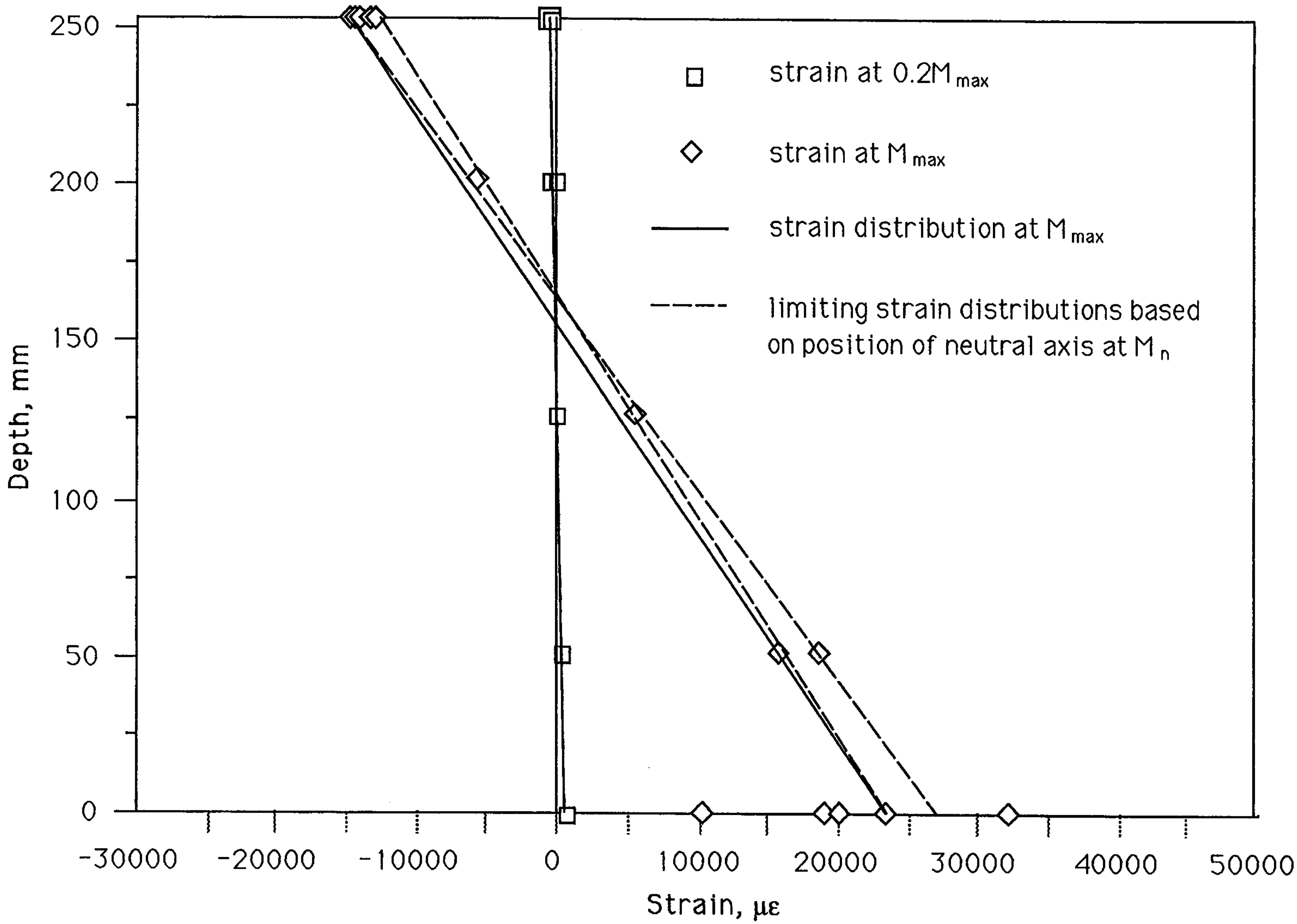

Figure 3.44 Strain Distribution Across Depth, CB33

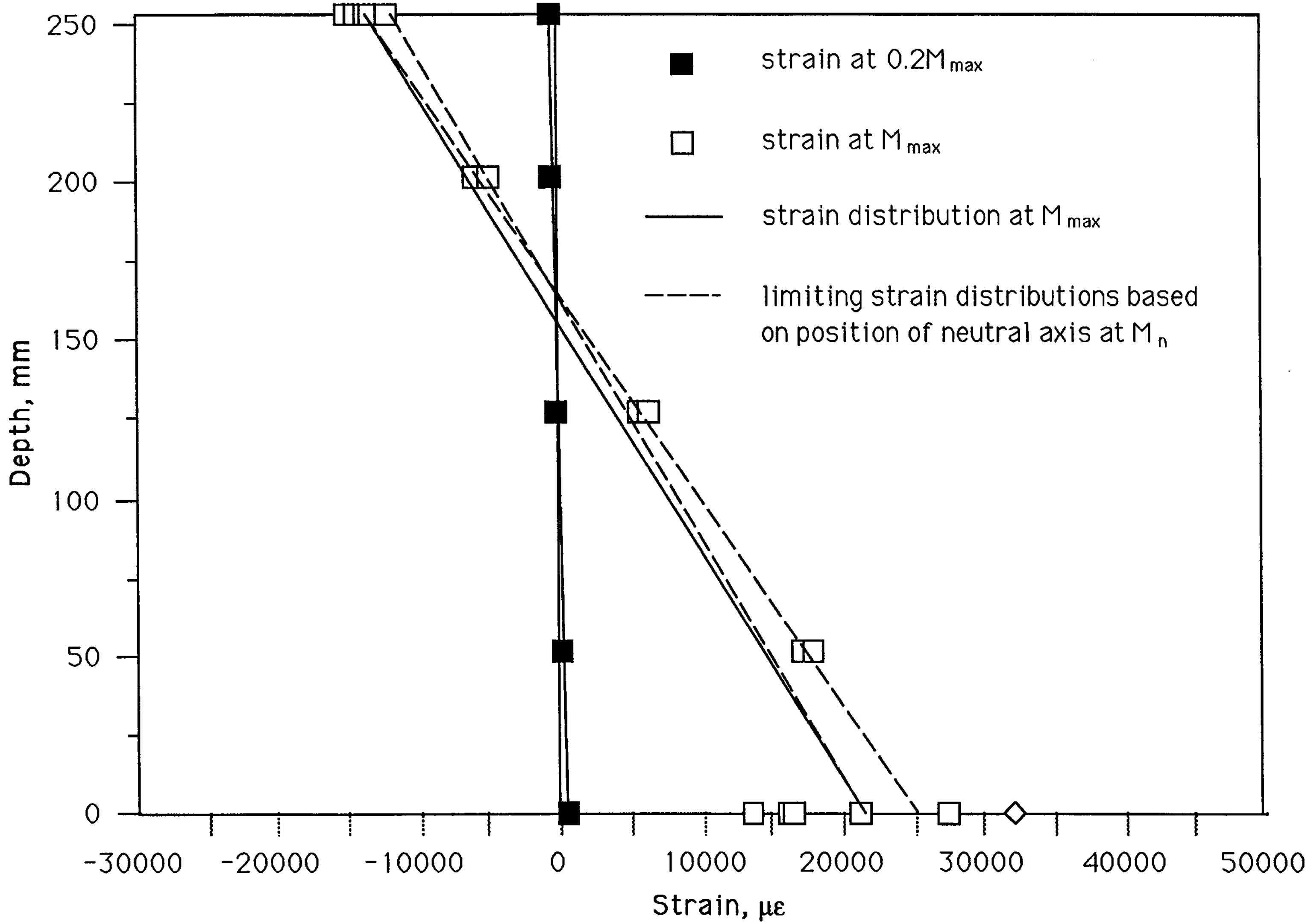

Figure 3.45 Strain Distribution Across Depth, CB35

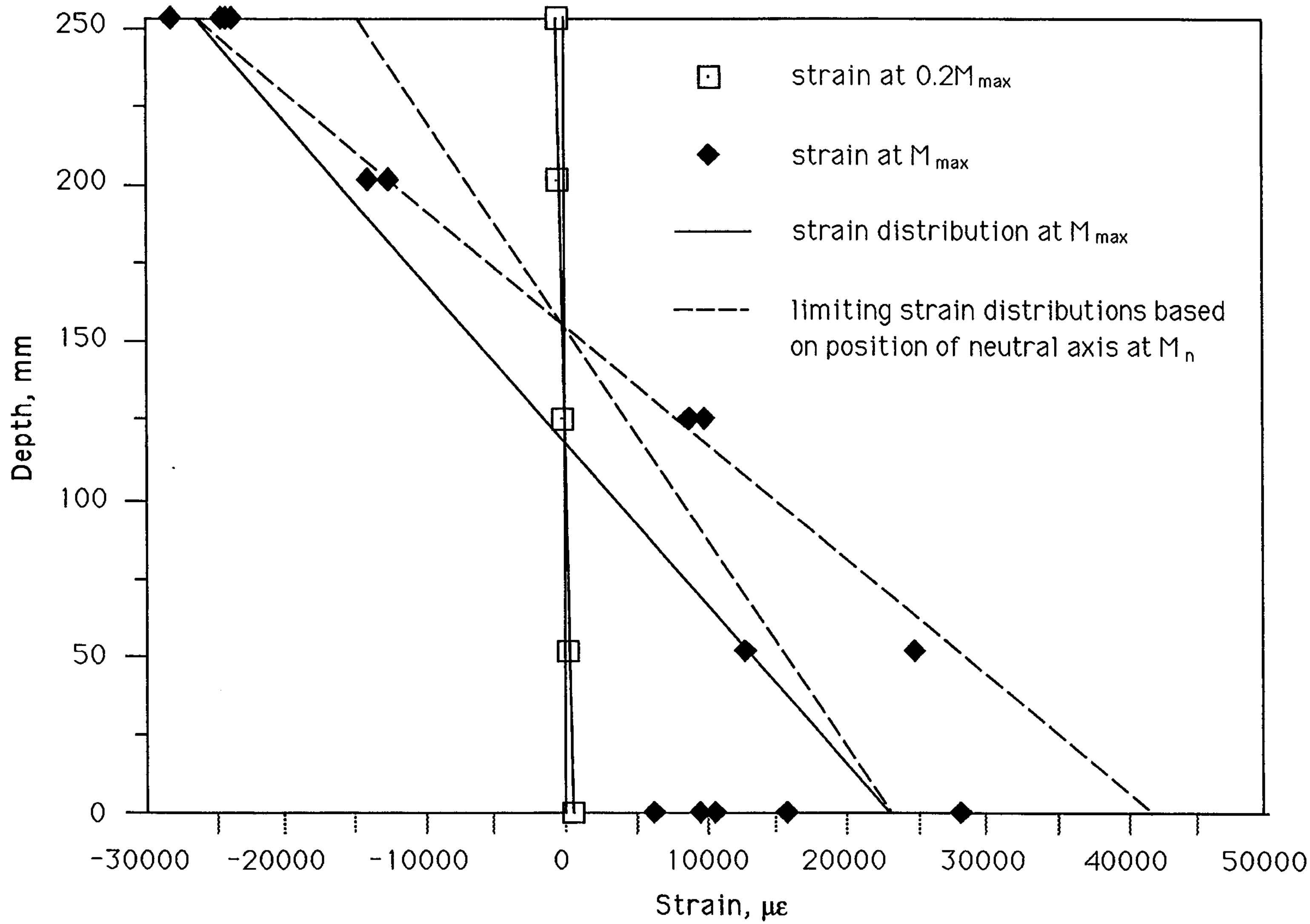

Figure 3.46 Strain Distribution Across Depth, CB41

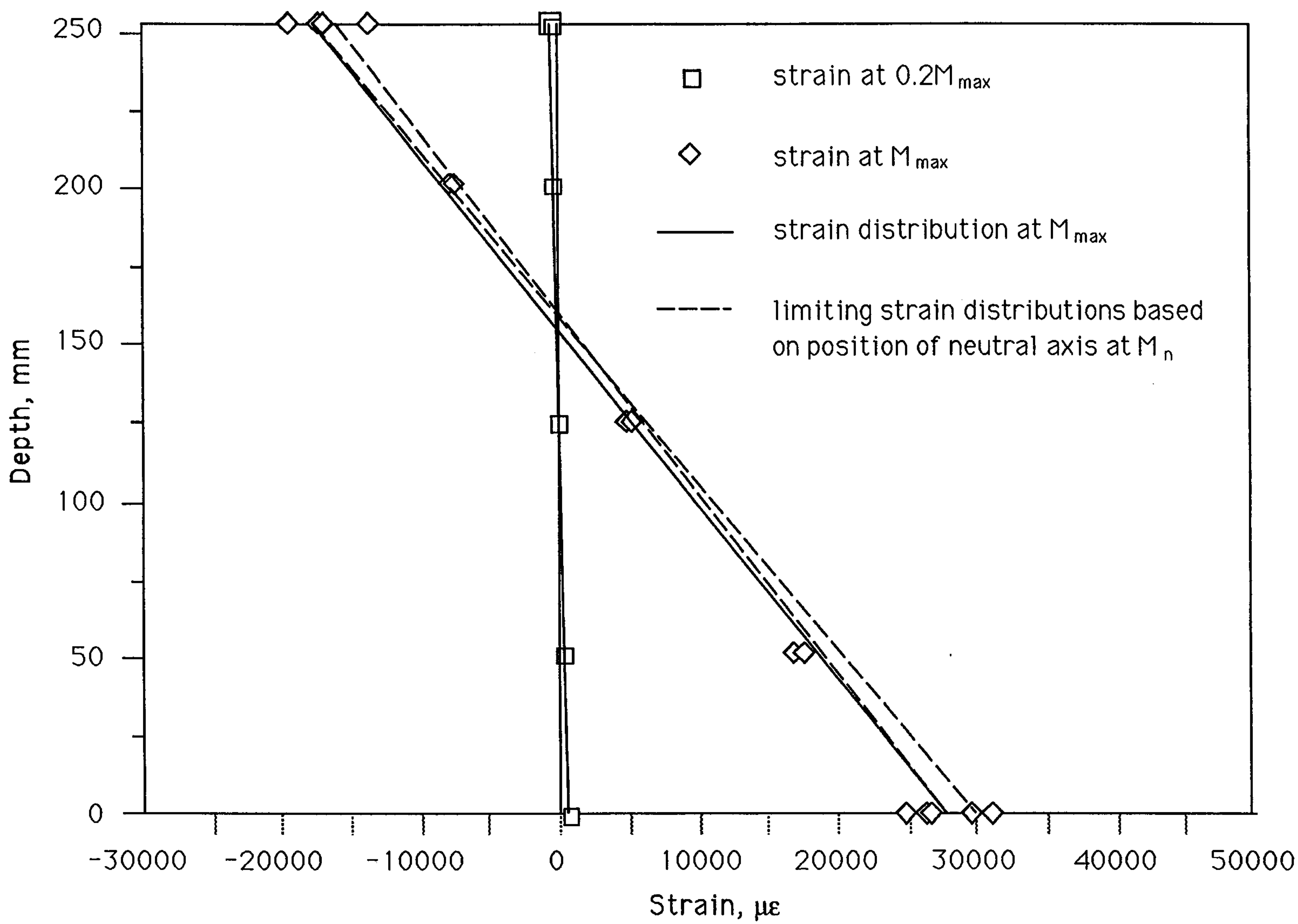

Figure 3.47 Strain Distribution Across Depth, CB45

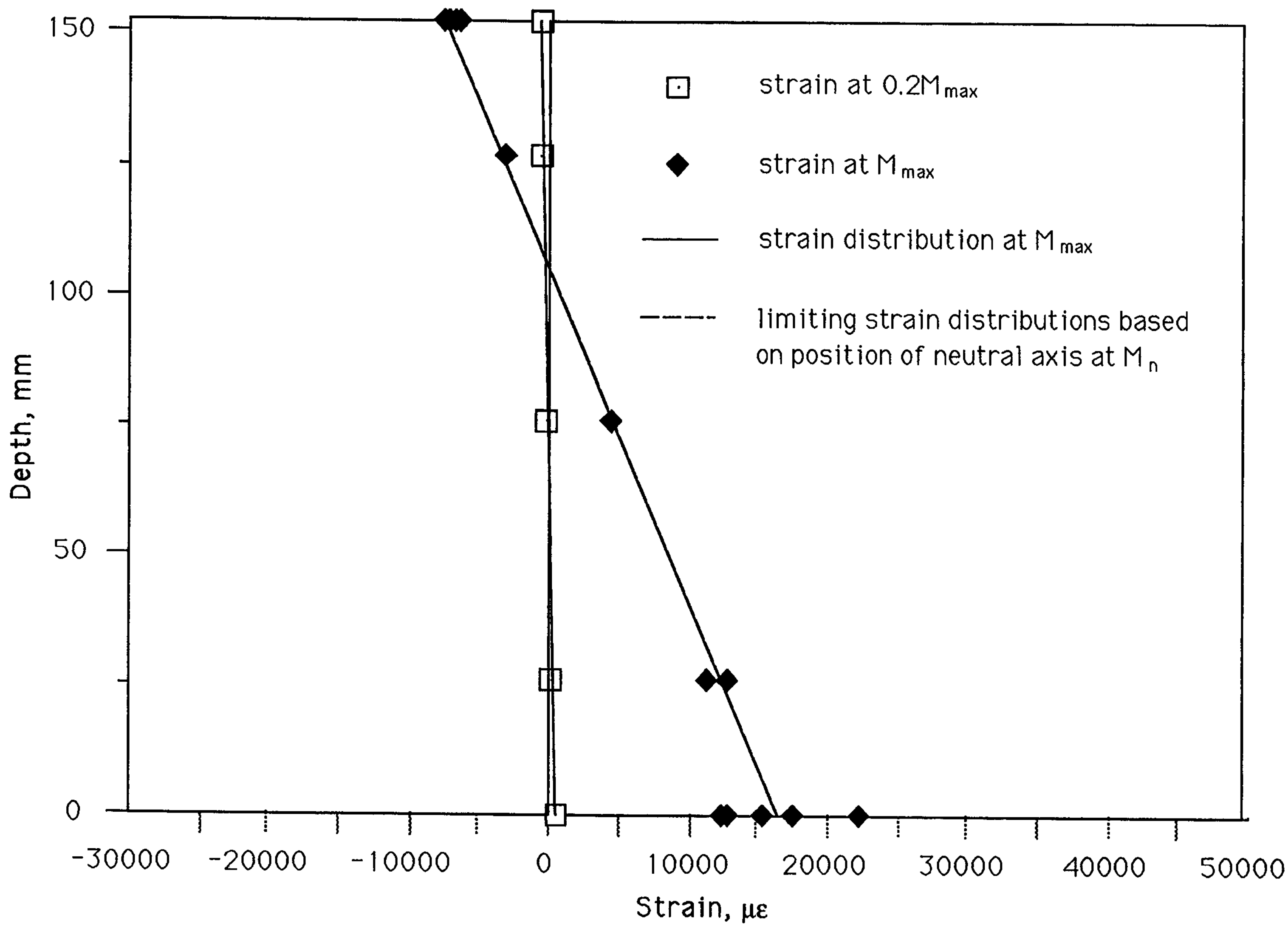

Figure 3.48 Strain Distribution Across Depth, CB52

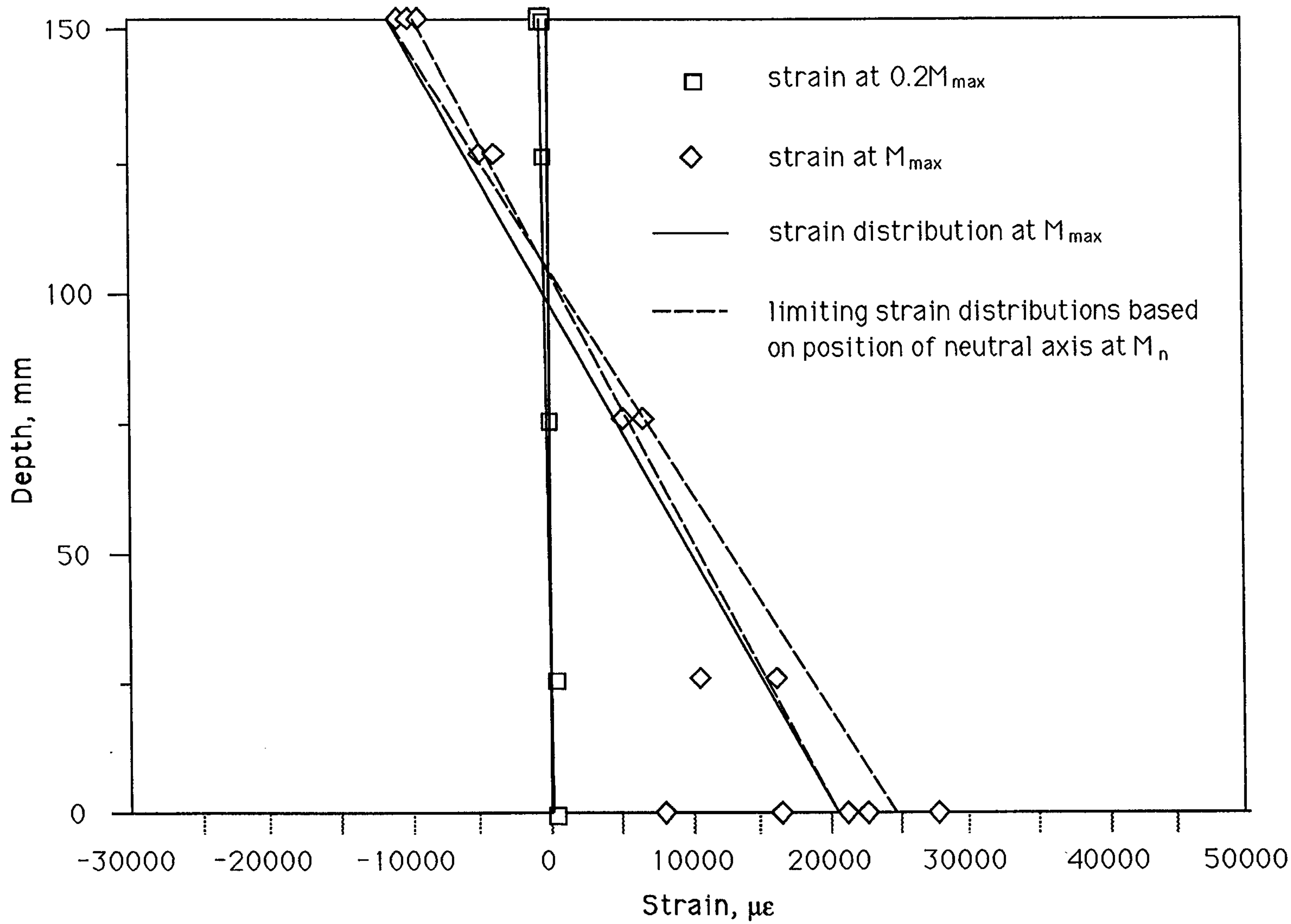

Figure 3.49 Strain Distribution Across Depth, CB53

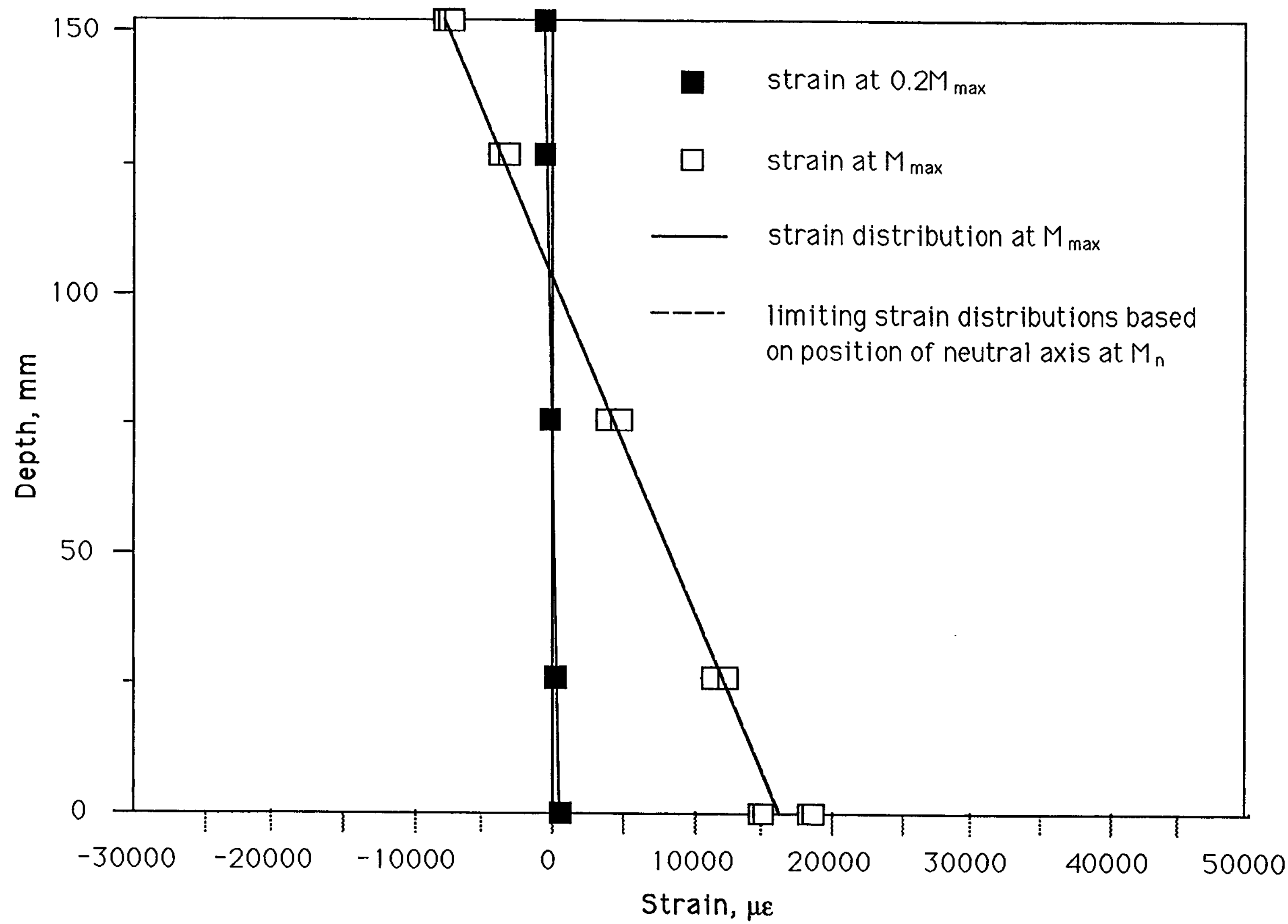

Figure 3.50 Strain Distribution Across Depth, CB55

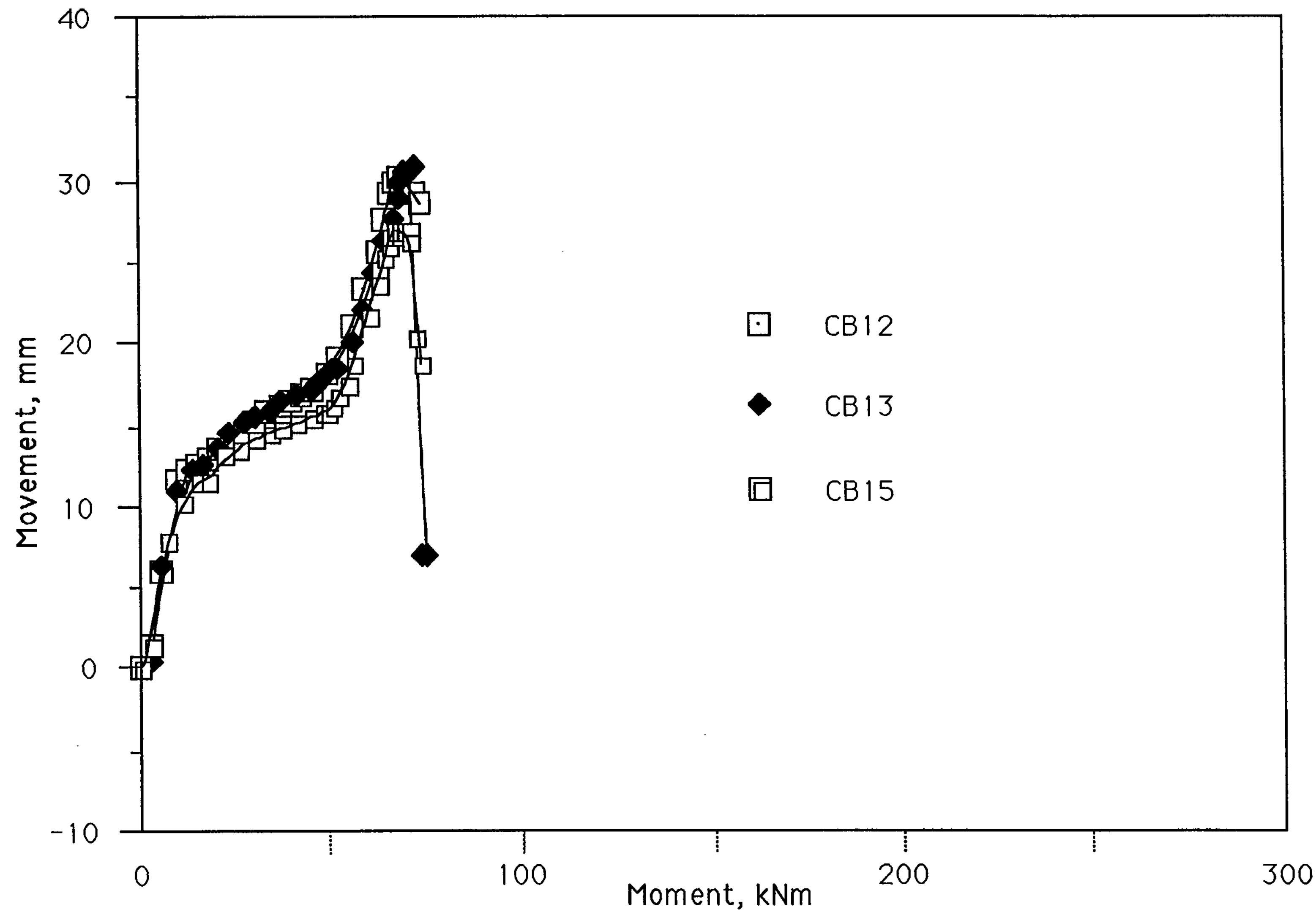

Figure 3.51 Movement of Neutral Axis with Moment, Section 1

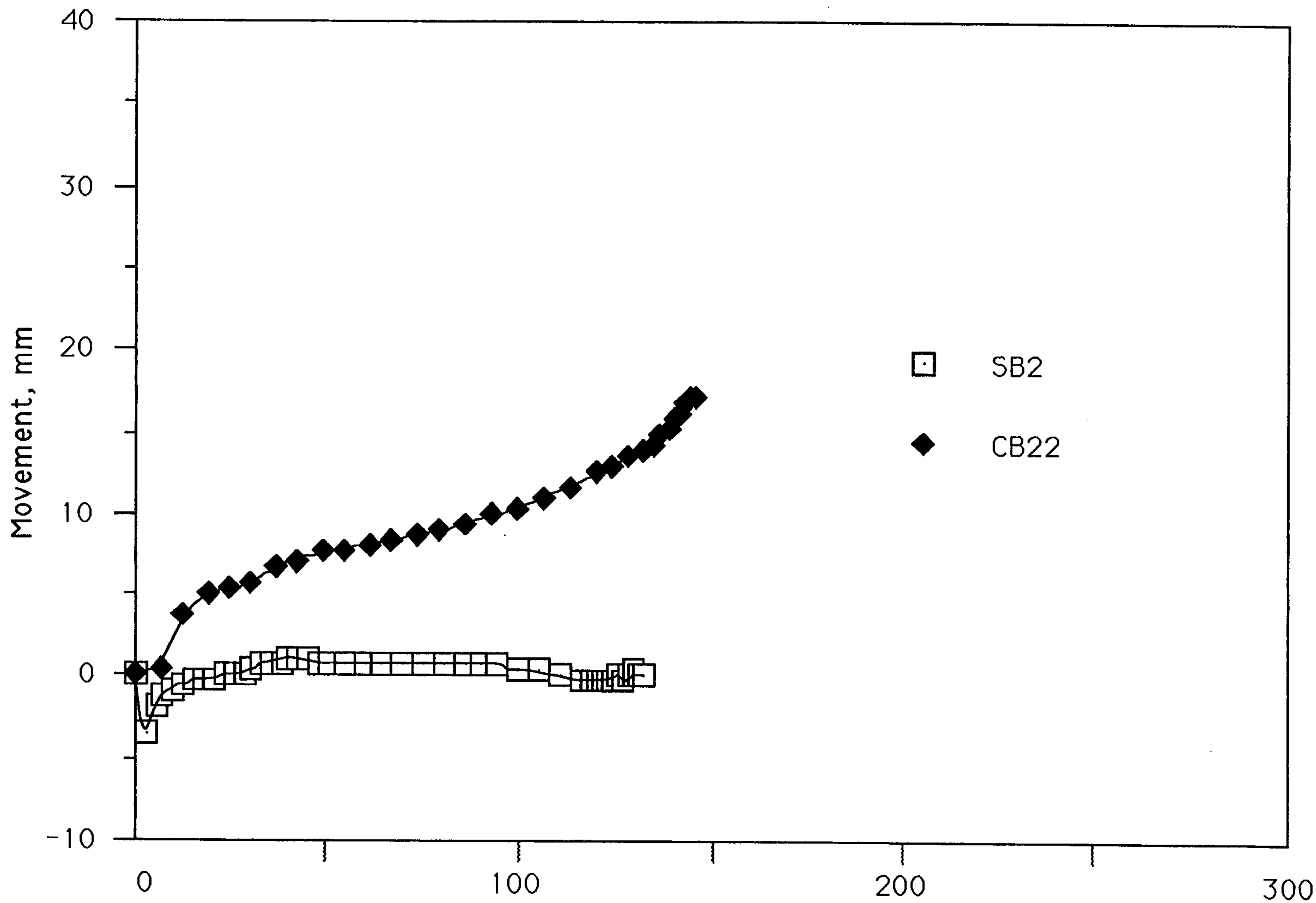

Figure 3.52 Movement of Neutral Axis with Moment, Section 2

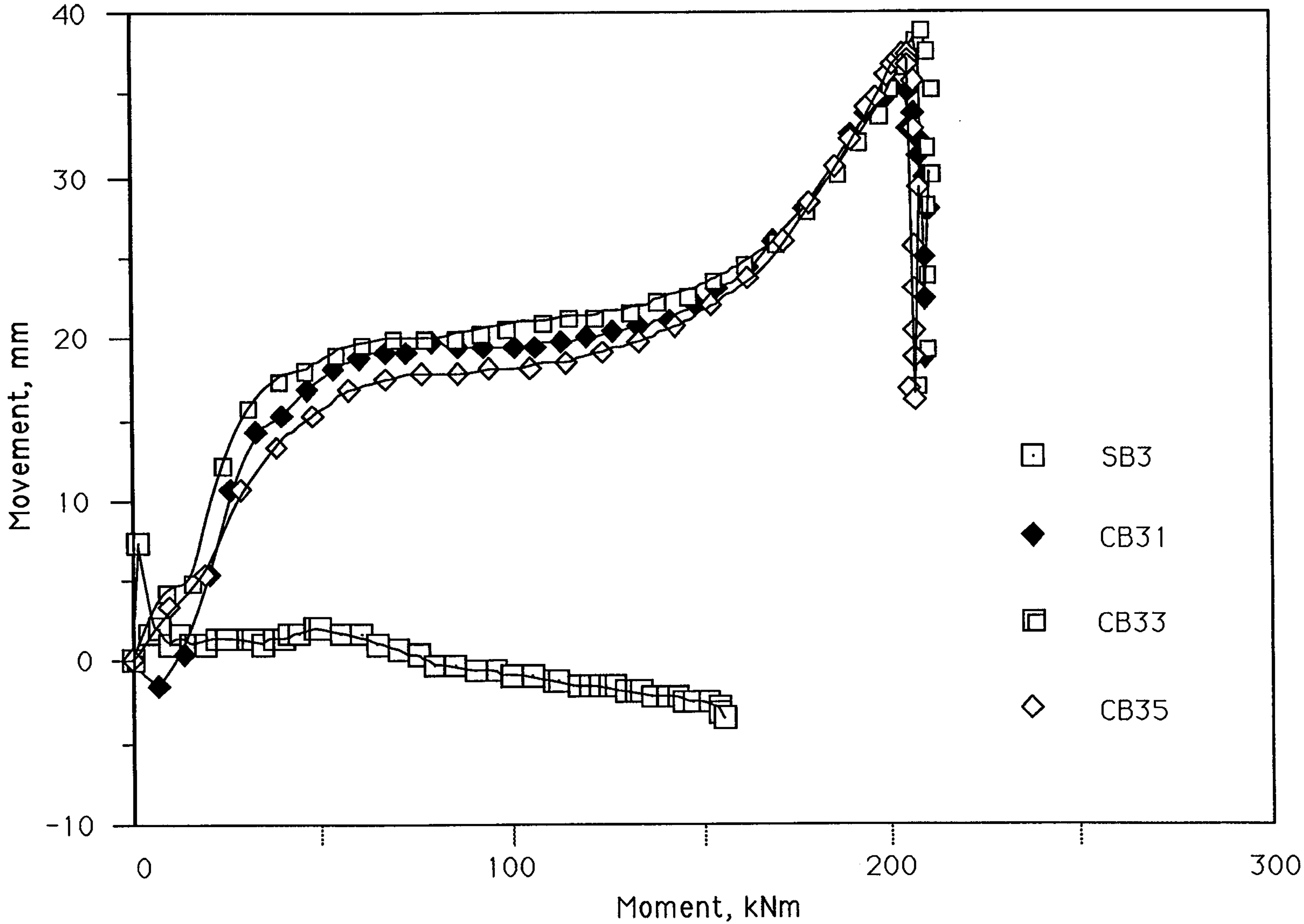

Figure 3.53 Movement of Neutral Axis with Moment, Section 3

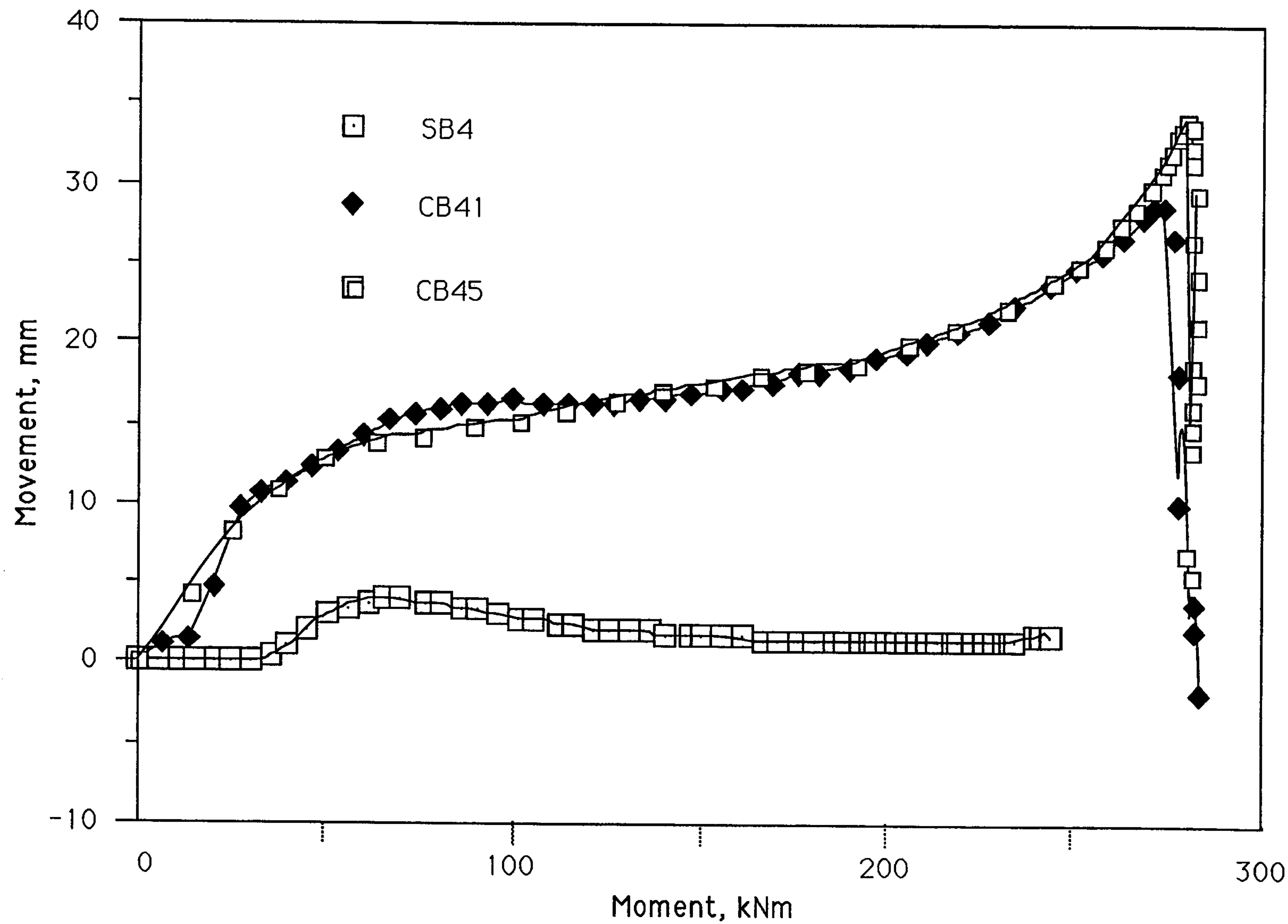

Figure 3.54 Movement of Neutral Axis with Moment, Section 4

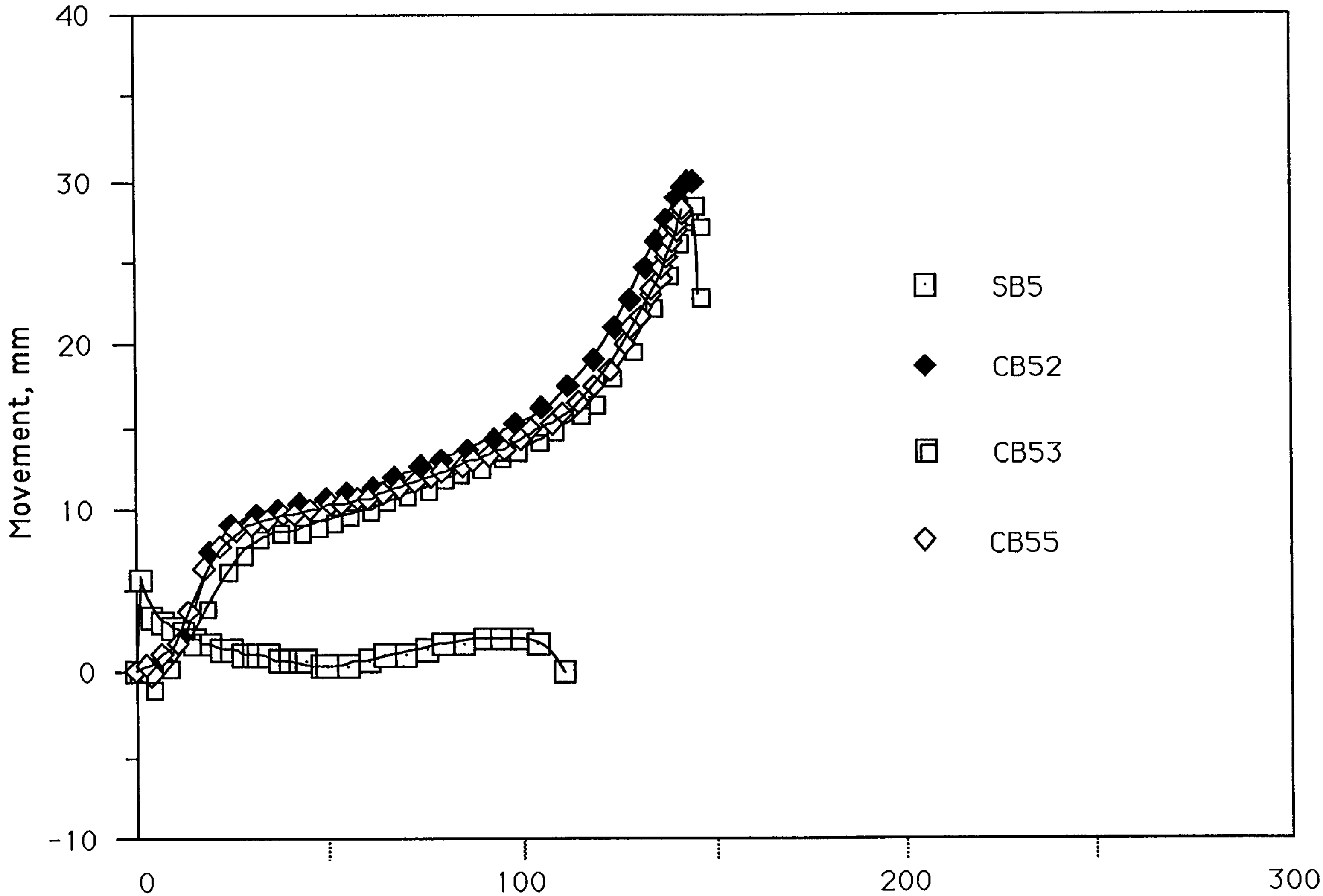

Figure 3.55 Movement of Neutral Axis with Moment, Section 5

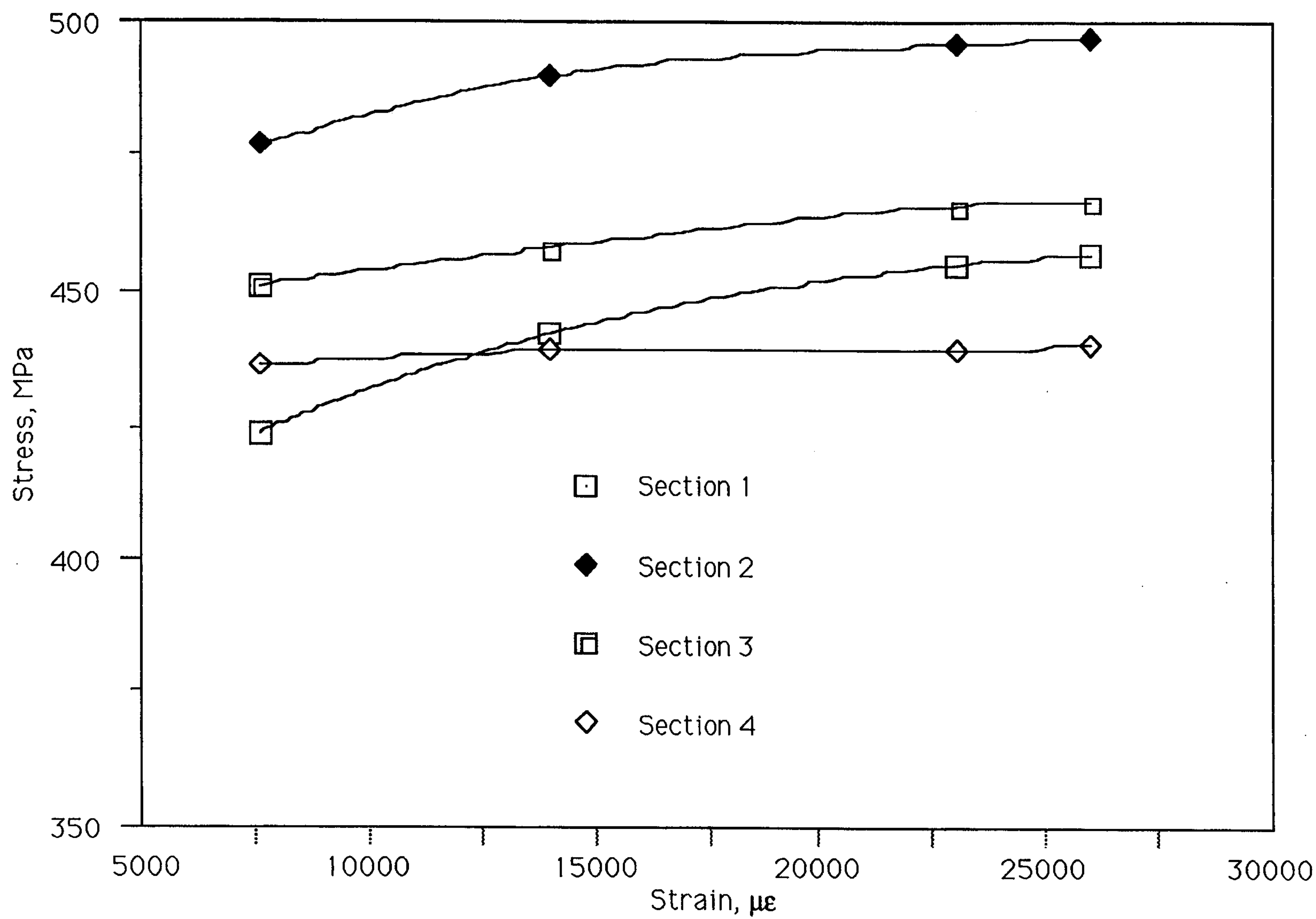

Figure 3.56 Stress-strain Relationship Used in Research Model

Chapter 4 Engineering Applications

4.1 Moment Resistance of Concrete Filled Hollow Structural Section

4.1.1 Research Model

For purposes of research, where accurate predictions of the moment resistance are required, the research model developed previously is appropriate. The steel, in compression or tension, is considered to be stressed to a stress equal to the average of that at 14 000 and 23 000 $\mu\varepsilon$ and the concrete to its cylinder strength in compression and to carry no load in tension. Rectangular stress blocks are used, with that of the concrete extending to 0.85 of the depth to the neutral axis which is located to satisfy equilibrium. No reduction of moment occurs when shear-spans, as short as the depth of the section, are used.

4.1.2 Design Model

For design, all the above provisions apply except that the steel stress both in tension and compression is taken as the specified yield stress of the steel and the concrete stress as the 28 day cylinder strength.

Based on the test/predicted ratios developed here and ratios of test to specified minimum material and geometric properties and the associated coefficients of variation, resistance factors could be developed for this design model but this is considered to be beyond the scope of this work.

Simultaneous equations can be developed to determine the design moment resistance based on the above assumptions and assuming the outside corner radius equals 2t.

The total depth of the concrete in compression, that is the depth to the neutral axis from bottom of the top flange, is

[4.1] $$c = \frac{\dfrac{A_s}{2t^2} + \left(1 - \dfrac{\pi}{4}\right)\dfrac{f'_c}{\sigma_y} - \left(\dfrac{3\pi}{2}\right) - \dfrac{b}{t} + 6}{2t + 0.85(b - 2t)\dfrac{f'_c}{2\sigma_y}} t^2$$

The area of the steel in compression is

[4.2] $$A_{sc} = (b - 6t + 3\pi t/2)t + 2tc$$

and therefore the area of the steel in tension is

[4.3] $$A_{st} = A_s - A_{sc}$$

thus the compressive force and tensile force in the steel and compressive force in the concrete are

[4.4] $$C_s = A_{sc}\sigma_y$$

[4.5] $$T_s = A_{st}\sigma_y$$

[4.6] $$C_c = T_s - C_s$$

The distance from the line of action of the steel tensile force to the neutral axis is

$$[4.7] \quad y_{st} = \frac{\int y \, dA_{st}}{A_{st}}$$

$$= \frac{t^2}{2A_{st}}\left[(b - 2t - 5\pi t/3) + 2(d - 3t - c)(b + d - c + 3\pi t/2 - 9t)t\right]$$

and to the steel compressive force is

$$[4.8] \quad y_{sc} = \frac{\int y \, dA_{sc}}{A_{sc}}$$

$$= \frac{t^2}{2A_{sc}}\left[(b - 2t - 5\pi t/3) + 2c(b + c + 3\pi t/2 - 6t)t\right]$$

The lever arm between the internal steel forces is

$$[4.9] \qquad e = y_{sc} + y_{st}$$

and between the concrete compressive force and the steel tensile force(neglects rounded corner) is

$$[4.10] \qquad e' = (1 - 0.85/2)c + y_{st}$$

Finally the unfactored resisting moment is

$$[4.11] \qquad M_r = C_s e + C_c e'$$

Design tables could easily be developed based on the above equations and should of course include resistance factors to give whatever reliability is desired.

4.2 Laterally Unsupported Beams

The lateral torsional buckling resistance of a concrete filled hollow structural section is only of concern when a rectangular cross section is bent about its strong axis. By CSA Standard S16.1-M89 (CSA 1989) the elastic critical moment for HSS's in general is given by

$$M_u = \frac{\omega_2 \pi}{L}\sqrt{EI_y GJ} \qquad [4.12]$$

Adapting this to concrete filled HSS's it is suggested, based on the table of stiffness (Table 3.2) that I_y in [4.12] be replaced by 1.12 times that of the steel section alone. Pending further investigation, conservatively J could be taken as that of the steel section alone.

As the moment curvature diagram becomes non-linear at moments as low as 20 percent of the maximum value, it would appear appropriate to use an inelastic transition for moments greater than this value up to the maximum moment of the concrete filled hollow structural section.

Chapter 5 Summary and Conclusions

5.1 Summary

The results of a series of 4 flexural tests on hollow structural sections and 12 tests on concrete filled hollow structural sections conducted by E. Barber are reported. All tests were made with 2 point loading to provide a constant moment region for observation and measurement. Rollers and knife edges were provided at all reaction and load points to allow longitudinal movements to occur as the beam deflected and unhindered rotation to occur. These are absolutely essential to give simple beam test conditions

Shear-span to depth ratios of 1 to 5 were tested to examine whether or not shear transfer problems existed between the steel and the concrete. The different section sizes and wall thicknesses of the HSS's allowed different proportions of the steel to concrete cross sectional areas to be investigated.

Material properties and behaviour were established from a series of ancillary tests which included steel stub column tests, composite stub column tests, tension coupon tests, residual stress measurements, and concrete cylinder tests.

The test data were analyzed to determine the behaviour of the concrete filled HSS's and to develop models to predict their moment resistance.

5.2 Conclusions and Recommendations

1. A considerable variation in the yield and ultimate strength of the steel exists around the perimeter of a hollow structural section. Stress-strain curves obtained from either tension tests on coupons or stub column tests on the cross section exhibit the typical curves of heavily cold worked material. No distinct yield plateau exists. Moduli of elasticity of the steel range from 200 000 to 211 000 MPa.

2. Longitudinal residual strains of up to 25% the yield strain in compression for Section 3 and 40% in tension for Section 2 exist because of the manufacturing process.

3. The process of cold forming a tube which is welded longitudinally and subsequently made rectangular induces longitudinal tensile residual strains on the outside fibers and compression residual strain on the inside fibers of up to 0.85 ε_y.

4. The concrete, of nominal 28 day strength of 30 MPa, showed a strength gain from about 30 MPa at 7 days to 48 MPa at 85 days. For this concrete the secant modulus of elasticity at 0.4 of the ultimate strength is given closely by $E_c = 3550\sqrt{f''_c}$ The tensile strength determined from split cylinder tests is only about $0.52\sqrt{f''_c}$.

5. The moment-curvature relationship for concrete filled HSS's is initially linear for only about 1/4 of the maximum moment, and is followed by increasing inelastic behaviour and then by a long plateau of slightly, increasing moment until failure occurs. Failure was

precipitated by an upward buckle of the top flange. Subsequent examination of the concrete revealed that the tension zone was heavily cracked and that concrete had crushed where the steel had buckled.

6. Steel strains at failure reached on the average 14 000 $\mu\varepsilon$ in compression and 23 000 $\mu\varepsilon$ in tension with the greater strains occuring in the more compact sections. The concrete prevented inward movement of the webs of the HSS's and therefore provided rotational restraint to the edges of the top flange and increased straining capability before failure.

7. The flexural stiffness of the concrete filled HSS's was about 1.12 times that of the bare steel sections, but only about 0.81 of that based on the uncracked concrete.

8. Three independent sets of observations, the consistent moment-curvature diagrams, the minimal slips that occured between the steel and concrete and the close correspondence between the steel and concrete strains at a given load, same ultimate moment reached, all indicate that there was no loss of full composite action between the steel and the concrete due to lack of shear transfer by friction or bond.

9. By back calculation from the known position of the neutral axis at the penultimate moment existing before any local buckling occured and the steel stresses from the steel strain measurements, it was determined that the effective rectangular stress block in the

concrete extending to 85% of the depth to the neutral axis was at the stress level of the concrete strength at the time of testing. Confinement of the concrete by the steel increased the load carrying capacity of the concrete appreciably. The ratio, k_3, of the maximum concrete compressive stress in flexure to the cylinder strength is therefore 1.00.

10. A research model, with rectangular stress blocks based on steel stresses taken as the average corresponding to steel strains at 14 000 and 23 000 $\mu\varepsilon$, with the concrete stressed to its cylinder strength and with the neutral axis located for equilibrium gave a mean test/predicted ratio of the maximum moment resistance of 1.016 with a coefficient of variation of 0.025. The use of a steel stress at these high strain levels is, based on these tests, valid for all sections with a b/t ratio of 36.0 or less in grade 350 steel.

11. A design model using the yield strength of the steel, but with all other factors as for the research model, resulted in a mean test/predicted ratio of the maximum moment resistance of 1.188 with a coefficient of variation of 0.0337. The increased mean value is due to the underassessment of the steel contribution.

12. Neither the ratio of the concrete in compression to that of steel that varied from 3.07 to 5.63 nor the ratio of shear-span /depth that varied from 1.03 to 5.05 had any effect of the test to predicted moment ratio.

5.3 Future Work

From this limited investigation, it is concluded that further research is required in the following areas:

1. These test results should be incorporated with statistical data on material and cross-sectional property variations to determine resistance factors.

2. Design tables should be developed to give the flexural resistance of concrete filled hollow structural sections for several grades of concrete.

3. The lateral torsional buckling resistance should be investigated. Some tests may be necessary.

4. The effective stiffness of composite beams up to specified load levels should be analyzed.

5. These results should be incorporated in beam-column equations.

References

American Society for Testing and Materials. 1977. Standard Methods and Definitions for Mechanical Testing of Steel Products. ASTM A370-77 Part (1), Philadelphia, PA.

Barber, E., Kennedy, S. J., Kennedy, D. J. L. and MacGregor, J. G. 1987. Flexural Strength of Concrete-Filled Steel Hollow Structural Sections. Proceedings of CSCE Centennial Conference, Montreal, QC. pp 493-509.

Canadian Standards Association. (CSA) 1990a. Compressive Strength of Cylindrical Concrete Specimens. National Standard of Canada CAN3-A23.2-9C, Canadian Standards Association, Rexdale, ON.

Canadian Standards Association. (CSA) 1990b. Splitting Strength of Cylindrical Concrete Specimens. National Standard of Canada CAN3-A23.2-13C, Canadian Standards Association, Rexdale, ON.

Canadian Standards Association. (CSA) 1984. Design of Concrete Structures for Buildings. National Standard of Canada CAN3-A23.3-M84 Canadian Standards Association, Rexdale, ON.

Canadian Standards Association. (CSA) 1989. Limit States Design of Steel Structures. National Standard of Canada CAN/CSA-S16.1-

M89, Canadian Standards Association, Rexdale, ON.

Furlong, R. W. 1967. Strength of Steel-Encased Concrete Beam Columns. Proceedings of the American Society of Civil Engineers, Journal of the Structural Division, ST5 Vol. 93, pp. 113-124.

Kennedy, S. J. and MacGregor, J. G. 1984. End Connection Effects on the Strength of Concrete Filled HSS Beam Columns. Structural Engineering Report No. 115, University of Alberta.

Knowles, R. B. and Park, R. 1969. Strength of Concrete Filled Steel Tubular Columns. Proceedings of the American Society of Civil Engineers, Journal of the Structural Division, Vol. 95, ST12 pp. 2565-2587.

Redwood, R. G. 1983. Design of Concrete Filled HSS. Report of CSA Task Group on Composite Construction, CSA Technical Committee S16 Steel Structures for Buildings, February, 17 pp.

Structural Stability Research Council. 1976. Guide to Stability Design Criteria for Metal Structures. John Wiley and Sons, New York, NY.

Tebedge, N., Alpsten, G. and Tall, L. 1973. Residual Stress Measurement by the Sectioning Method. Experimental Mechanics, Vol. 13, pp. 88-96

Todeschini, C. E., Bianchini, A. C. and Kesler, C. E. 1964. Behaviour of

Concrete Columns Reinforced with High Strength Steels, Proceedings, Journal of the American Concrete Institute, Vol. 61, No. 6, pp. 701-716.

Tomii, M. and Sakino, K.1979. Experimental Studies on the Ultimate Moment of Concrete Filled Square Steel Tubular Beam-Columns. Transactions of the Architectural Institute of Japan, No. 275, pp. 55-63.

Bibliography

American Society for Testing and Materials. 1961. Standard Test Method for Young's Modulus at Room Temperature. ASTM E111-61 Part (10), Philadelphia, PA.

American Society for Testing and Materials. 1971. Splitting Tensile Strength of Cylindrical Concrete Specimens. ASTM C496-71, Philadelphia, PA.

Bridge, R. Q. 1976. Concrete Filled Steel Tubular Columns. Civil Engineering Transactions, Australia. Vol CE 18, No. 1 pp.127-133.

Cai, Shao-Huai. 1986. Limit Analysis and Application of Concrete-Filled Steel Tubular Columns. The First Asian Conference on Structural Engineering and Construction, Bangkok, January 15-17.

Canadian Standards Association. (CSA) 1990a. Methods of Test for Concrete. National Standard of Canada CAN3-A23.2-M90, Canadian Standards Association, Rexdale, ON.

Canadian Standards Association. (CSA) 1990b. Flexural Strength of Concrete (using simple beam with third point loading). National Standard of Canada CAN3-A23.2-8C, Canadian Standards Association, Rexdale, ON.

Canadian Standards Association. (CSA) 1989. Limit States Design of Steel Structures. National Standard of Canada CAN/CSA-S16.1-M89, Canadian Standards Association, Rexdale, ON.

Dunberry, E., Leblance, D. and Redwood, R. G. 1987. Cross-section Strength of Concrete-Filled HSS Columns at Simple Beam Connections. Department of Civil Engineering and Applied Mechanics, McGill University, Montreal, QC. pp 408-417.

Furlong, R. W. 1983. Column Rules of ACI, SSLC, and LRFD Compared. Proceedings of the American Society of Civil Engineers, Journal of the Structural Division, Vol. 109, ST10, pp 2375-2386

Galambos, T. V. 1968. Structural Members and Frames. Prentice-Hall Inc., Englewood Cliffs, N. J.

Gardner, N. J., and Jacobson, E. R. 1967. Structural Behaviour of Concrete Filled Steel Tubes. Journal of the American Concrete Institute, Vol. 64, No. 7, pp. 404-413.

Janss, J. Composite Steel and Concrete Construction. Part 3. Tests on Concrete Filled Tubular Columns. Report Published by the Centre of Scientific Research and Industrial Techniques of Metal Fabrication (CRIF), Brussels, Belgium

MacGregor, J. G. 1988. Reinforced Concrete, Mechanics and Design. Prentice Hall Inc. Englewood Cliffs, N. J.

Pekoz, M. V. T. 1983. Limit Design in Cold-Formed Steel. Journal of Structural Engineering Vol 109. pp. 2033-2047.

Sabnis, G. M. 1979. Handbook of Composite Construction Engineering. Van Nostrand Reinhold Company, Toronto, ON.

Sabnis, G. M., Harris, H. G., White, R. N., and Mirza, M. S. 1983. Structural Modelling and Experimental Techniques. Prentice-Hall Inc., Englewood Cliffs, N. J.

Salani, H. J. and Sims, J. R. 1964. Behaviour of Mortar Filled Steel Tubes in Compression. Proceedings of American Concrete Institute, October. pp. 1271-1283

Sherman, D. R. 1969. Residual Stress Measurement in Tubular Members. Proceedings of the American Society of Civil Engineers, Journal of the Structural Division, Vol. 95, ST4, pp. 635-647

Somayasi, S. and Shah, S. P. 1981. Bond Stress Versus Slip Relationship and Cracking Response of Tension Members. Journal of the American Concrete Institute, pp. 217-225

Toshiyuki K., Yasuki, Y. and Hiroshi, N. 1987. Fundamental Study on Elastoplastic Behavior of Concrete Encased Steel Short Tubular Columns. Osaka, City Univ. Vol. 28, pp. 237-253.

Troke, R. W. 1976. Improving Strain-Measurement Accuracy with Using Shunt Calibrations. Experimental Mechanics, October. pp.

397-400

Walker, A. C. (Editor) 1975. Design and Analysis of Cold-Formed Sections. International Textbook Company Limited.

Window, A. L. and Holister, G. S. 1982. Strain Gauge Technology. Applied Science Publishers Ltd., Essex, England.

Yam, H. J., and Sims, J. R. 1981. Design of Composite Steel-Concrete Structures. Surrey University Press, London.

Appendix A

A.1 Relaxation of Residual Strains

When, using the method of sectioning, a coupon is cut from a member to determine the relaxation of residual strains, a correction must be applied if the coupon does not remain straight. Fig. A.1(a) shows that the measured relaxation length of the straight coupon is L_m where the original length was L. There is a positive relaxation strain $(L_m - L)/L$ and therefore, before sectioning, there must have existed a compressive residual strain of the same magnitude. In Fig. A.1(b), for a coupon that curves on sectioning, the measured relaxed lengths determined from the strain gauge on the chord are L_{im} and L_{om} for the inside and outside surfaces respectively assuming that the coupon is convex outward as is usually the case for a coupon cut from a HSS. The true relaxed lengths on the arc are greater than L_{im} and L_{om}.

For the case when the relaxed length is greater than the original length, the relaxation strain is positive. Measuring on the chord, giving too small a relaxed length, results in too small a relaxation strain. The apparent residual strain of opposite sign (negative) is also too small. The true residual strain has a larger negative value. To get the true residual strain, a negative correction would be applied to the apparent residual strain.

For the case when the relaxed length is less than the original length, the relaxation strain is negative. Measuring on the chord, giving too small a relaxed length, results in too great a relaxation strain. The apparent residual strain of opposite sign (positive) is also too great. The true residual strain is of lesser magnitude. To get the true residual strain a negative correction would be applied to the apparent residual strain.

The effect of the curvature correction is always to reduce the residual strain, compressive residual strains are increased in magnitude and tensile residual strains are decreased in magnitude. As established subsequently, the correction is of essentially the same magnitude, $\Delta\varepsilon_r$, for the inside strain, ε_i, outside strain, ε_o and the mean strain ε.

A.2 Correction of Relaxation Strains

Considering Fig. A.2, L_{im} and L_{om} are relaxed lengths measured on the inside and outside chords, L_i and L_o are relaxed lengths along the arc, that is:

[A.1a] $$\Delta_{im} = L_{im} - L$$

[A.1b] $$\Delta_{om} = L_{om} - L$$

[A.1c] $$\Delta_i = L_i - L$$

[A.1d] $$\Delta_o = L_o - L$$

and,

[A.1e] $$\Delta = (\Delta_i + \Delta_o)/2$$

[A.1e] gives:

[A.2] $$\varepsilon = (\Delta_i + \Delta_o)/2L$$

also:

[A.3] $$L + \Delta = 2\theta\rho$$

where, $\theta \neq 0$

$AB = (L + \Delta_{im} + L + \Delta_{om})/2 = (2L + \Delta_{im} + \Delta_{om})/2 = 2(\sin\theta)\rho$, thus,

[A.4] $$\theta = \sin^{-1}(2L + \Delta_{im} + \Delta_{om})/4\rho$$

and by similar triangles:

$$\frac{L + \Delta_{im} - (L + \Delta_{om})}{t} = \frac{2L + \Delta_{om} + \Delta_{im}}{2\rho}$$

therefore,

[A.5] $$\rho = \frac{2L + \Delta_{om} + \Delta_{im}}{2(\Delta_{im} - \Delta_{om})}t = \frac{2 + \varepsilon_{om} + \varepsilon_{im}}{2(\varepsilon_{im} - \varepsilon_{om})}t$$

from [A.4] and [A.5],

[A.6] $$\theta = \sin^{-1}\frac{(2L + \Delta_{om} + \Delta_{im})(\varepsilon_{im} - \varepsilon_{om})}{2(2 + \varepsilon_{om} + \varepsilon_{im})\,t} = \sin^{-1}\frac{(\varepsilon_{im} - \varepsilon_{om})}{2t}L$$

from [A.3],

[A.3a] $$1 + \Delta/L = 2\theta\rho/L$$

thus,

[A.7] $$\varepsilon = 2\theta\rho/L - 1$$

Substituting [A.5] and [A.6] into [A.7], gives:

$$\varepsilon = \frac{(2+\varepsilon_{om}+\varepsilon_{im})}{(\varepsilon_{im}-\varepsilon_{om})}\frac{t}{L}\sin^{-1}\frac{(\varepsilon_{im}-\varepsilon_{om})}{2t}L - 1$$

Similarly, ε_o and ε_i can be computed by replacing ρ by $(\rho + t/2)$ for inside strains and by $(\rho - t/2)$, for outside strains, that is,

$$\varepsilon_i = \left(\frac{(2+\varepsilon_{om}+\varepsilon_{im})}{(\varepsilon_{im}-\varepsilon_{om})} + 1\right)\frac{t}{L}\sin^{-1}\frac{(\varepsilon_{im}-\varepsilon_{om})}{2t}L - 1$$

and,

$$\varepsilon_o = \left(\frac{(2+\varepsilon_{om}+\varepsilon_{im})}{(\varepsilon_{im}-\varepsilon_{om})} - 1\right)\frac{t}{L}\sin^{-1}\frac{(\varepsilon_{im}-\varepsilon_{om})}{2t}L - 1$$

These are the corrected relaxation strains.

A.3 Comparison of Corrected and Uncorrected Relaxation Strains

The uncorrected relaxation strains, measured on the chord are ε_m, ε_{im} and ε_{om}, are:

$$\varepsilon_m = \frac{\varepsilon_{im}+\varepsilon_{om}}{2}$$

$$\varepsilon_{im} = \frac{L_{im} - L}{L}$$

$$\varepsilon_{om} = \frac{L_{om} - L}{L}$$

the difference between the corrected and uncorrected relaxation strains are then,

$$\Delta\varepsilon = \varepsilon - \varepsilon_m = \frac{L_{im} + L_{om}}{2}\left(\frac{2t}{L_{im} - L_{om}} \sin^{-1}\frac{L_{im} - L_{om}}{2t} - 1\right)\frac{1}{L}$$

$$\Delta\varepsilon_i = \varepsilon_i - \varepsilon_{im} = L_{im}\left(\frac{2t}{L_{im} - L_{om}} \sin^{-1}\frac{L_{im} - L_{om}}{2t} - 1\right)\frac{1}{L}$$

$$\Delta\varepsilon_o = \varepsilon_o - \varepsilon_{om} = L_{om}\left(\frac{2t}{L_{im} - L_{om}} \sin^{-1}\frac{L_{im} - L_{om}}{2t} - 1\right)\frac{1}{L}$$

Because L_{im} and L_{om} will differ by only a very small amount, the three corrections are virtually identical.

A.4 Residual Strains

The residual strains are the negative of the relaxation strain, therefore, the final corrected residual strains are:

$$\varepsilon = -\frac{(2 + \varepsilon_{om} + \varepsilon_{im})}{(\varepsilon_{im} - \varepsilon_{om})}\frac{t}{L}\sin^{-1}\frac{(\varepsilon_{im} - \varepsilon_{om})}{2t}L + 1$$

$$\varepsilon_i = -\left(\frac{(2 + \varepsilon_{om} + \varepsilon_{im})}{(\varepsilon_{im} - \varepsilon_{om})} + 1\right)\frac{t}{L}\sin^{-1}\frac{(\varepsilon_{im} - \varepsilon_{om})}{2t}L + 1$$

$$\varepsilon_o = -\left(\frac{(2 + \varepsilon_{om} + \varepsilon_{im})}{(\varepsilon_{im} - \varepsilon_{om})} - 1\right)\frac{t}{L}\sin^{-1}\frac{(\varepsilon_{im} - \varepsilon_{om})}{2t}L + 1$$

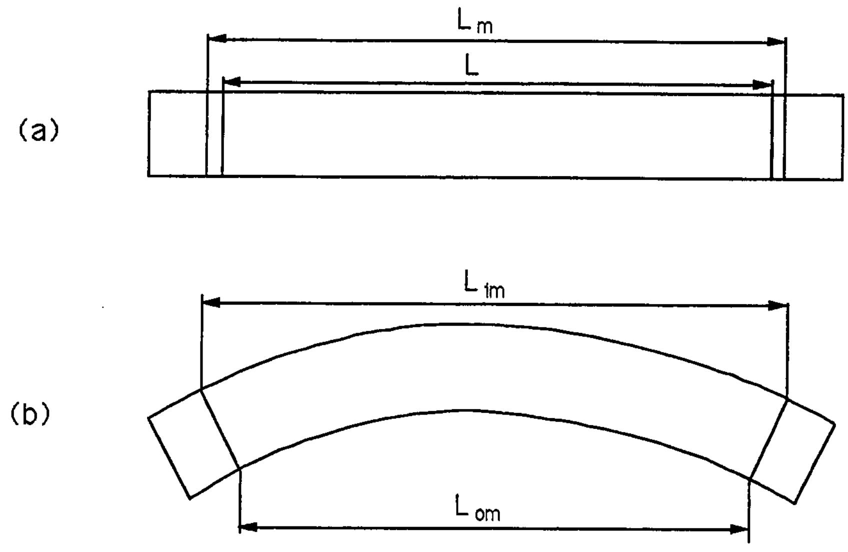

Fig. A.1 Residual Strain Measurement

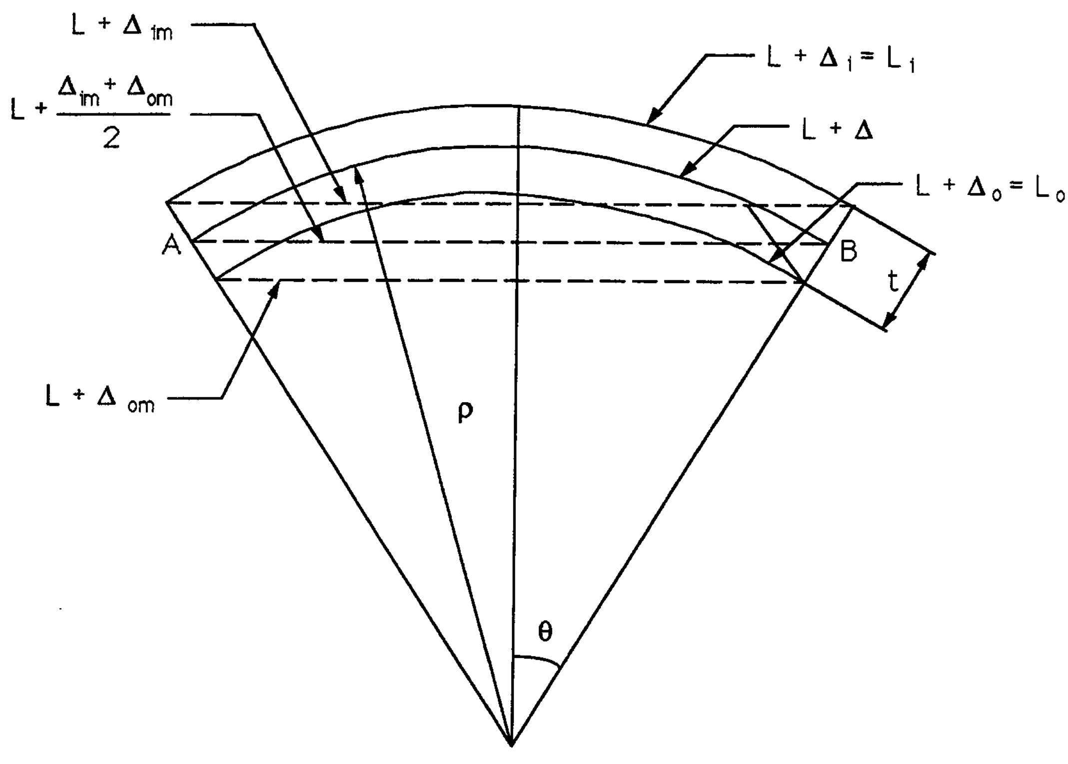

Fig. A.2 Geometric Dimension